Polarimetry of the crab nebula and NGC 1569

C. White

Polarimetry of the Crab Nebula and NGC 1569

A Thesis Submitted to the University of Durham for the Degree of Master of Science

by

Cathleen White BSc (Dunelm)

January 1977

Abstract

This thesis contains a description of the technique used to measure the optical linear polarisation of the Crab Nebula, and the irregular galaxy NGC 1569, and the results obtained from these measurements. This work was undertaken while the author was a member of the Durham University Astronomy Group.

The first chapter is an outline of the differing states of polarisation and the method used to describe these states via the Stokes Parameters. A short review of the mechanisms producing linear polarisation of the optical radiation from astronomical objects is included.

Chapter 2 contains a brief account of the design and operation of the Durham University polarimeter used to detect and measure optical linear polarisation, with a short description of the electronographic camera used as a recording device. The technique for the reduction of the data, from its initial electronograph form to the final extraction of the Stokes parameters for over 1000 points in the object observed is also described.

The following three chapters contain a review of the present information known about the Crab Nebula, an account of the technique employed to measure the optical linear polarisation of the nebula, together with a final map of the polarisation, and a comparison of the results obtained by the present method and the previous photographic measurements of Woltjer made in 1957.

The final chapter is devoted to the study of the irregular galaxy NGC 1569. A short review of the known parameters of the galaxy is included and the results of the present polarisation measurements are shown. An interpretation of the results follows in which it is suggested that the polarisation detected is not intrinsic to the NGC 1569 but produced as the light from the galaxy passes through our interstellar medium. An attempt is made to remove the interstellar polarisation leaving NGC 1569 apparently unpolarised.

Preface

The work presented in this thesis was carried out during the period 1974-1976 while the author was a research student under the supervision of Dr. S.M. Scarrott in the Physics Department of the University of Durham. During this period the author visited the Florence and George Wise Observatory, University of Tel Aviv, Israel (February 1975, May 1976).

Contents

Introduction

Astronomy is the oldest and perhaps the broadest of the physical sciences, encompassing as it does, varied aspects of all these subjects, on a scale wider than can be produced on earth, spanning periods not merely of thousands of years but thousands of millions of years.

With the advent of new, sophisticated techniques, especially in the latter half of this century, astronomers have been able to look farther and in more detail at the nature of the universe about us, gathering information not only in the optical but in the γ ray, x-ray, infrared and radio regions of the spectrum.

All that we can observe are the properties of the radiation from astronomical objects, but the interpretation of this data leads to the derivation of theories describing the processes, that we cannot directly see, which produce the observed results. Of these properties, polarisation must surely be one of the most interesting and informative.

Interstellar linear polarisation was measured in our galaxy in the 1940's. Subsequent work produced a wealth of information on the polarisation of starlight which lead to a better understanding of the role of magnetic fields in the structure of the galaxy. This moved astronomers to look in more detail at the polarisation of radiation from other galaxies in the hope of increasing the information already known of the mechanisms at work in these galaxies. Detailed polarisation measurements have been made for many galaxies including M82 and the Sombrero galaxy.

The theory of synchrotron radiation has been well developed for many years to explain the results obtained from the large synchrotron and cyclotron accelerators designed for the production of very high energy electrons and other charged particles. Astronomers realised the possible significance of the synchrotron mechanism for astronomical sources.

Soviet theorists predicted that high linear polarisation of the radiation from the Crab nebula should be observed if the synchrotron mechanism was involved and the subsequent observation of significant linear polarisation in the nebula both confirmed the earlier prediction and prompted detailed investigation of the properties of the nebular radiation in all wavebands. The discovery of a pulsar in the central region of the nebula in the late 1960's, renewed interest in the formation and structure of magnetic fields within the nebula, and the necessity for more detailed polarimetry of the Crab nebula became apparent.

Chapter One Polarised Light

1.1 States of Polarisation

The classical description of light is that of a series of superimposed transverse electromagnetic waves, characterised by the electric (E) vector, vibrating in a plane perpendicular to the direction of propagation.

When the electric vector vibrates randomly in this plane, the light is called natural or unpolarised light.

If the electric vector exhibits a preference for a fixed direction, the light is described as being plane polarised. The amplitude of the electric vector can be divided into two orthogonal components which are sinusoidal and exactly in phase, so that the resultant of these components is at a fixed angle in the plane of vibration. For a mixture of plane polarised and unpolarised light, the degree of polarisation is defined as the ratio of the intensity of the plane polarised light and the total intensity.

When the two component beams have a phase difference introduced between them the electric vector traces out an ellipse in both time and position along the wave (See figure 1.21). The ratio b/a of the semi axes is called the ellipticity, and the eccentricity, less commonly referred to is given by $(a^2 - b^2)^{\frac{1}{2}}/a$. If the phase difference is 90° and the two components have equal amplitude, the major and minor axes are the same length and the radiation is described as being circularily polarised.

1.2 Methods of Describing Polarised Light

The most useful form of describing polarised light is by the Stokes Parameters, I, Q, U, V, which are directly related to the signals produced by a device for measuring polarisation.

Consider a beam of light travelling in a fixed direction with a certain frequency. If we choose a plane of reference through the direction of propagation, then $\vec{r}$ is the unit vector along the normal of the plane of reference, and $\vec{l}$ is a unit vector in this plane and perpendicular to the direction of propagation, such that $\vec{r} \times \vec{l}$ is in the direction of propagation (See figure 1.21).

We now consider a simple wave with elliptical polarisation, for which the locus of the E vector is an ellipse.

FIGURE 1.21

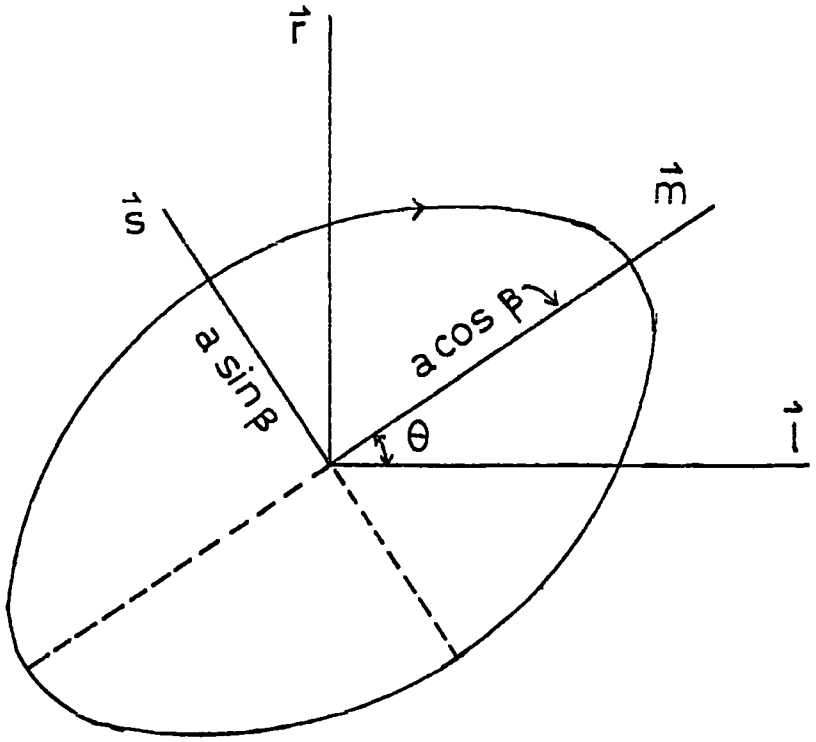

Parameters defining the state of polarisation of a simple (elliptically polarised) wave. The direction of propagation is into the paper.

A geometric representation of this simple wave $\vec{m}$ and $\vec{s}$ being the unit vectors along the major and minor axes of the ellipse respectively, a^2 the intensity of the beam, α the phase angle and $\tan\beta$ the ellipticity, is given by:

$$\vec{E} = a\vec{m}\,\mathrm{Cos}\beta\,\mathrm{Sin}\,(\omega t - kz + \alpha) + a\vec{s}\,\mathrm{Sin}\beta\,\mathrm{Cos}\,(\omega t - kz + \alpha)$$

where E is the transverse electric vector, θ the orientation of the ellipse, k the wave number = $2\pi/\lambda$, z the position along the axis of propagation. The Stokes parameters in this notation are:

$$I = a^2$$

$$Q = a^2\,\mathrm{Cos}\,2\beta\,\mathrm{Cos}\,2\theta$$

$$U = a^2\,\mathrm{Cos}\,2\beta\,\mathrm{Sin}\,2\theta$$

$$V = a^2\,\mathrm{Sin}\,2\beta$$

If $\tan\beta$ is 0 we have linear polarisation, if -1 left handed circular polarisation, and +1 right handed circular polarisation.

The measured intensities of an actual beam of light are a super position of many simple waves with independant phases. Thus the Stokes parameters of the entire beam are:

$$I = \Sigma I_i \qquad U = \Sigma U_i \qquad Q = \Sigma Q_i \qquad V = \Sigma V_i$$

Unless θ and β are the same for all simple waves we have $I^2 > Q^2 + U^2 + V^2$.

If they are the same than the light is completely polarised. If they are not, then the light is partially polarised, except in the case where $Q^2 = U = V = 0$ when the light is unpolarised.

For partially polarised light, where I is the total intensity, and Pe is the degree of polarisation, the degree of linear polarisation P is given by $Pe\mathrm{Cos}2\beta$ and the degree of ellipticity is given by $Pv = Pe\mathrm{Sin}2\beta$.

The intensity of unpolarised light is given by I (1-Pe), and the intensity of elliptically polarised light is IPe = $Q^2 + U^2 + V^2$.

Now $Q = IPe \cos 2\beta \cos 2\theta = IP \cos 2\theta$

$U = IPe \cos 2\beta \sin 2\theta = IP \sin 2\theta$

$V = IPe \sin 2\beta = IPv$

Therefore

$$P = \frac{(Q^2 + U^2)}{I}$$

$$\theta = \tfrac{1}{2} \tan^{-1} (U/Q)$$

1.3 Mechanisms Producing Plane Polarisation

Optical Polarisation has been observed in many astronomical objects. From these observations it is possible to deduce, in many cases, the mechanism responsible for the production of polarisation. Magnetic fields in particular play an important role in the polarising mechanisms, either directly in the emission process, or indirectly by the alignment of scattering particles.

Some of the mechanisms involved in the production of polarisation are listed here:

1. Reflection from solid surfaces, for example the moon and some of the minor planets.
2. Scattering by small particles or grains. This has been observed in the galaxy M82 (Elvius 1963), and more recently by Bingham et al 1975.
3. Scattering by molecules (Rayleigh Scattering), for example, by the molecules in the atmosphere of Venus.
4. Scattering by free electrons (Thompson Scattering) as seen in the solar corona.

5. Zeeman effect, which produces both circular and linear polarisation, found in the emission lines of molecules and neutral hydrogen in the interstellar medium.

6. Synchrotron Emission. This is of the greatest importance in the study of the Crab Nebula and is discussed in detail below.

1.4 Synchrotron Emission

The theory has been well recorded in the literature e.g (Schwinger 1949, Pacholczyk 1970) so a brief outline of the results is shown here.

The Larmour formula (1) gives the total power P radiated by an accelerated electron moving at non-relativistic velocities, p is the momentum, e the electronic charge, m the mass of the electron, c the speed of light.

$$P = \frac{2}{3} \frac{e^2}{m^2 c^3} \left(\frac{dp}{dt}\right)^2 \qquad (1)$$

A generalised form of this equation for an arbitrary electron velocity, since the power must be lorentz invariant is given by:

$$P = \frac{2}{3} \frac{e^2}{m^2 c^3} \gamma^2 \left(\left(\frac{dp}{dt}\right)^2 - \frac{1}{c^2} \left(\frac{de}{dt}\right)^2 \right) \qquad (2)$$

where e is the total energy, $\gamma = \frac{e}{mc^2}$, $p = \gamma mv$

If the particles are moving in a circular trajectory, the momentum changes much more rapidly than the energy change per revolution

therefore: $\frac{dp}{dt} = \omega_{op} \gg \frac{1}{c} \frac{de}{dt}$, so to a good approximation

$$P = \frac{2}{3} \frac{e^2}{m^2 c^3} \gamma^2 \left(\frac{dp}{dt}\right)^2 = \frac{2}{3} e^2 \omega_o \gamma^4 \beta^3 \qquad (3)$$

Where $R = V/2\omega_o$ is the radius of curvature and ω_o the instantaneous angular velocity, $\beta = V/C$. The energy (de) radiated per revolution is then

$$de = \frac{2\pi}{\tau\omega_0} P = \frac{4\pi}{3} \frac{e^2}{R} \gamma^4 \beta^3 \text{ eV} \qquad (4)$$

For relativistic electrons $\beta \sim 1$. The rate of radiation for the same energy proton is a factor of 1/2000 down on that of the electron. Therefore only electrons and positrons are important for the synchrotron mechanism in astronomical sources.

However physically the electrons will not be travelling in circular motion but in arbitrary motions. But for relativistic electrons the arbitrary motion round a field can be reasonably approximated by circular motion. Schwinger (1946) derives an expression for the power radiated in unit solid angle in some direction n, where the instantaneous velocity and acceleration are in the Z and X directions respectively, and the direction of observation is defined by the polar angles θ and ϕ

$$P(n,t) = \frac{e^2}{4\pi m^2 c^3} \dot{p}^2 (1-\beta^2) \frac{1}{(1-\beta\cos\theta)^3} - \frac{(1-\beta^2)\sin^2\theta\cos^2\phi}{(1-\beta\cos\theta)^5}$$

For small electron velocities since $\beta \sim 0$, the angular dependance of the emission goes as $1-\text{Sin}^2\theta\ \text{Cos}^2\phi$. For larger velocities the radiation is emitted increasingly in the forward ($\theta \to 0$) direction in the plane of motion. See figure 1.31.

FIGURE 1.31

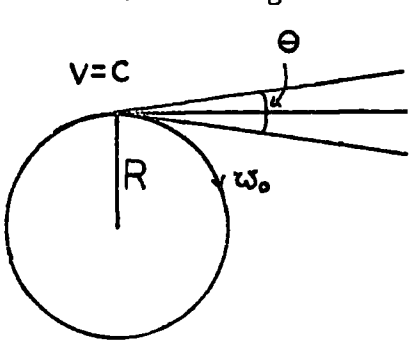

For the relativistic case a measure of the angle of emission is given by $\langle \text{Sin}^2\theta \rangle = 1-\beta^2 = \frac{1}{\gamma^2}$ so that the angle between the electrons direction of motion and its direction of emission is given by

$$\langle \theta^2 \rangle^{\frac{1}{2}} = \frac{1}{\gamma}$$

Since the radiation is confined to a very narrow cone it will sweep past the observer as a pulse of duration $\Delta t' = R/c\gamma$ in its own time. Because of the Doppler shift, the duration will appear to the observer to last for $\Delta t \sim R/c\gamma^3$ (since $\Delta t \sim \Delta t'/\gamma^2$). Since from the uncertainty principle $\Delta\omega\,\Delta t \sim 1$, the spectrum of the pulse will contain frequencies up to a critical frequency $\omega c \sim \omega o\ \gamma^3$, where ωo is the gyrofrequency.

It would seem then that the radiation emitted by a relativistic electron would be polarised primarily in the orbital plane. However this is not the case, because the polarisation depends not only on the orbital orientation but also on the confinement of the radiation to a cone, the size of which is frequency dependant.

The radiation at high frequencies is more nearly 100% linearly polarised than for low frequencies.

In general then, the radiation is elliptically polarised with components nearly in and perpendicular to the orbital plane of the electron.

References

Bingham, R.G. et al (1976) Nature 259 463

Elvius, A. 1963 Lowell Obs Bull 5 281

Pacholczyk, A.G. Radio Astrophysics Chapter 3 p.77 (W.H Freeman and Co San Francisco)

Schwinger, J. (1949) Phys. Rev. 75 1912

Chapter Two. Technique

2.1 The Electronographic Camera

Photographic techniques for observing polarisation of light from astronomical objects have inherent disadvantages. The quantum efficiency is low in most cases, except for IIIa J plates, so they do not make full use of the light from the object, and the density/intensity relation is not linear but logarithmic, making calibration essential to find the relative intensities of points on the plates.

Photoelectric techniques are extremely accurate, very sensitive, but slow since only small areas can be studied at one time. Also the results are in digital form and must await reduction before the final picture emerges.

The obvious next step is to find a device, which produces pictures and has sensitivity approaching that of photoelectric devices. This exists in the form of the electronographic camera.

There are many designs of these e.g Spectracon, Kron Camera, but for these studies the electronographic camera, built at the Royal Greenwich Observatory by Dr. D. McMullan was used.

A diagram of the camera is shown in figure 2.11. The light image is focused on the photocathode, which is a thin layer of a compound of Na-K-Cs -Sb, and is formed on the inside surface of a glass window at the end of the camera.

The photocathode is affected by small amounts of oxygen or water vapour, and so a mica window is introduced between the photocathode and the inserted electronographic film. The enclosure made by the window and film is evacuated by means of an ion appendage pump.

The electrons emitted from the photocathode when it is irradiated by light are accelerated down the camera by means of an electric field produced by electrodes made up of titanium annuli spaced by soda lime glass cylinders 10 mm long.

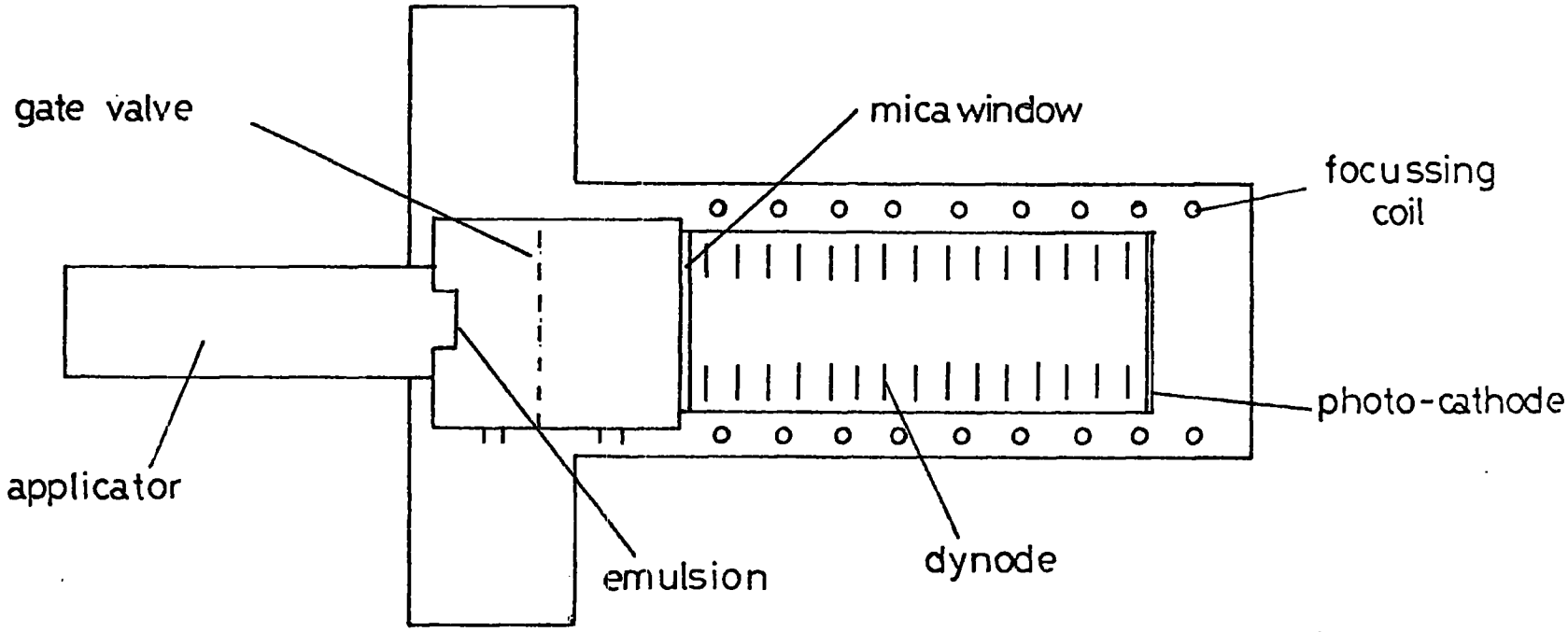

FIGURE 2.11 Schematic diagram of the electronographic camera.

The structure is fused with solder glass and the metal resistors, forming the potential divider, are mounted on the electrode structure.

The electrons are accelerated through 40 kv produced by the electrodes and are constrained to tight spiral paths by a magnetic field produced by an external coil.

The electron image is formed at the mica window, which has the property of transmitting at least 80 per cent of electrons accelerated by 40 kv and is 40 mm in diameter and 4 μ thick.

Against the mica window the electronographic film (nuclear emulsion 10 μ thick, on melinex 50 μ thick). The air pressure on this side of the window is maintained at 1 Torr by a mechanical pump, and the film is mounted in a film holder and brought into contact by a pneumatic activator, through a gate valve which acts as a vacuum lock. The mechanism for loading and unloading the film is automatic.

2.2 Polarimeter Design and Operation

The design of the optical system was based on the ideas of Pickering (1873) and Ohman (1939). They used a doubly refracting prism to produce two adjacent images in orthogonally polarised light. When this system is used electronographically the effect is to reduce large scale positional variations in the sensitivity of the photo-cathode and non-uniformity of development.

A schematic diagram of the polarimeter used (of which full details are given in Axon 1976, Pallister 1976) is shown in figure 2.21 and the properties of the optical components are listed in table 2.2a. Figure 2.22 shows a photograph of the polarimeter.

Light from an astronomical object, passing through the telescope is focused on a series of opaque bars (grids) made of blackened perspex to reduce edge polarisation effects.

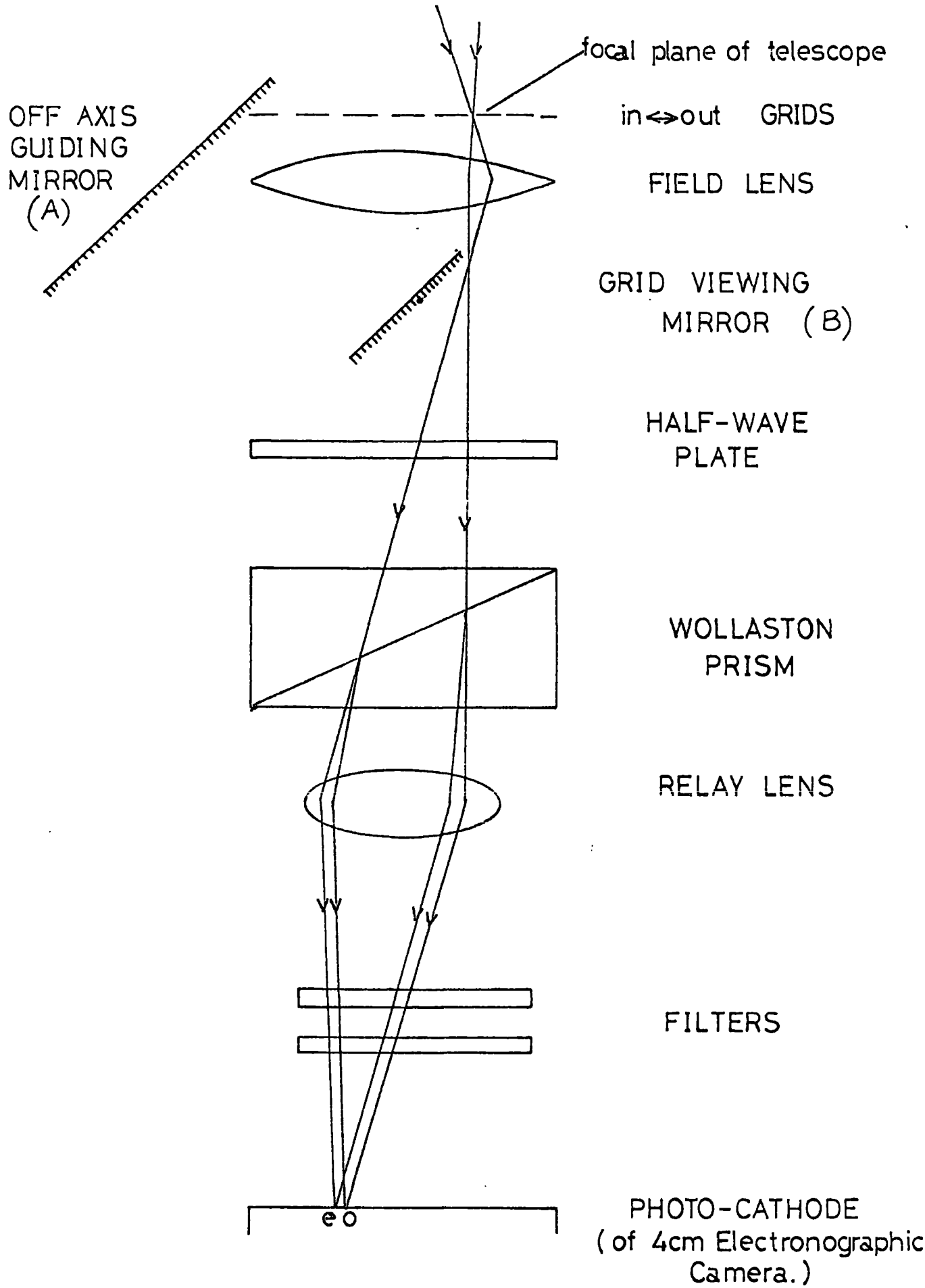

FIGURE 2.21

Schematic diagram of the polarimeter showing passage of light ray.

FIGURE 2.22

THE POLARIMETER

As these grids by necessity block out half the field of view, they are attached to a brass rod, which, when operated externally moves the grid system, transverse to the axis of the polarimeter by exactly one grid spacing. The grid dimensions, 3.2 mm width, are chosen such that the Wollaston prism will produce two adjacent images with a mutual displacement of one grid spacing. A variable diaphragm is incorporated, set at 4 cm diameter for the observations.

All the light is constrained to pass through the optical system by means of a field lens of 20 cm focal length. An achromatic half wave plate is then encountered. In its initial position 0^{o}, its optic axis is aligned north-south. When the half wave plate is rotated through $22\frac{1}{2}^{o}$ the plane of polarisation of the light is rotated through twice this angle, and it is designed to rotate in $22\frac{1}{2}^{o}$ steps.

TABLE 2.2a

Properties of the Optical Components of the Polarimeter

Component	Properties
Field Lens	20 cm focal length. f4 Achromatic doublet
Half-Wave Plate	Magnesium fluoride and quartz. Achromatic in Range 4000 Å - 5000 Å
Filters	Blue glass BG 12 Red-absorbing BG 38
Wollaston Prism	Quartz cemented 4 cm width
Relay Lens	Nikon f1.4, 50 mm Bloomed for all wavelengths
Mirrors	Aluminised perspex
Eyepieces	2 cm focal length orthoscopic

Since the $\lambda/2$ plate is achromatic over the range of 4500 Å ± 500 Å a blue filter BG 12 and a red absorbing filter BG 38 are placed between the grids and the half wave plate to limit the waveband of the incoming light.

The Wollaston prism then produces two adjacent images in orthogonally polarised light. By rotating the half wave plate in steps of $22\frac{1}{2}$ we can obtain electronographs of an object in planes or polarisation of 0° and 90° on one film, 45°, 135°; 90°, 0°; 135° 45°, see figure 2.21. These four electronographs give all the information required to calculate the degree of polarisation and its angle.

To regulate the exposure time of each electronograph taken, an electronic shutter is used which is operated externally.

As the exposure time for plates with the system described so far would be long, a relay lens is included in the system to demagnify the image and focus it on the photocathode of the RGO electronographic camera. It demagnifies 4 x linearily, which means sixteen times in area, therefore the exposure time is reduced by a factor of 16. The lens used is a Nikon f1.4, 50 mm lens bloomed for all wavelengths.

These are the main components of the polarimeter, but two mirrors have been incorporated to aid the method of operation.

The first mirror, the off axis griding mirror A (fig 2.21) is made of aluminised perspex and has an elliptical hole drilled through its centre, of such a size that its circular projection (since it is placed at 45° to the axis of the polarimeter) on the grid system is slightly larger than the aperture of the grids. It is positioned along the polarimeter axis such that its distance to the viewing telescope is the same as the distance from its centre front face to the grids.

Therefore the objects of the axis of the polarimeter can be seen in focus on the illuminated telescope, lens and eyepiece, thus providing a guiding facility.

The second mirror B, again aluminised perspex is mounted such that it can be moved in and out of the field of view of the polarimeter. When the mirror is at 45° to the axis of the system, an image of the field of the polarimeter can be seen through the second viewing telescope, useful both for finding the astronomical objects required and for positioning them so that they lie central on the electronograph.

The whole system is enclosed in a box, with a steel frame and aluminium sides, of approximate dimensions 2 ft long by 1 ft wide by 1 ft 6 ins deep. The controls for the half wave plate and rotatable mirror, the shutter, the focus knob for the relay lens, and the knob for moving the grids, are situated on the side of the casing.

When the electronographs have been completed for one half of the object under view, the grids can be moved to complete the other half without moving the position of the telescope.

Before observations take place, the optics of the system are aligned to lie central on the axis of the polarimeter. If the Wollaston prism is tilted in its holder, the images seen are elliptical, with the major axis of one parallel to the minor axis of its counterpart.

A thin wire, drawn across the grids, when viewed through the relay lens shows if the prism and holder are in square. (See figure 2.23)

FIGURE 2.23

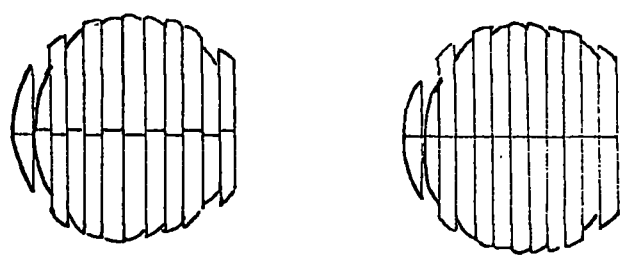

Prism not in square Prism in square

When the prism is not in square the two images of the wire are mutually vertically displaced. The correct position is when the images form a straight line.

The image tube is connected by an aluminium adaptor plate to the polarimeter which is mounted on the telescope in a similar way. The grids are finely focused on the photocathode by adjusting the relay lens position and taking electronographs until the thin wire is sharply in focus.

The telescope is then focused on the grids, using a bright star, viewed via the mirror B. To check that north is at the top of the grids, and that the grids lie north-south, the telescope is moved in declination and the orientation of the polarimeter on the telescope adjusted, until the star appears to move parallel to the grids.

The system is now ready for operation.

2.3 Digitisation of the Plates

The completed, developed, electronographs, were digistised on the Royal Greenwich Observatory's microdensitometer - the PDS machine, with an aperture size of 24 μ x 24 μ, in 26 μ steps, over an area of 512 x 512 pixels. Each pixel corresponds to an area of 1.4 arc secs x 1.4 arc secs.

Since the density/intensity relation for the electronographic film is linear the digital results are directly proportional to the actual intensity of the light from the source, after a small correction has been made for the response of the microdensitometer.

2.4 Reduction of the Data

A series of eight plates of any one astronomical object were taken, four with the grids in the "IN" position and four in the "OUT" position, to obtain information about both halves of the object.

Figure 2.41 shows a diagram of a typical electronograph.

FIGURE 2.41

Diagram showing a sketch of an electronograph with the Wollaston prism removed.(a)

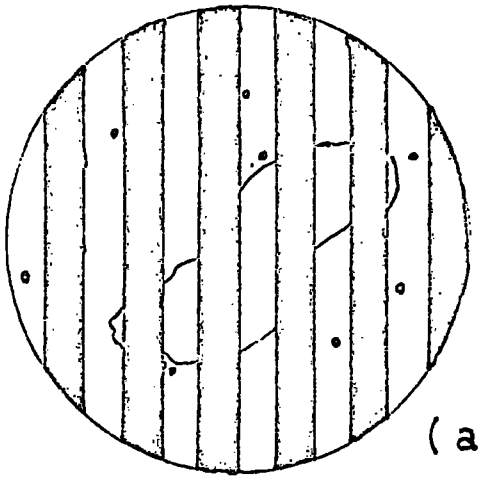

(a)

(b) with the Wollaston prism.

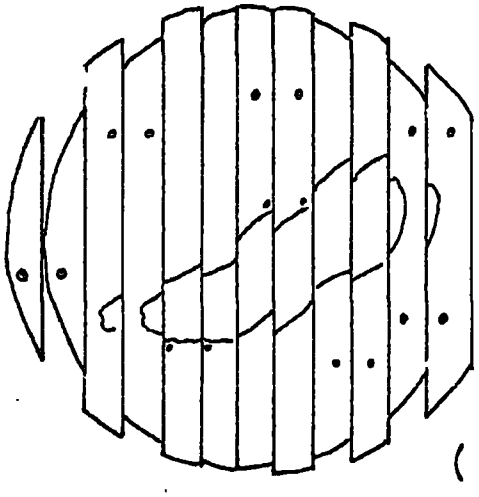

(b)

Our convention is to call the intensity of the left hand strip i1, corresponding to the intensity of the unpolarised component plus the polarised component, component at angle θ, plus the clear plate. Its adjacent strip has intensity i2. Similarily for the other three plates we define i3, i4; i5, i6; i7, i8;

Figure 2.42 shows a partially polarised beam of light passing through the half wave plate at position 0°.

FIGURE 2.42

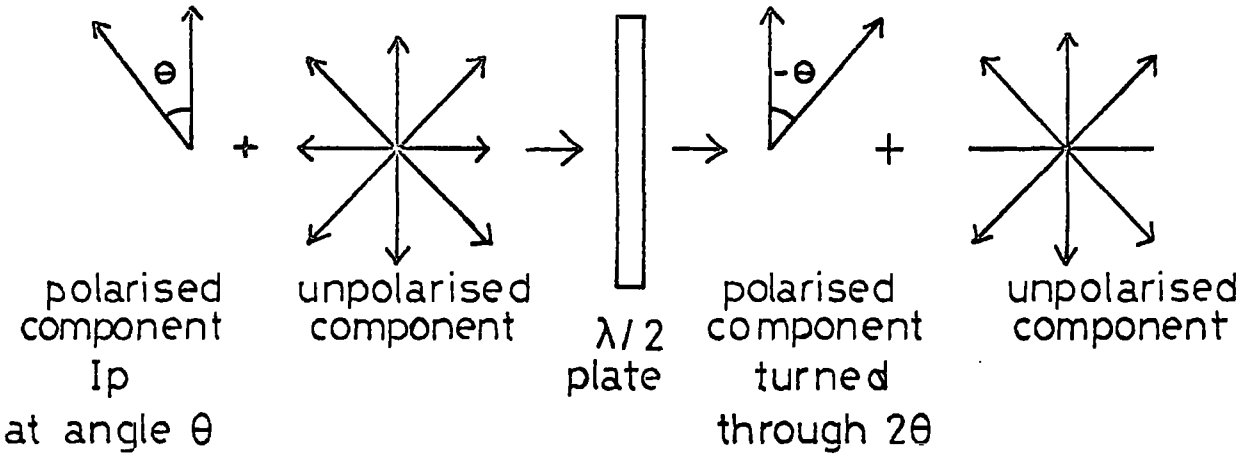

Therefore

$$i1 = \frac{I - Ip + Ip\cos^2(-\theta)}{2} \quad (1)$$

and its orthogonal image

$$i2 = \frac{I - Ip + Ip\cos^2(90-\theta)}{2}$$

$$i2 = \frac{I - Ip + Ip\sin^2(-\theta)}{2} \quad (2)$$

2.4.1 Photocathode Response

The sensitivity of the photocathode is not constant in position. The deviations are small ∓ 5% quoted by the manufacturers. However since we wish to compare exactly the intensity of a point on one strip with its counterpart on the adjacent strip we need to correct for this small variation.

For plate 1, the half wave plate position is 0° and the two adjacent strips are orthogonal. For plate 3, the half wave plate position is 90°. Therefore i1 on plate 1 must correspond to i6 on plate 3, i2 corresponding to i5.

We define a photocathode response factor

$$f1 = \frac{i2\ i6}{i5\ i1}$$

Plates 2 and 4 give another estimate

$$f2 = \frac{i4\ i8}{i3\ i7}$$

Both these estimates should equal 1 if the response is constant. However in practise this is not the case and the restriction on points used is that $|f1-f2| \leq 0.05$. So the f factor used is the average of f1 and f2.

$$f = \frac{f1 + f2}{2} \qquad (3)$$

and strip 2 is normalised to be i2/f

2.4.2 Exposure Factor

As well as checking the checking the correspondance from strip to strip, the total intensity should be constant from plate to plate. Obviously this may not be the case, because the intensity observed depends on the time of exposure and the brightness of the sky which could change over the time taken for all plates to be obtained.

To allow for this we introduce exposure factors e1, e2, e3 to normalise from plate 1 to the other three plates.

Now $i1 = \frac{I-Ip}{2} + Ip\ Cos^2(-\theta)$

$$i2 = f\left(\frac{I-Ip}{2} + Ip\ Sin^2(-\theta)\right)$$

Therefore the total intensity I = i1 + i2/f on plate 1, i3 + i4/f on plate 2, i5 + i6/f on plate 3 and i7 + i8/f on plate 4.

So we define

$$e1 = (i3 + i4/f)/(i1 + i2/f) \qquad (4)$$

$$e2 = (i5 + i6/f)/(i1 + i2/f) \qquad (5)$$

$$e3 = (i7 + i8/f)/(i1 + i2/f) \qquad (6)$$

Our basic equations then become:

$$i1 = \frac{I-Ip}{2} + Ip \cos^2(-\theta) \qquad (7)$$

$$i2 = f\left(\frac{I-Ip}{2} + Ip \sin^2(-\theta)\right) \qquad (8)$$

$$i3 = e1\left(\frac{I-Ip}{2} + Ip \cos^2(45^\circ-\theta)\right) \qquad (9)$$

$$i4 = fe1\left(\frac{I-Ip}{2} + Ip \sin^2(45^\circ-\theta)\right) \qquad (10)$$

$$i5 = e2\left(\frac{I-Ip}{2} + Ip \cos^2(90^\circ-\theta)\right) \qquad (11)$$

$$i6 = fe2\left(\frac{I-Ip}{2} + Ip \sin^2(90^\circ-\theta)\right) \qquad (12)$$

$$i7 = e3\left(\frac{I-Ip}{2} + Ip \cos^2(135^\circ-\theta)\right) \qquad (13)$$

$$i8 = fe3\left(\frac{I-Ip}{2} + Ip \sin^2(135^\circ-\theta)\right) \qquad (14)$$

Knowing the form that the Stokes Parameters take (Sect 1.2) we can derive them from the observational parameters i1-i8 in equations (7) to (10)

$$i1 - i2/f = Ip\left(\cos^2(-\theta) - Ip \sin^2(-\theta)\right) = Ip \cos(-2\theta) = Q1$$

$$\frac{i3-i4/f}{e1} = \left(Ip \cos^2(45-\theta) - Ip \sin^2(45-\theta)\right) = U1$$

The total intensity as before is $I = i1 + i2/f$

Therefore the degree of polarisation P1 is:

$$P1 = \frac{(Q1^2 + U1^2)^{\frac{1}{2}}}{I}$$

at angle $\theta 1 = -\frac{1}{2} \tan^{-1}\left(\frac{U1}{Q1}\right)$

Two more estimates of the Stokes parameters can be made from equations 11-14 Q2 and U2 from which independant estimates P2 and θ2 can be made.

If we take $Q = \frac{Q1 + Q2}{2}$ and $U = \frac{U1 + U2}{2}$

We find the degree of polarisation $P = \frac{(Q^2 + U^2)^{\frac{1}{2}}}{I}$ (15)

at angle $\theta = -\frac{1}{2} \tan^{-1} \left(\frac{U}{Q}\right)$ (16)

2.5 Computer Analysis

A full description of the computer techniques is given by Pallister (Phd Thesis). The data is analysed in stages, with checks to remove any erroneous measurements at various intervals, see flow chart figure 2.43.

Stage I To find the Star Positions

It is important to align the plates to obtain the exact corresponding points on one plate and the others. Firstly the plates are shortened to contain 384 pixels x 384 pixels to reduce storage in the computer. The positions of stars on each plate are found roughly by eye, from a computer printout of the data, and then more accurately by computer.

Stage II To find Plate Transformation Coefficients

Using these star co-ordinates, a minimising routine is used to find the coefficients A, B, C, D, E, F, to transform from one set of co-ordinates X', Y' on plate 2 to the co-ordinates of the same stars X, Y on plate 1, so that

$$X = A + BX' + CY'$$

$$Y = D + EX' + FY'$$

and similarily for X", Y" on plate 3, X"', Y"" on plate 4.

Stage III To Transform the Plates

Plates 2, 3, 4 are then transformed using these coefficients, and the star positions are again found on the transformed plates. These co-ordinates should be the same on all four plates, the acceptable level of difference being to within $\frac{1}{2}$ pixel.

Stage IV To find Strip Comparison Coefficients

Using the same minimising routine as in Stage II, the star co-ordinates on one strip are compared to the star co-ordinates on the adjacent strip, the coefficients are found to establish the relationship of the position of points on one strip to the corresponding points on the adjacent strip.

Stage V To Extract Values of i1 to i8

For each plate the positions on the odd strips are found at distances of 5 pixels apart which would give the best information about the object observed, but avoiding the areas where the strip overlaps appear.

When these positions a computer program is used to add the points in 5 pixel x 5 pixel areas in steps of 5 pixels. Thus producing the values of i1, for all points on the odd strips in integrated areas of 7" x 7". Also the coefficients from Stage IV are used to find the values of i2 for all points corresponding to the odd strips on the even strips.

Stage VI To Find the Clear Plate Levels

A histogram is drawn, from the information on the original 512 x 512 plates to find the intensity of the clear plate. If the distribution is narrow, a constant clear plate level is subtracted from the i1-i8 values. If the distribution is broad, and the residual density down the plate is not constant, a variable background is subtracted, using the values of the clear plate levels from the program used in Stage V, choosing strip positions in areas of clear plate used, thus ensuring that the correct clear plate intensity is removed from each point on the plate.

Stage VII To Find the Stokes Parameters for the Object Plus Sky

Using the i1-i8 values from stage V and incorporating the clear plate subtraction, the f1 and f2 factors are calculated together with the mean value f, the three exposure factors e1, e2, e3, the total intensity I, the three values Q1, Q2, Q and U1, U2, U. From these P1, P2, P and θ1, θ2, θ for all points in the object.

Stage VIII To Find the Stokes Parameters for the Sky

At this stage the output from the previous stage is used both to check the quality of the observations, and to effect the subtraction of the contribution of the sky to the intensity and the polarisation observed.

Various histograms are drawn, to check the distributions of f1, f2, f, e1, e2, e3. If they are narrow distributions, the data is of good quality. The distributions of e factors with both x and y are also drawn and should be well regulated for acceptable data.

The parameters checked for each object included in this thesis, will be described and shown in more detail in the Chapters relating to the analysis of these objects.

Also displayed in histogram form are the Intensity, Q and U distributions for the sky alone. The intensity of the sky is easily distinguishable on the plates, since the objects observed were chosen not to fill the entire field of the electronograph thus leaving a wide area of the plate containing sky only.

Stage IX To Find the Stokes Parameters of the Object

The values of I sky, Q sky, U sky are subtracted from the I, Q, U of all the points on the plates therefore leaving the Stokes Parameters of the objects above from which the degree of polarisation and angle can be found for many points in the object observed.

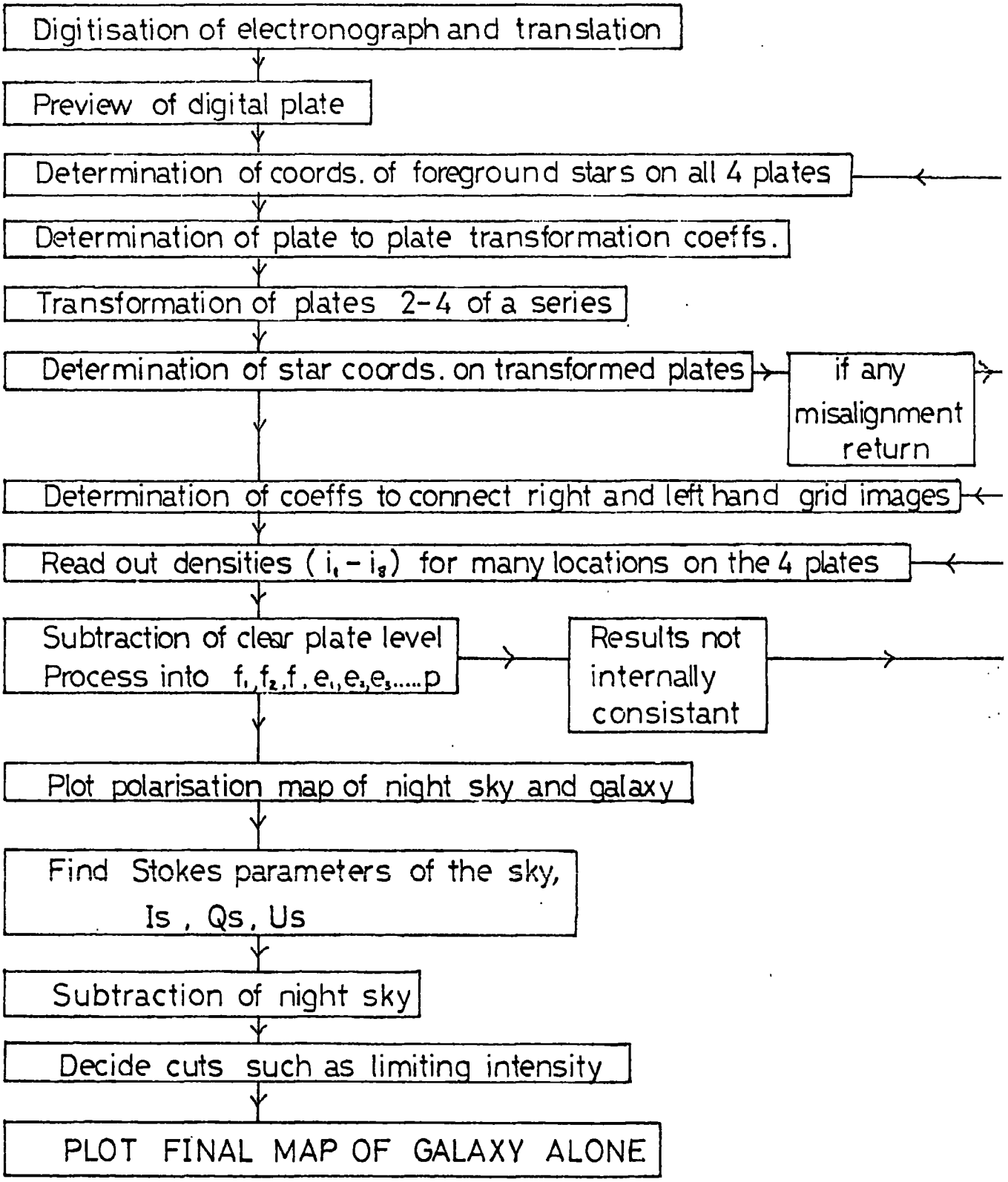

FIGURE 2.43

FLOW CHART OF THE REDUCTION TECNIQUE

2.6 Instrumental Errors

The errors encountered in the observation of the objects involved will be discussed further in the chapters reserved for the description of the analysis of these objects. The instrumental errors alone will be discussed here.

A number of standard polarised stars (whose degree and angle of polarisation are known from the photoelectric measurements), were observed, slightly defocused, on the same observing run, as the objects in this thesis were observed.

Table 2.6a shows the comparison of our results with those from standard reference sources.

TABLE 2.6a Comparison between our measurements and published values for polarised stars. (Mathewson and Ford (1970))

Star	Tabulated value		Our measurements	
	P%	θ°	P%	θ°
HD 43884	2.75 ± 0.05	170 ± 1	2.3 ± 0.4	172 ± 5
HD 122945	0.1 ± 0.07	56 ± 18	0.3 ± 0.4	69 ± 20
HD 155528	4.6 ± 0.09	93 ± 1	4.3 ± 0.4	90 ± 3
HD 80083	0.13 ± 0.09	140 ± 17	1.4 ± 0.4	128 ± 10

As no systematic error in the comparison of these results, and indeed the agreement is extremely good, we can conclude that no instrumental corrections are necessary.

References

Axon, D.J. (1976) Phd Thesis (Durham)

Ohman (1939) MNRAS 13 No 11

Pallister, W.S. (1976) Phd Thesis (Durham)

Pickering, (1873) American Academy of Arts and Sciences Vol IX, 1

Mathewson, D.S. and Ford, V.L. 1970 Mem RAS 74 139-182

Chapter Three The Crab Nebula

3.1 The History of the Nebula

In 1054 AD Chinese and Japanese observers noticed a bright new star in the constellation Taurus, near the tip of one of the horns of the imaginary Bull. It remained visible to the naked eye for 650 days.

Over 700 years later in 1731, English physicist and amateur astronomer John Bevis observed nebulosity in the same position as the bright star had been seen. Messier, in 1758, found it and described it as "being of whitish light and spreading like a flame". He included the nebula in his catalogue as M1.

Lord Rosse, an Irish astronomer, who made the first studies of spiral galaxies with his 60 inch reflector observed this nebulous object in 1844, and so named it the CRAB NEBULA.

This century brought extensive information about the nebula, starting in 1921 when Lampland discovered that the nebula was expanding and noted variability in brightness in patches. Baade in 1942, measured the expansion rate and concluded that it exploded 758±36 years previously.

In 1948 Bolton and Stanley made the first identification of the Crab Nebula as a galactic radio source, and in 1954 the first optical polarisation measurements of M1 were made by Russian Scientists Vashakidze and Dombrovsky, prompted by the prediction that optical polarisation would be observed, from the theory of a synchrotron mechanism of emission for the Crab Nebula by Shlovsky.

Mayer (1957) first measured the radio polarisation of the nebula and in 1963 Bowyer et al, detected a small x-ray source near the nebula.

The discovery of the pulsar NP0532 by Staelin and Reifensten (1968) prompted more extensive research into the properties of the nebula, and in 1969 the pulsar was identified in the optical by Cocke et al. X-ray and γ-ray emission were subsequently detected from the pulsar.

3.2 Present Properties of the Crab Nebula

The Crab Nebula, otherwise known as M1 or NGC 1952 is the remnant of a supernova explosion which took place in 1054 AD. It is situated in the constellation Taurus, about 1° north and slightly west of Zeta Tauri, having RA (1950) $05^h\ 31^m\ 5$ and DEC (1950) + 21° 59'.

The distance from the earth to the nebula is known to be about 2 kpc and its size is 6' x 4' which corresponds to a diameter of 2 or 3 pc.

The lower limit for the mass of the nebula has been estimated from the intensity of HB (Minkowski 1968) to be 1 $M_\odot$. The upper limit is 10 $M_\odot$ (Gott et al 1970) and swept up interstellar matter is thought to account for only a few per cent of the mass of the nebula.

The nebula is expanding, and by extrapolating proper motion measures back in time Baade (1942) found that convergence occurred, not in 1054 A, but 1140 $\mp$ 10 AD. If this result is interpreted as a constant acceleration over the history of the nebula then the acceleration is 0.0014 cm sec^{-1} and the initial expansion velocities are 1700 km sec^{-1} along the major axis and 1100 km sec^{-1} along the minor axis.

The crab nebula, because of its low expansion velocity and irregular shape is not typical of either type I or type II supernovae, it therefore belongs to the 10% of supernovae that make up types III, IV, V of the Zwicky classification.

In the radio frequency range $10^7 < \nu < 2.5\ 10^{"}$ Hz, there is a relatively large power flux available for measurement, the photon flux is in excess of 10^{10} sec^{-1}. In the radio region intensity in the centre is less strongly peaked than in the optical, (Wilson 1972 II) and the emission can be well described as a power law with spectral index α, defined by flux density $\propto$ (frequency)$^{\alpha}$, of -0.26.

In the infrared and optical regions (reviewed by Scargle 1969, 1970) the experimental evidence is vast. In the optical region there is very little disagreement between observers and the spectral index is quoted to be -2.5. The main uncertainty in these measurements lies in the correction for visual obscuration. However if value of Av of 1^m 7 is used, the corrections for visual obscuration as a function of frequency given by Becklin and Neugebauer (1968) yield a fairly smoothed unabsorbed spectrum of index -0.9.

The x-ray source is much smaller than in the optical region. The spectral index for the region $2 \times 10^{17} < \nu < 10^{20}$ Hz is -1.2. Above 10^{20} Hz there are only upper limits to the flux density, the results of the data available having been reviewed by Peterson and Jacobson (1970).

Figure 3.21 shows the electromagnetic spectrum of the total radiation from the Crab Nebula. The thickness of the lines covers the limits of uncertainty at any frequency.

The pulsar NP 0532, discovered by Steilin and Reifenstein (1968), is situated near the centre of the nebula RA (1950) $05^h\ 31^m\ 31^s\ 4$ and DEC (1950) + 21° 58' 54.4". It is one of the youngest pulsars recorded, and has the shortest period 0.033 secs. The flux density, after correction for interstellar absorption, shows a broad maximum in the visible, with a decrease in both the ultraviolet and the red, the latter continuing into the infrared to at least 2 μ (OKE 1969). The ultraviolet and x-ray intensities can fit into this shape, whereas the radio observations show a positive slope at 12 cm. The general effect is that of a two humped energy distribution, with one hump at radio wavelengths, and the other in the visible to x-ray region.

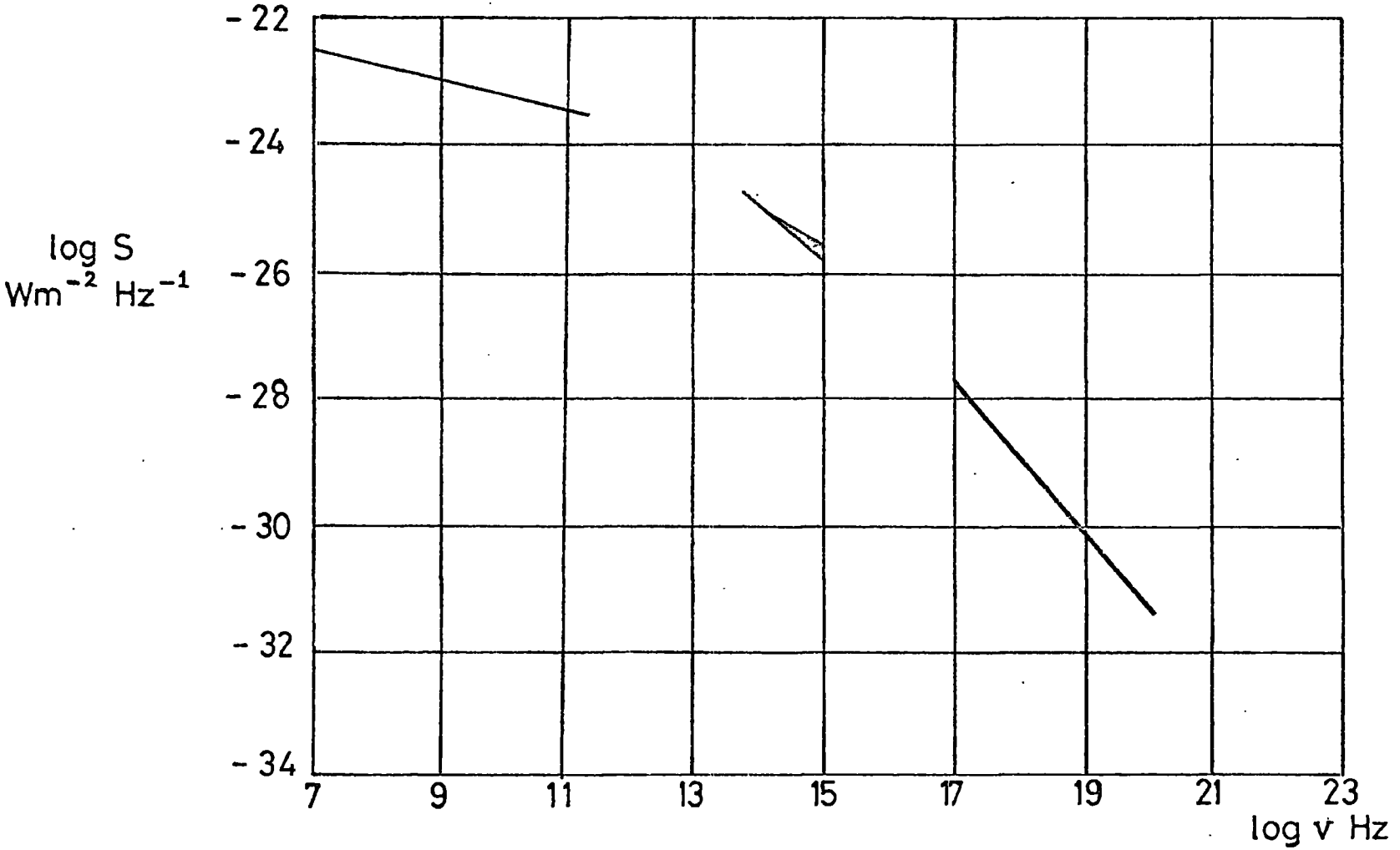

FIGURE 3.21 The electromagnetic spectrum of the Crab Nebula total radiation. The thickness of the lines covers the limits of uncertainty at any frequency.

Reproduced from Baldwin (1970)

3.3 Appearance of the Nebula

The optical emission from the nebula (figure 3.31) consists of two distinct components, line emission and continuum synchrotron emission. The line emitting features, the filaments, are red, due to the predominance of Hα and (NII) emission. The continuum emission is more strongly concentrated in the centre of the nebula, than the filaments, and is also seen in the radio, infrared and x-ray regions of the spectrum.

Continuum Emission

The continuum image is somewhat S shaped, probably related in some way to the electrodynamics of the pulsar. There are noticeable large scale features, a "hole" near the centre of the nebula, two indented bays in the east and west sides of the object, and regions of high and low intensity especially noticeable in the north west region. The continuum image can be resolved into a system of complex fine fibres, reminiscent of a stretched ball of cotton wool. Polarisation data suggests that these fibres are aligned with the magnetic field lines.

The work of Scargle (1969) indicates that the nebula is rather bluer at the centre than at the edges. This is in accord with the difference in the radio and optical spectra where, although the outermost contours in the two regions are approximately the same size the optical emission is more strongly peaked in the centre. The x-ray source is much smaller than the optical continuum, which suggests that the nebula is successively smaller at higher frequencies.

The activity in the continuum emission is concentrated towards the centre of the nebula. The wisp structure (figure 3.32) changes noticeable over a period of a few months to a year. The thin wisp nearest the pulsar (the south proceeding of the two 16th magnitude stars near the centre of the nebula) comes and goes as well as changing shape and position.

FIGURE 3.31

Photograph of the Crab Nebula taken in the red (6300Å - 6750Å)

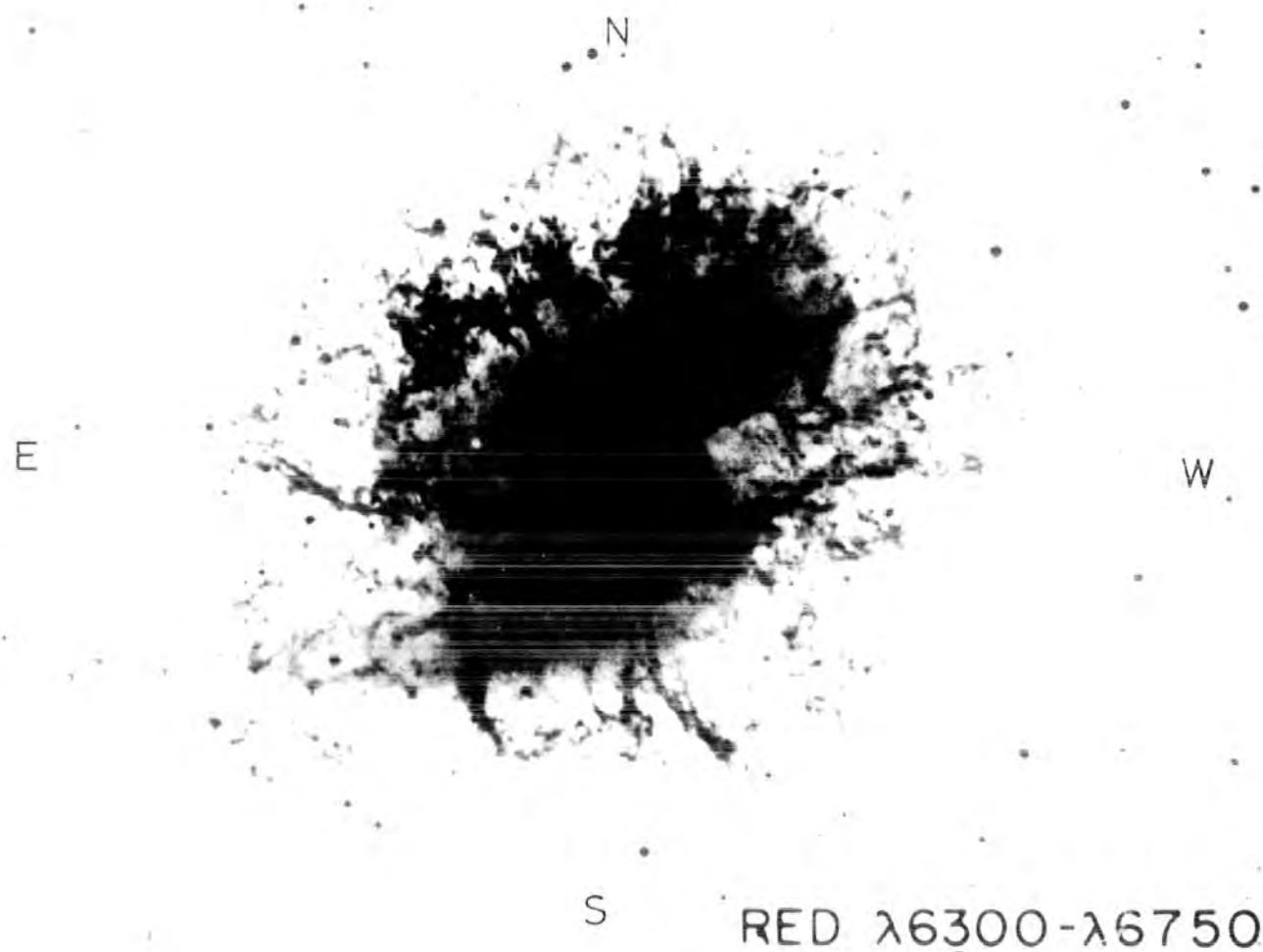

FIGURE 3.32

Drawing of the characteristic configuration of the central region of the Crab Nebula.

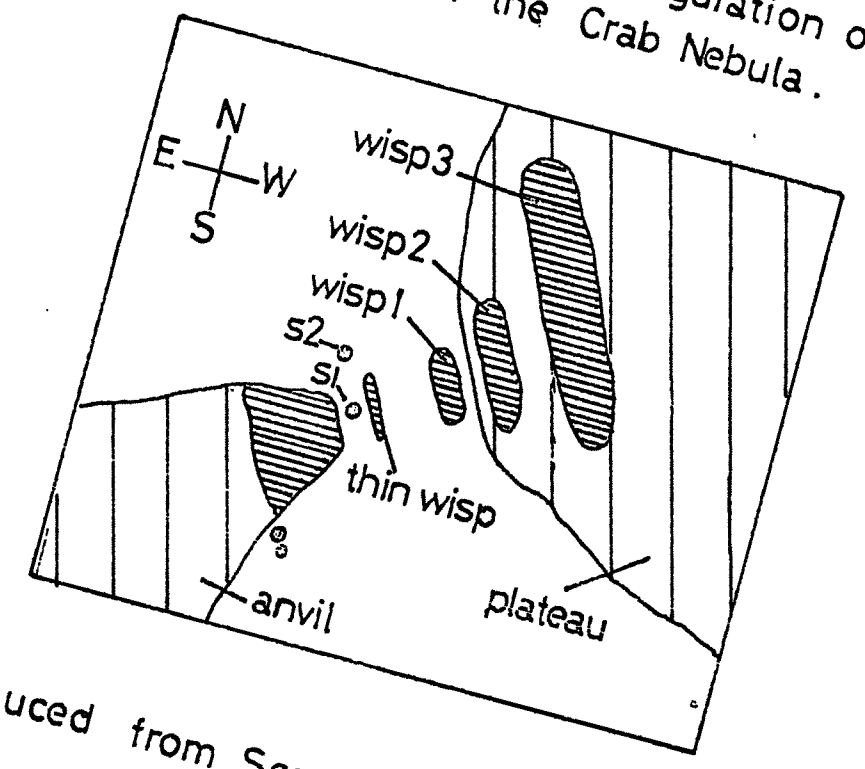

Reproduced from Scargle (1969)

The Line Emission

The line emission is concentrated in a filamentary structure, irregularily distributed. The main contribution comes from Hα and (NII) emission. Other strong lines are (SII), (OIII), (OII), (OI), HeI + II, (NeIII) and hydrogen. The emission comes from gas at densities of the order of 10^3 cm^{-3}, at temperatures around 10^4 °K.

Some information about the three dimensional structure of the filaments can be extracted from the radial velocity measurements, assuming that the velocity is proportional to distance from the centre of the nebula along the line of sight, as it is in the plane of the sky. The radial velocity data, by Trimble (1968) suggests that the line emitting material is in discontinuous clumps. There is no evidence that the filaments lie in a thin shell around the nebula. Only a few faint filaments are found in the centre of the nebula, but about half the features measured lie less than two thirds of the distance from the centre to the outer surface of the nebula, and some of the strongly emitting features extend approximately radially outward in the outer half of the object.

Comparison of the line emission photographs taken ten years apart, show that the nebula is expanding on a time scale, of the order of the age of the nebula, and from a centre within 10" of the pulsar.

3.4 Optical Polarisation Studies of the Crab Nebula

The first observations of the optical linear polarisation of the CRAB NEBULA were made by Vashakidze and Dombrovsky (1954). Subsequently, more detailed results were obtained photoelectrically by Walraven (1957), superceded only by the more extensive photographic measurements of Woltjer (1957).

The photoelectric measurements of Walraven took place in the winter of 1956 on the 80 inch reflector of the Observatoire de Haute Provence. The optical linear polarisation as measured for some 300 points in the nebula, with a diaphragm of diameter 18 arc seconds and without a colour filter. The results of these observations are shown in figure (3.41). At the same time, observations through colour filters showed that the bright central parts of the nebula have colour index B-V = 0.82 in the Johnson-Morgan system.

In the autumn of 1955 Baade took a series of plates through a polaroid filter on the 200 inch telescope at Mount Palomar. The orientations of the polaroid were 0°, 45°, 90°, 135°, with respect to the north. All plates were taken in the wavelength region 5200 Å to 6200 Å, so the contribution from the filaments was small. The plates were analysed by Woltjer (1957), measurements being taken every half a millimetre on the plate in both directions with a diaphragm of 0.47 mm in diameter, corresponding to 5 seconds of arc.

Measurements of the degree and angle of polarisation were obtained for over 1000 points in the nebula, and the results are shown in figure 3.42.

The net optical polarisation of the entire nebula is about 9.2% in position angle 159.6° (Oort and Walraven 1956). Woltjer pointed out that the interstellar polarisation toward the nebula was at approximately the same position angle so that about 2% must be subtracted from the observed integrated polarisation to get the intrinsic synchrotron polarisation.

The photographs of Baade, taken at successive orientations of the polaroid pick out regions where the local projected magnetic field is perpendicular to the transmission direction, from which it seems that the fibres, seen clearly in the north east region of the nebula, trace the magnetic field lines.

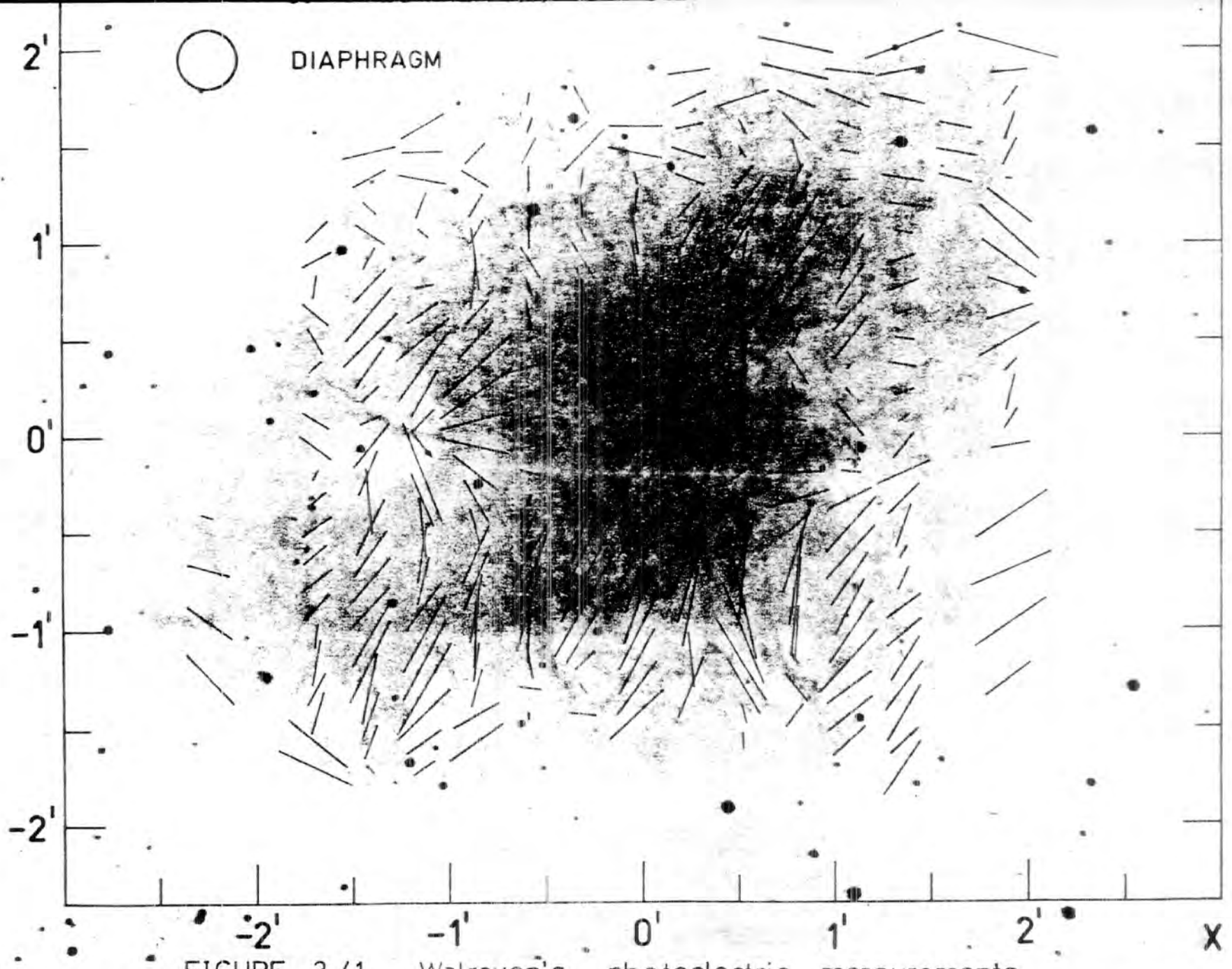

FIGURE . 3.41 Walraven's photoelectric measurements of the optical linear polarisation of the Crab Nebula.

From Walraven (1957)

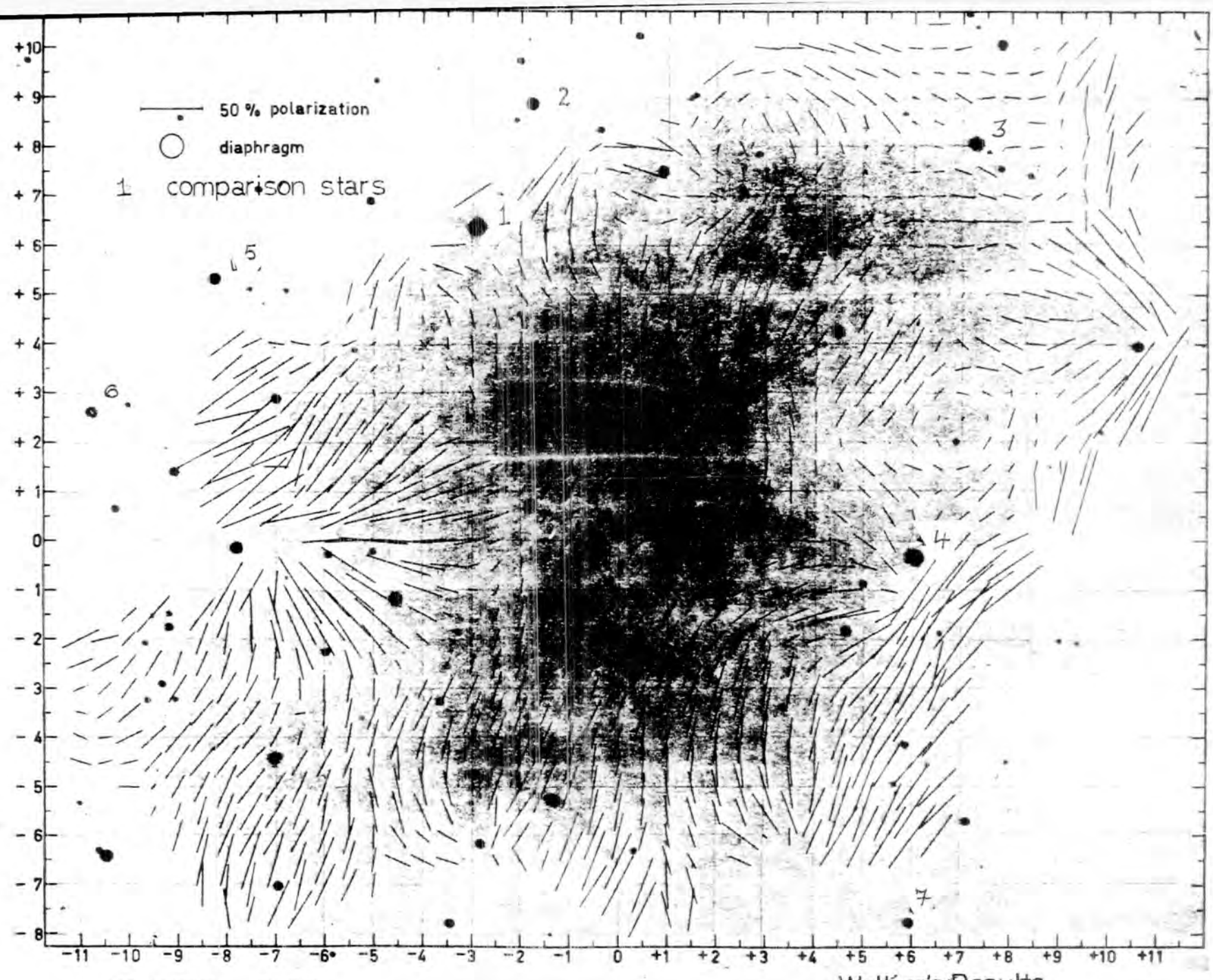

FIGURE 3.42

Polarizations in the Crab Nebula, measured photographically

Woltjer's map shows a rather uniform pattern over the central region of the nebula, the magnitude and direction of the polarisation changing on a scale of the same dimensions as the nebula itself, although in this region we see a projection average, as we look through the total thickness of the nebula. However the general pattern suggests that the field here is smooth and simple, typical polarisation values being 20%.

In the outer regions the loops, shown on Baade's plates, have linear polarisation value higher than this, of the order of 30% - 40% as would be expected, since in the outer regions we are looking through less volume of the nebula.

Woltjer (1958) suggests that the general polarisation pattern is related to the gaseous filaments, in that the magnetic field lines circle round the filaments, however some features, notably the fan like structure on the eastern edge of the nebula, centred on the dark bay in this region, seem more closely related to the continuum than the filamentary structure.

3.5 Optical Linear Polarisation of the Crab Nebula Pulsar

One interesting problem, which has yet to be resolved, is the relationship between the optical linear polarisation of the Crab nebula pulsar with that of the nebula itself.

The total integrated polarisation of the main pulse of the pulsar, NP 0532, has been measured by many authors (Kristian et al 1970, Cocke et al 1970, Wampler et al 1969). The agreement between the results quoted by these authors is good, the values of degree of linear polarisation and angle, uncorrected for interstellar polarisation being $P = 6.8 \mp 0.5\%$, $\theta = 98° \mp 3°$ (Kristian et al); $P = 6.5 \mp 0.5\%$, $\theta = 96° \mp 2°$, (Cocke et al); $P = 6.5 \mp 0.9\%$, $\theta = 107° \mp 6°$ (Wampler et al).

Cocke also presents the same result corrected for interstellar polarisation as P = 7.2∓0.5% at angle 88°∓2°.

All authors agree that, in general, the polarisation is high, of the order of 20%, in the wings of both the main and subpulse, but falls to near zero near the pulse centres (See figure 3.51), and the polarisation vector sweeps through a large angle, approximately 140°, for the duration of the pulse.

The differences in the measurement occur in the details of the individual polarisation measurements for the measured points in the pulses. These variations in results cause the interpretation of the nebula/pulsar relationship to be unresolved.

Cocke et al find that within about 0.2 pc of the pulsar, the optical polarisation of the nebula varies between 10 and 25 percent but with consistent position angle close to 140°. No simple relationship can be deduced from this between the nebula and pulsar optical polarisation, since the integrated main and secondary pulses are polarised at about 90°. The intensity peaks are polarised at 110° (main) and 95° (secondary) whereas at the polarisation troughs the angles are 122° (main) and 160° (secondary). The mean of these last two angles is near 140°, but Cocke et al, conclude that it is difficult, without a detailed emission model, to know what significance to attach to this coincidence.

On the other hand Kristian et al propose the following model: They assume that for each of the two pulses there is a unit vector $\vec{p}$, fixed in and rotating with the pulsar, such that the apparent direction of the electric vector θ, at any instant is parallel or perpendicular to the projection of $\vec{p}$ on the plane of the sky.

FIGURE 3.51

Average time changes of linear polarisation within the main and sub-pulses.
The zero of time is taken to be the peak of main pulse.

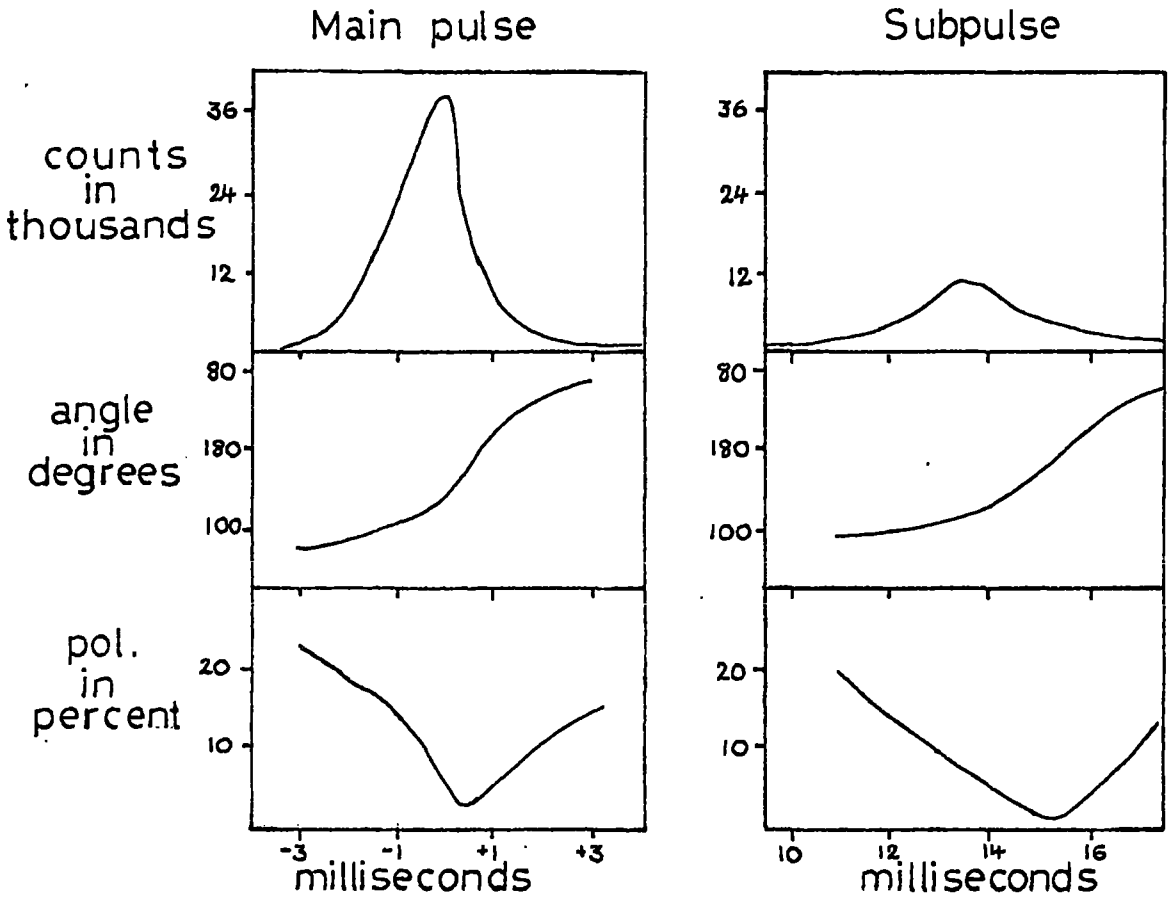

Reproduced from Kristian et al.(1970)

It is assumed that $\vec{p}$ is associated with a single fixed longitude (in pulse-centred co-ordinates), but not with a single latitude, such that if the emission pattern is a fan beam, $\vec{p}$ will be determined by an average of the emission properties of the beam in latitude.

The variation of θ is given by the following formula

$$\text{Cot } \theta = \frac{\tan \beta \text{ Cos } b - \text{Cos } (\omega t + e) \text{ Sin } b}{\text{Sin } (\omega t + e)}$$

where ω is the rotation frequency, b the latitude of the observer with respect to the pulsar, β the angle between $\vec{p}$ and the equator of the pulsar, and e is the angle between the projection of $\vec{p}$ on the pulsars equator and the meridian plane of the longitude associated with $\vec{p}$. If $(Pz, P_\rho, P\phi)$ are the cylindrical co-ordinates of $\vec{p}$ in a frame rotating with the pulsar then

$$\tan \beta = \frac{Pz}{(P\rho^2 + P\phi^2)^{\frac{1}{2}}} \quad \text{and} \quad \tan (\omega t + e) = \frac{P\rho}{P\phi}$$

The phase is chosen so that at t = o, the observer is at the longitude associated with $\vec{p}$.

Kristian's observation that there is a sweep of the polarisation vector of 150° during only 60° of the pulsars rotation, together with the details of the pulse polarisation places the following restriction on the values of b and β.

(i) That β cannot be more than 25°

(ii) That b must be within 10° of β

so the rotation axis of the pulsar must be within 35° of the plane of the sky.

In the model the change of θ with time will show an inversion symmetry about the moment $\omega t + e = 0$, when $\vec{p}$ lies in the plane defined by the rotation axis and the direction of the observer, at which time the direction θ will be either parallel or orthogonal to the projection of the rotation axis on the plane of the sky. The symmetry is observed in both pulses, occurring at the polarisation minimum (figure 3.51).

The observed direction of θ at the centre of symmetry is 160°∓70, which agrees well with the angle of polarisation in the nebula of 159°∓2° found by Kristian et al.

Kristian concludes then that the pulsar's rotation axis is either orthogonal to or parallel to the general magnetic field in the immediate vicinity of the pulsar.

Of interest too, is the comparison of the optical and radio polarisation observations of the pulsar. The results of radio observations at 430 MHZ (Campbell et al 1970) show that the main pulse is about 18% polarised during its rise and peak, and more strongly polarised during the decay, together with no detectable rotation of angle within the main pulse.

One would expect from the simultaneity of pulse arrival times in radio and optical wavelengths (Conklin et al 1969) and the general correspondance of intensity profiles, that the radio and optical pulses of the pulsar NP0532 are closely related. However the difference in detail of the polarisation profiles for the two wavelength bands, together with large intensity changes in the radio profiles (Heiles et al 1970), point to the conclusion that the emission mechanisms for the optical and radio radiation are different.

3.6 The Synchrotron Nature of the Radiation from the Crab Nebula

It is now universally believed that the continuum radiation from the Crab nebula is of synchrotron nature. It is interesting, therefore, to compare some of the results of the observations of the nebula with the theoretical predictions. The standard theory of synchrotron radiation from relativistic electrons in a uniform field gives a value of the degree of linear polarisation to be $P = \frac{\gamma + 1}{\gamma + 7/3}$ where γ is the spectral index of the electrons (Pacholczyk 1970).

Taking the value of the spectral index in the optical region to be γ = 2.5 (Section 3.2) the expected value of the degree of polarisation is approximately 70%.

In the central region of the nebula, where the alignment of the polarisation vectors implies that the field is fairly uniform, the average value of the degree of polarisation is 20% (Woltjer 1957), which is considerably lower than the expected value of 70%. However, projection effects must be allowed for, since in this region we are looking through the total thickness of the nebula, therefore seeing several looped lines of force crossed, in projection. In some areas in the outer regions of the nebula values approaching 70% have been measured, which indicate that here we are seeing just a single looped line of force.

At present, the magnetic energy of the nebula is so large that the nebula cannot have expanded isotropically with the field frozen in (Woltjer 1971), if the usual theory of synchrotron radiation of the nebula is correct. This prompted Gunn and Ostriker (1971) to propose a synchro-compton model for the radiation, where the electrons are confined to an area filled with 30 Hz electromagnetic waves generated by the rotating pulsar. Rees (1971) extended this proposal to predict that significant circular polarisation should be present. Martin, Illing and Angel (1972) have detected circular polarisation of order 0.2%, which is too small to fit the "synchro-Compton" model. This model has now been abandoned.

Several authors have attempted to account for the large magnetic flux, by the lines of force being continually stretched by winding round the supernova remnant, and carried outward by a flux, wrapping them round the outer filaments (Wilson 1972).

References

Baade, W. (1942) Ap. J 96 109

Beckin, E.E and Neugebauer, G. (1968) Ap. J 151 145

Campbell, D.B, Heiles, C, and Rankin, J.M (1970) Nature 225 527

Cocke, W.J, Disney, M.J, Muncaster, G.W (1970) Nature 227 1327

Conklin, W.J, Howard, H.T, Miller, J.S and Wampler, E.J (1969) Nature 222 552

Gunn, J.E and Ostriker, J.P (1971) Ap. J 165 523

Heiles, C and Rankin, J.M (1970) IAU Symposium No 46 p 103

Kristian, J, Visvanathan, N, Westphal, J.A and Snellen, G.H (1970) Ap J 162 475

Martin, P.G, Illing, R, Angel, J.R.P, (1971) Nature 230 103

Minkowski, R (1968) Nebula and Interstellar matter Univ of Chicago Press

Oke, J.B (1969) Ap. J Letts 156 L49

Oort, J.H and Walraven, T. (1956) BAIN 12 285

Pacholczyk, A.G (1970) Radio Astrophysics (Pubs. Freeman & Co San Francisco)

Peterson, L.E and Jacobson, A.S (1970) PASP 82 412

Rees, M.J (1971) The Crab Nebula IAU Symposium No 46 p 407

Scargle, J.D. (1969) Ap. J 156 401

Scargle, J.D and Harlan, E.A (1970) Ap. J 159 L143

Staelin, D.H, Reifenstein, E.C (1968) Science 162 1481

Trimble, V (1968) Astron J. 73 535

Walraven, T (1957) BAIN 13 293

Wilson, A.S (1972 II) MNRAS 160 355

Wilson, A.S (1972 III) MNRAS 160 373

Woltjer, L. (1957) BAIN 13 301

Woltjer, L. (1958) BAIN 14 39

Woltjer, L. (1971) IAU Symposium No 46 p 389

Chapter Four. Present Observations of the Optical Linear Polarisation of the Crab Nebula

4.1 Introduction

The ideal position in the sky of the Crab Nebula together with its size (4 x 2 arc mins) has made the nebula one of the most extensively studied of the extended astronomical objects, not least in the field of optical linear polarisation measurements. The great wealth of observational evidence in this field makes the Crab Nebula an ideal subject to study with the nebular polarimeter described in Chapter Two of this thesis, both to use the results to check the performance of the polarimeter against previous measurements, and, hopefully to augment the information already known about the optical linear polarisation of the nebula. Accordingly, in the spring of 1975, a series of eight plates, with varying positions of the half wave plate, were taken of the Crab Nebula, in the wavelength region 4000 Å - 5000 Å, on the 1 metre telescope of the Wise Observatory, Tel Aviv University Israel. These eight plates, in two series of four plates, one for each half of the nebula, gave full information to extract the degree and angle of polarisation for over 1000 points in the Crab Nebula.

4.2 Technique

The technique used to reduce the data, from the original electronograph form to the obtainment of the Stokes parameters, to describe the degree and angle of polarisation of radiation from the Crab nebula, was in essence that described in Chapter Two, with some important amendments.

The four electronographs for one half of the nebula gave intensities i1 - i8 corresponding to components 0°, 90°; 45°, 135°; 90°, 0°; 135°, 45°; of the radiation measured from the north, called plates 1, 2, 3, 4 respectively.

FIGURE 4.31

FLOW DIAGRAM OF THE THREE PLATE ANALYSIS .

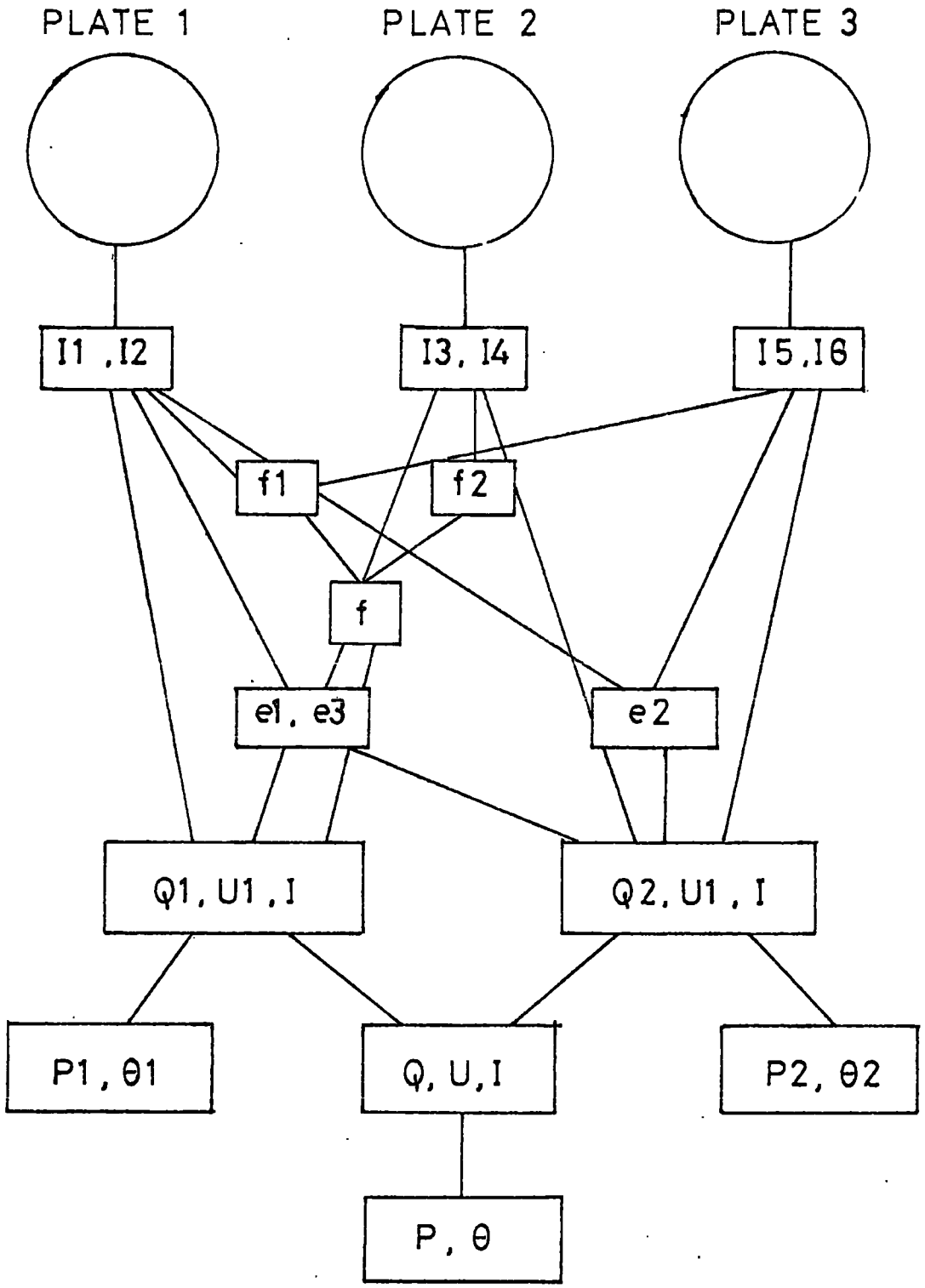

However, when histograms were drawn to find the residual density level of the clear plate on each of the four plates, it was found that on one of the plates, Plate 4, the residual density distribution was disturbingly broad. On careful examination of this plate it became obvious that the plate was fogged over half its area, therefore rendering it useless for analysis. Unfortunately the same appeared to be the case for one of the plates for the other half of the nebula. Therefore the technique had to be altered to obtain the most information from the remaining plates.

4.3 The Three Plate Analysis

The three remaining plates, for one half of the nebula, gave intensity values i1 - i6 for components of the radiation 0°, 90°; 45° 135°, 90°, 0°. It was possible, then, to obtain only one estimate of the photocathode response $f1 = \frac{i2\ i6}{i5\ i1}$ and subsequently one set of estimates of the Stokes parameters. However if the second plate was used twice, in place of the fogged plate 4, two estimates, albeit not wholly independant, of the Stokes parameter could be obtained, therefore using all the available information from the three good plates.

The procedure adopted is shown in diagramatic form in figure 4.31, and described below.

Photocathode Response

One estimate of the photocathode response factor $f1 = \frac{i2\ i6}{i5\ i1}$ from plates 1 and 3 was determined in the usual way (Section 2.41) and a histogram showing the f1 distribution is shown in figure 4.32. The other estimate $f2 = \frac{i4\ i8}{i3\ i7}$, since i7, i8 from plate 4 were replaced by i4, i3 on plate 2, was set to 1, for all points on the plate.

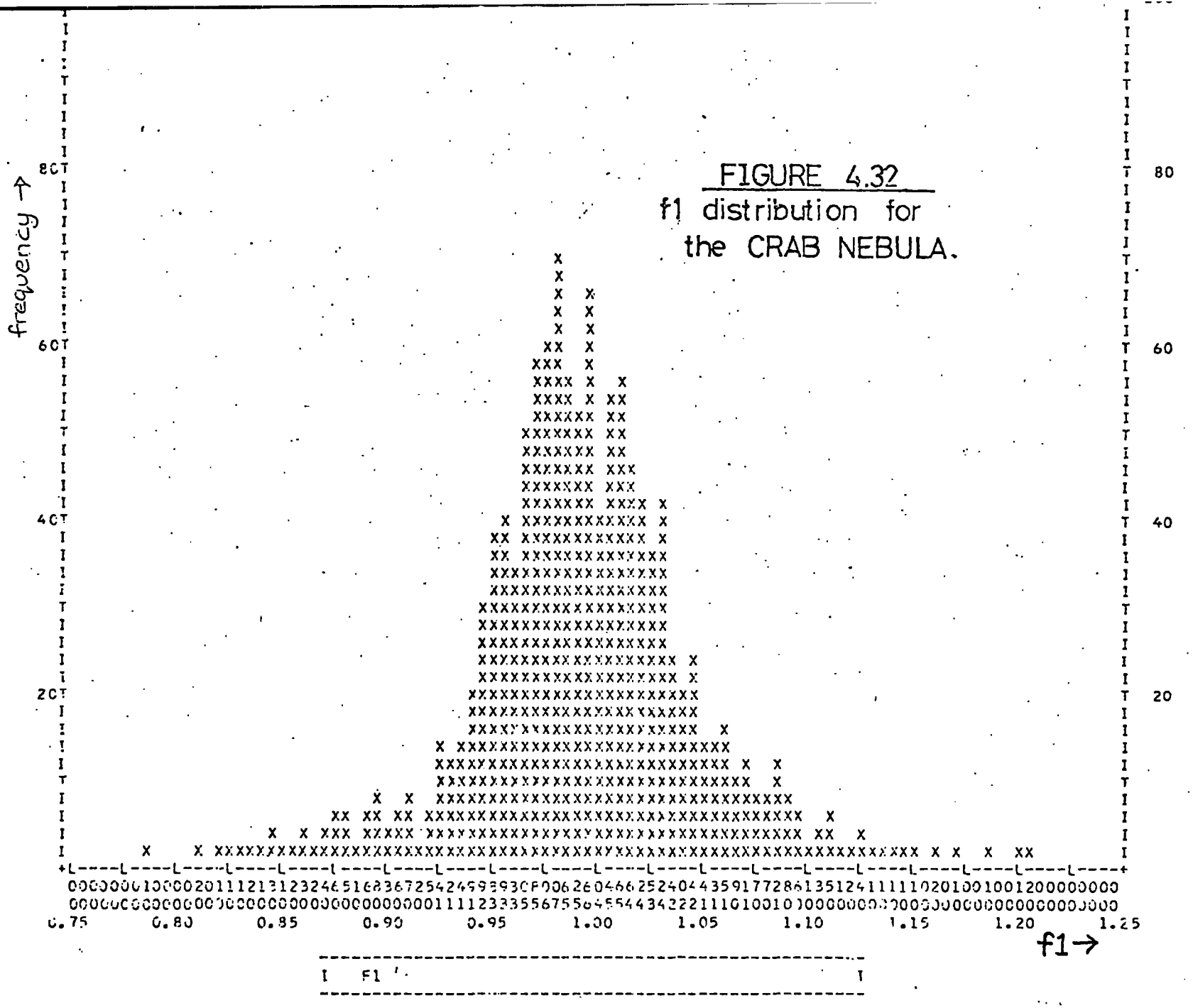

FIGURE 4.32
f1 distribution for the CRAB NEBULA.

The photocathode response factor f used, was then the average of these f = (f1 + f2)/2.

Exposure Factors e1, e2, e3

The values of e1, e2, that is the exposure factors normalising the intensity from plate 1, to the intensities of plates 2 and 3 were calculated from the measured values of i1 - i6 that is e1 = (i3 + i4/f)/(i1 + i2/f), and e2 = (i5 + i6/f)/(i1 + i2/f) and since plate 2 replaced plate 4, the exposure factor e3 was set to equal e1 for all points. A check on whether the clear plate level had been removed correctly was made by plotting the value of the exposure factor against the position from north to south down the plate. Figures 4.33 and 4.34 show these distributions for e1 and e2 respectively. A variable level for the clear plate was removed and the figures 4.33, 4.34 indicate that the correct clear plate level was removed.

Stoke's Parameter I

The intensity value I = i1 + i2/f, was calculated from the first plate and since the intensities of the other plates were normalised to that of the first plate, by the exposure factors, the intensity, I, was calculated in the same way as for the four plate analysis. Figure 4.35 shows the intensity distribution of all points on the plate, the first peak giving the intensity level of the sky on the plate.

Stoke's Parameter Q

The two estimates of Q, Q1 = i1 - i2/f and Q2 = (i6/f - i5)/e2 remained unaltered by using only three plates. The Q factor for the sky alone was determined from a histogram of Q values for the intensity level of the sky, and shown in figure 4.36.

Stoke's Parameter U

Since U1 = (i3 - i4/f)/e1, U2 = (i8/f - i7)/e3, the two estimates U1, U2 were the same value, as plate 2 replaced plate 4.

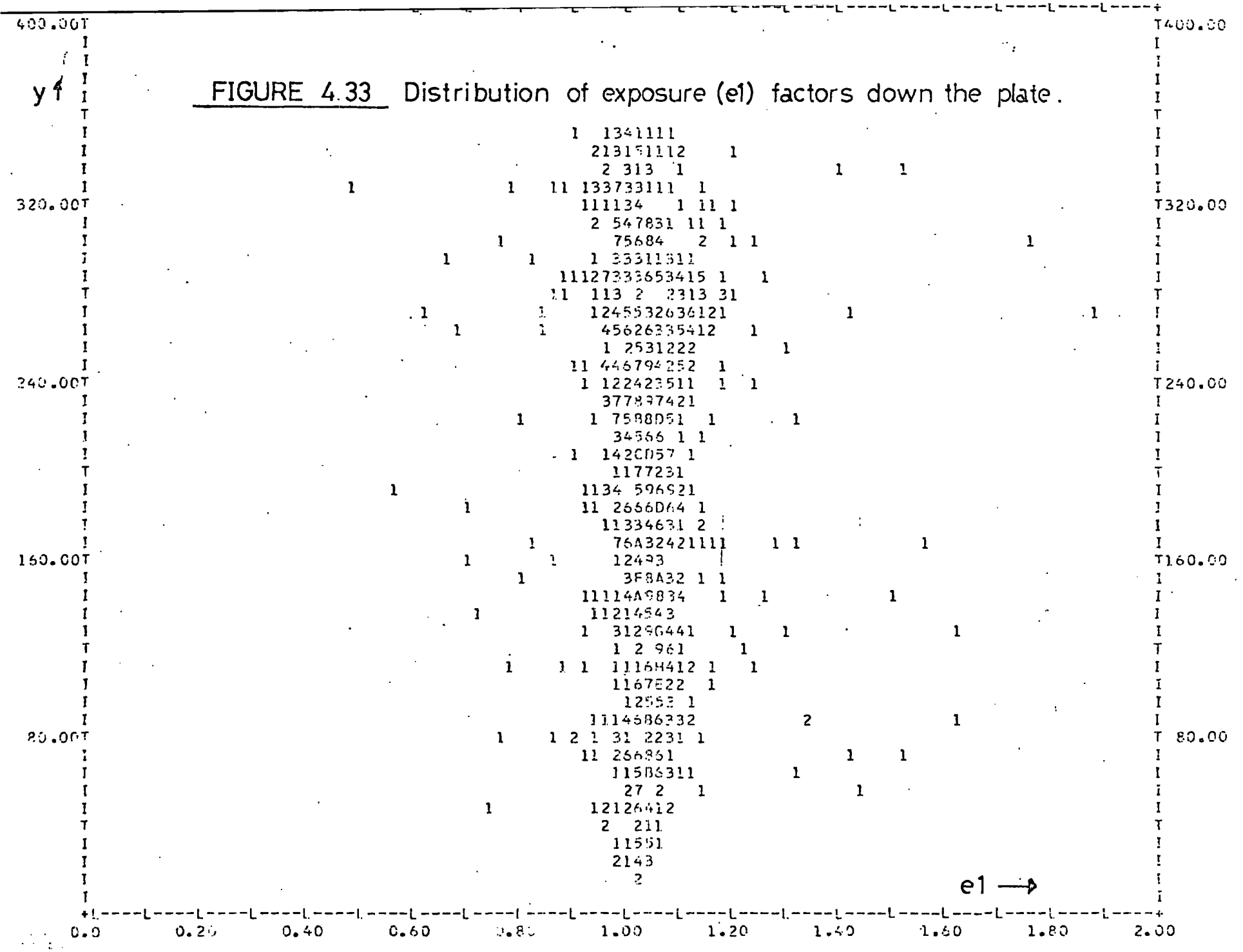

FIGURE 4.33 Distribution of exposure (e1) factors down the plate.

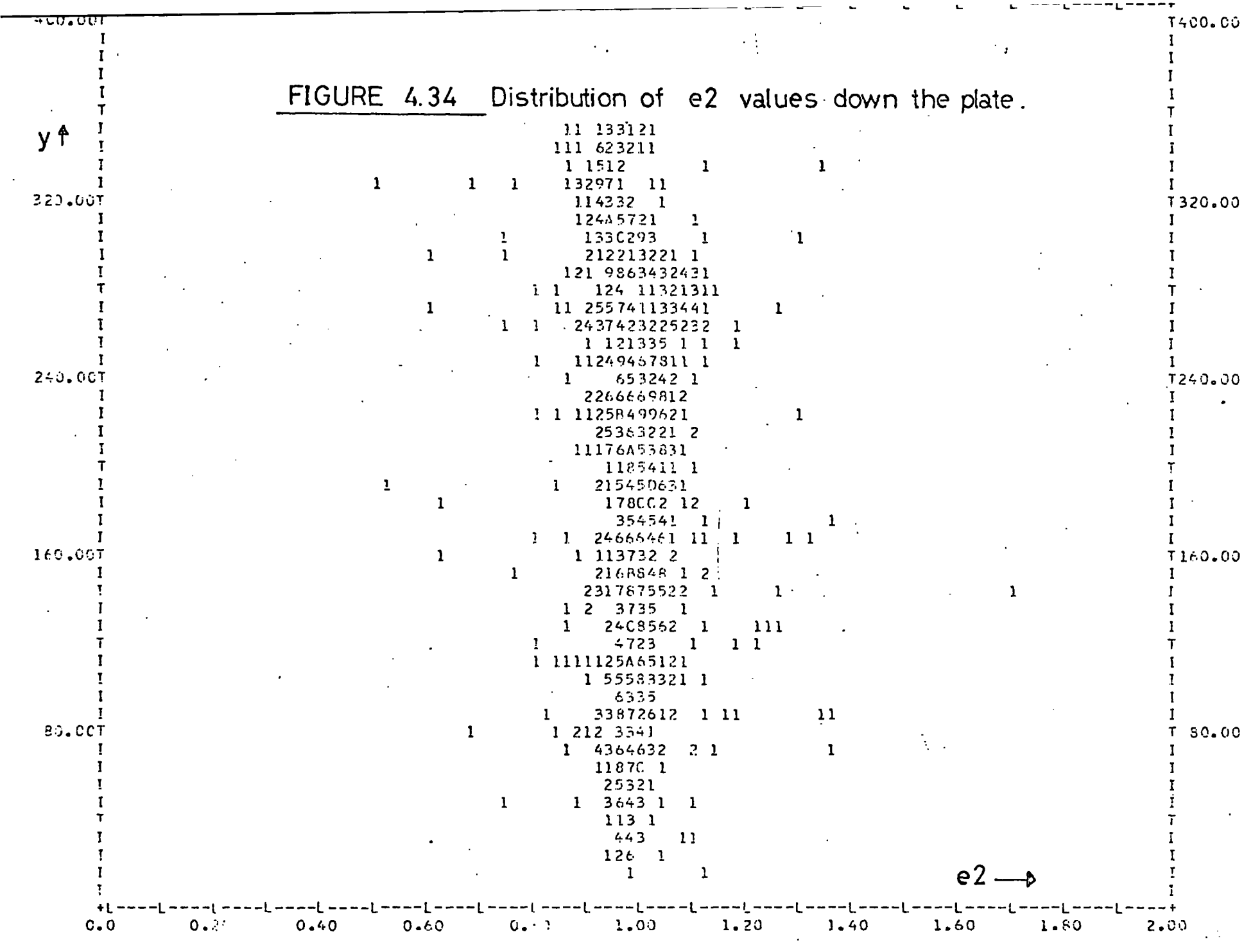
FIGURE 4.34 Distribution of e2 values down the plate.
y
e2
400.00
320.00
240.00
160.00
80.00
0.0
0.40
0.60
1.00
1.20
1.40
1.60
1.80
2.00

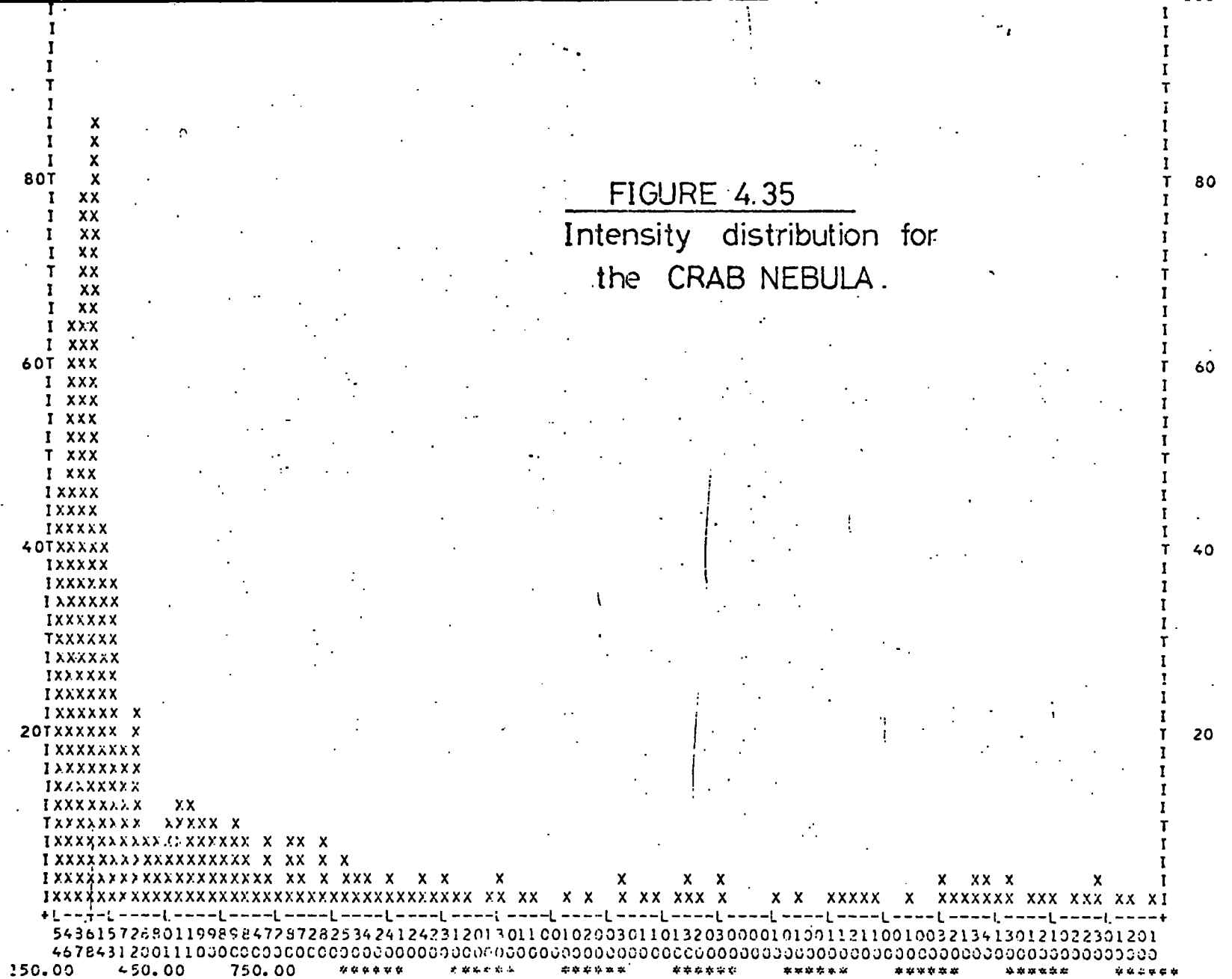

FIGURE 4.35

Intensity distribution for the CRAB NEBULA.

PLOT NUMBER 6

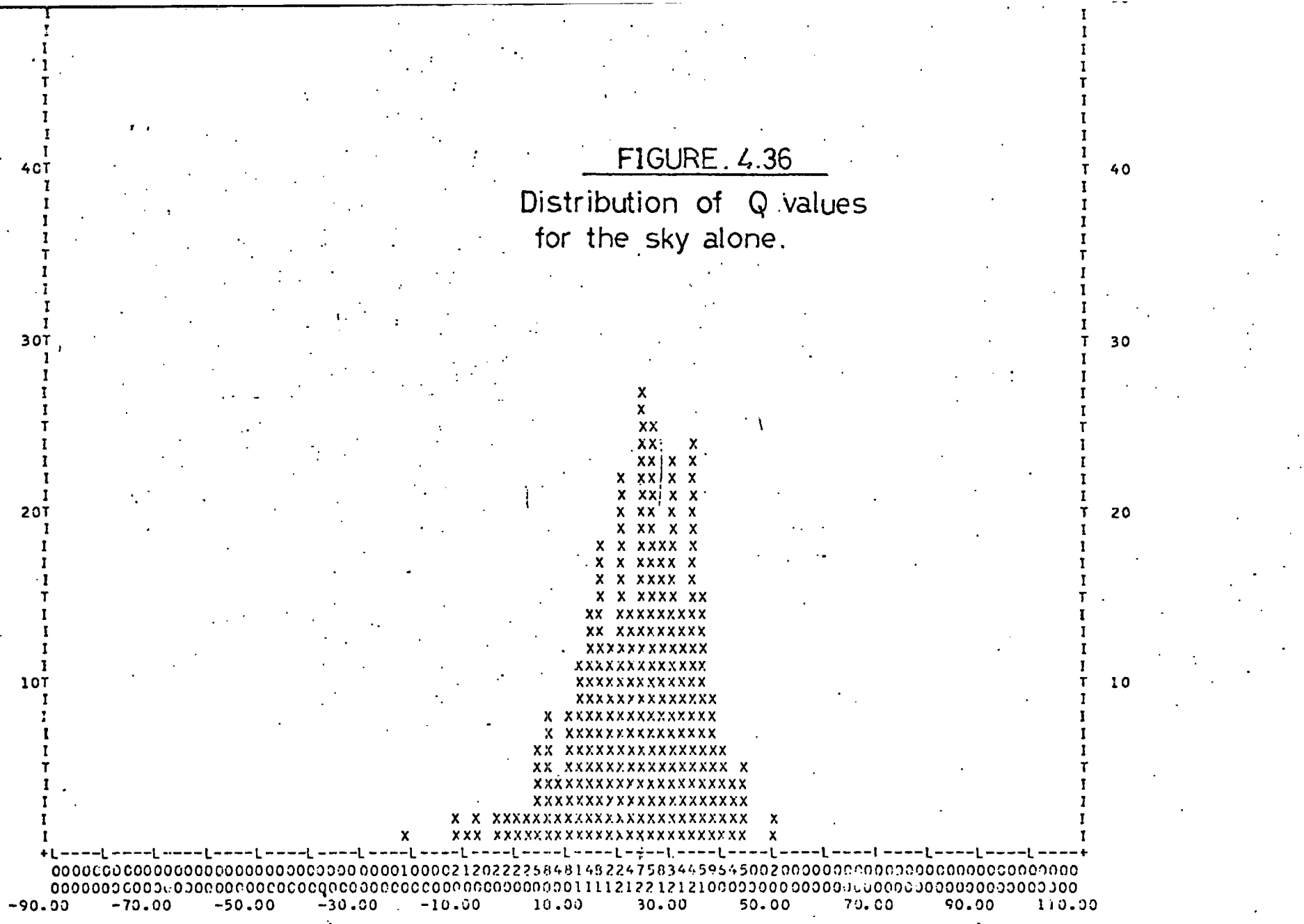

FIGURE. 4.36

Distribution of Q values for the sky alone.

FIGURE 4.37

Distribution of U values for sky alone.

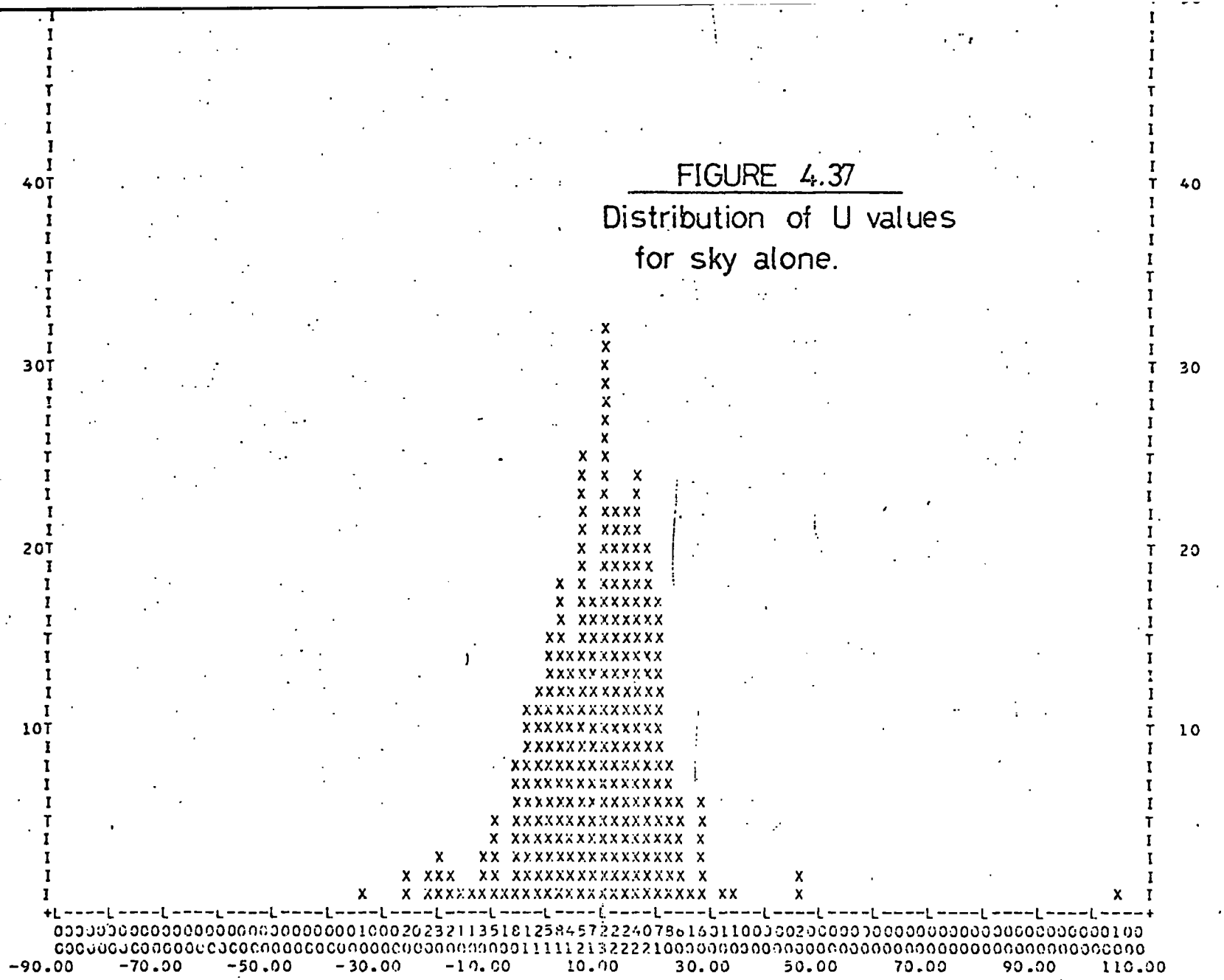

The distribution for the U factor of the sky is shown in figure 4.37.

The Degree of Polarisation P and Angle θ

Two estimates of the degree of polarisation P1, P2 were calculated knowing $P1 = (Q1^2 + U1^2)^{\frac{1}{2}}/I$, and $P2 = (Q2^2 + U2^2)^{\frac{1}{2}}/I$, and the two estimates of the angle θ1, θ2 were calculated from $\theta 1 = \frac{1}{2} \tan^{-1}\left(\frac{U1}{Q1}\right)$ and $Q2 = -\frac{1}{2} \tan^{-1}\left(\frac{U2}{Q2}\right)$. These two estimates of the degree of polarisation are independant measures in the four plate analysis. However, when only three plates are used the two estimates of P1, P2 are not wholly indepandant since the Stokes parameter U is the same in both cases.

The degree of polarisation P is calculated from $P = (Q^2 + U^2)^{\frac{1}{2}}/I$ at angle $\theta = -\frac{1}{2} \tan^{-1} \left(\frac{U}{Q}\right)$

4.4 Results of the Present Observations of M1

The analysis of the data resulting from the present observations of the Crab Nebula gave information on the degree and angle of polarisation for well over 1000 points in the nebula. The results are shown in map form in figure 4.41 superimposed on a photograph taken in the blue (4000 Å - 5000 Å).

The length of each line is directly proportional to the degree of polarisation and is drawn parallel to the electric vector. Angles are measured positive from the north anticlockwise through west to south, and each vector represents the integrated polarisation over an area 7" x 7".

The wavelength region (4000 Å - 5000 Å) used for the measurements contains the Hβ emission line, which although not one of the strongest lines of emission from the filaments, nevertheless means that not all of the observed radiation is continuum synchrotron emission and some contribution from the filaments is to be expected.

FIGURE 4.41

Results of the present observations of the optical linear polarisation of the Crab Nebula superimposed on a blue photograph.

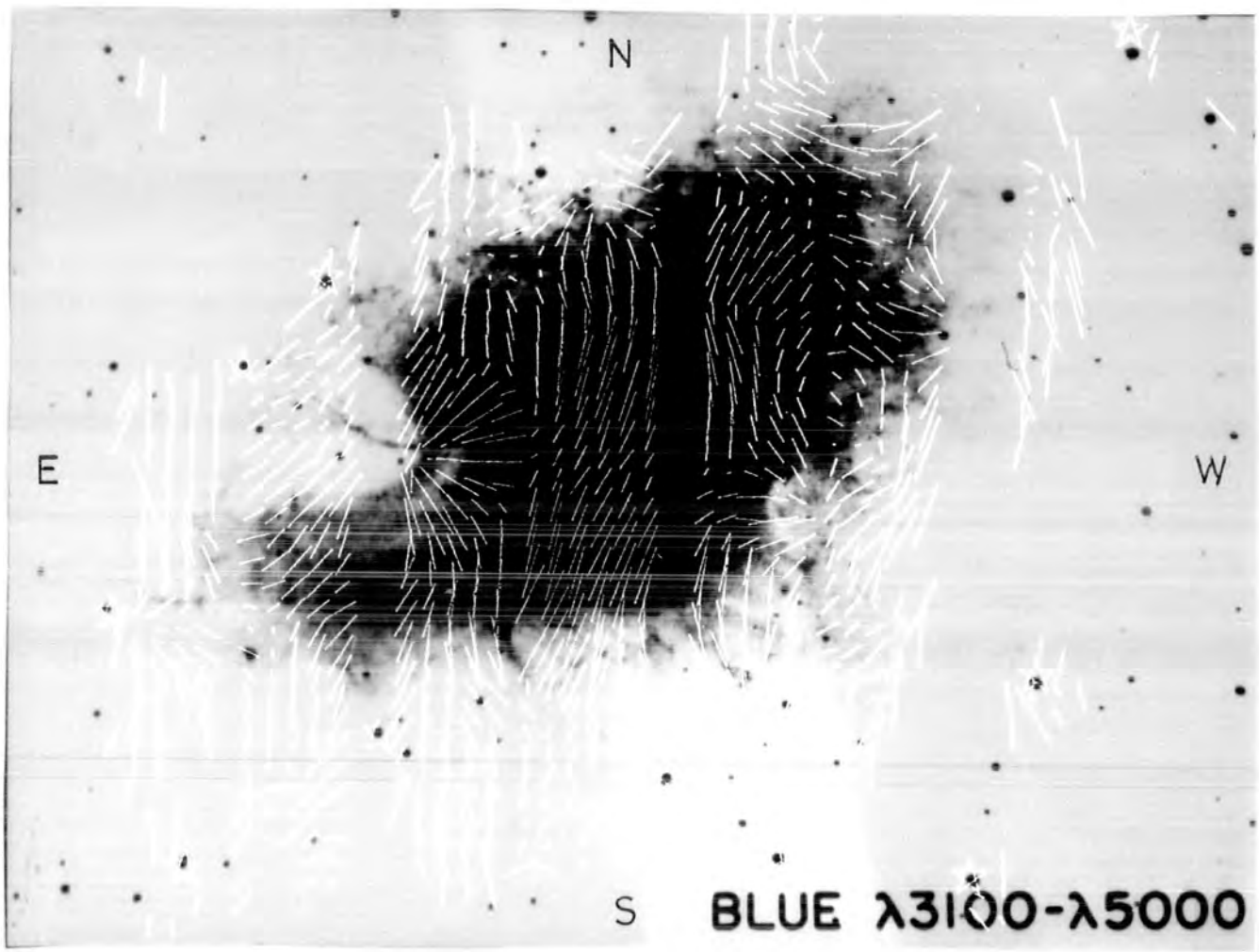

⟵ 30 % polarisation

FIGURE 4.42 (a) Results of the 4" x 4" analysis for the Crab Nebula

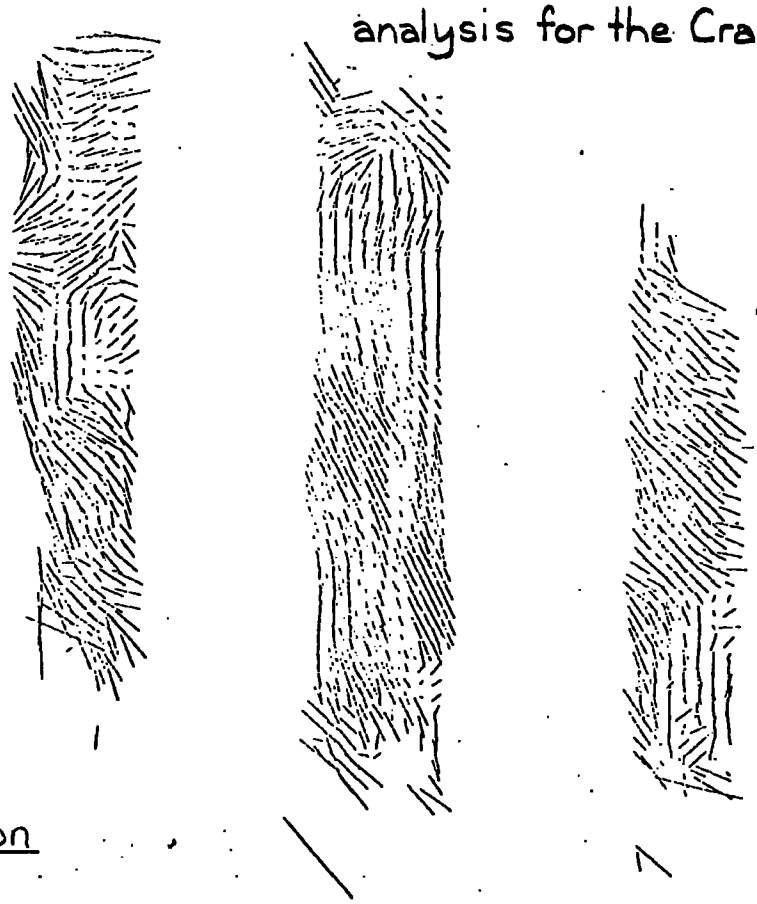

30% Polarisation

(b) Results superimposed on the contour map.

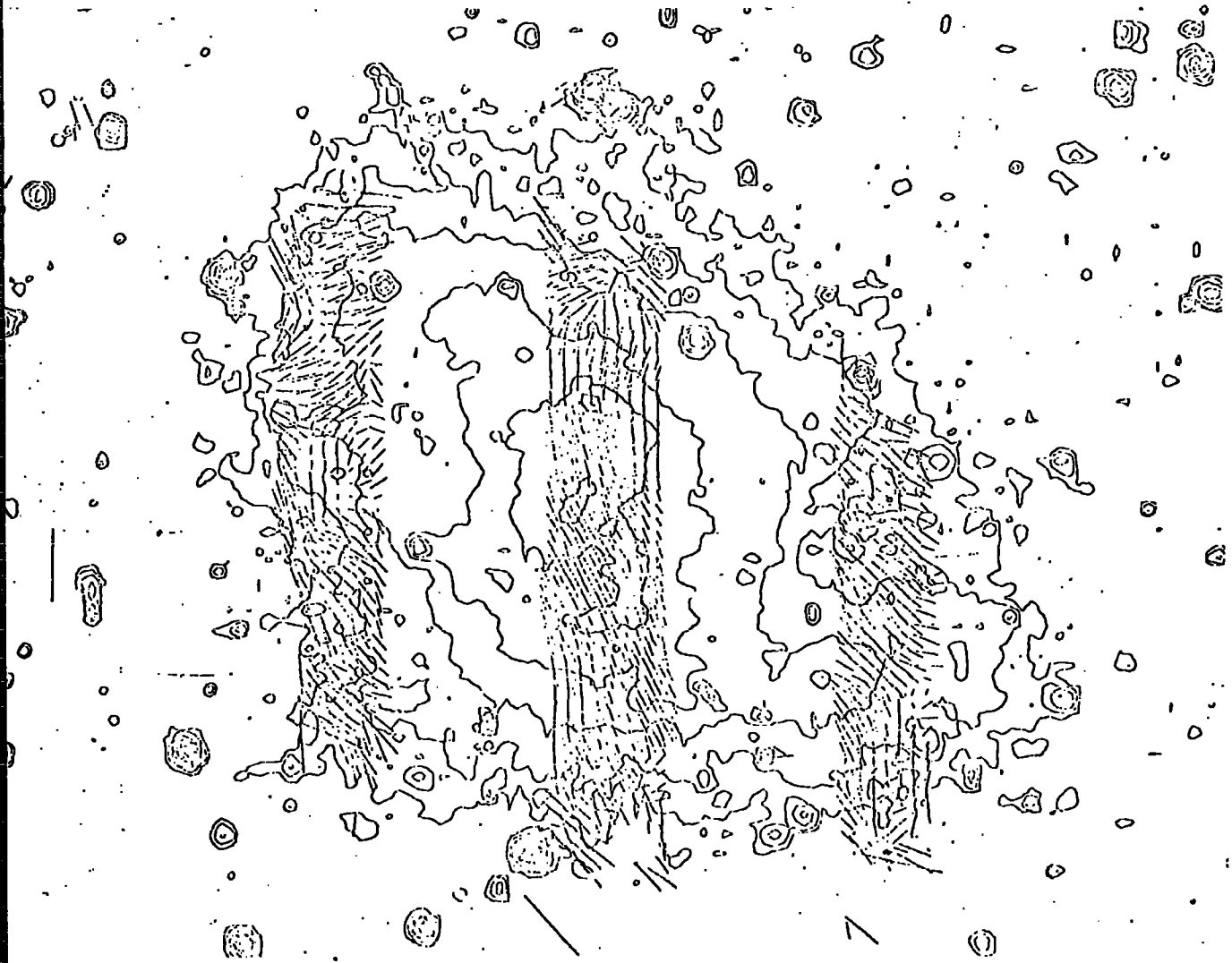

At the same time, the data for one half of the nebula was analysed over an integrated area of 3 pixels by 3 pixels, corresponding to 4" x 4". The results are shown in figure 4.42.

In the winter of 1975, an electronograph of the entire nebula, in the same wavelength region as the polarisation plates, was taken on the 36" telescope at the Royal Greenwich Observatory. A contour map of this plate shows that the nebula extends further than is easily seen on the photographic plates (figure 4.43) and the superposition of the polarisation map on the contour map (figure 4.44) clearly indicates that the total area of the nebula has been measured.

4.5 Errors on the Measurements

It is difficult to determine the individual errors on each point on the polarisation map, since this involves detailed knowledge of the individual errors on the values i1 - i6. However some estimate of the relative errors on various points on the plate can be made by examining the variation of the difference of the two estimates of the degree of polarisation P1 - P2, and those of the angle θ1 - θ2, with the intensity and degree of polarisation measured. Of course, since only three plates have been used in the analysis the value of U is the same for both estimates, which reduces the independance of the estimates, nevertheless the variation of P1 - P2 gives a measure of the error on the degree of polarisation albeit slightly underestimated. It has already been established (Section 2.6) that instrumental errors can be ignored.

One would expect that since $P = (Q^2 + U^2)^{\frac{1}{2}}/I$ and that $\theta = -\frac{1}{2} \tan^{-1} (U/Q)$ that the error on the degree of polarisation depends more critically on the intensity than does the error on the angle.

FIGURE 4.43

Contour map of the Crab Nebula superimposed on a blue photograph.

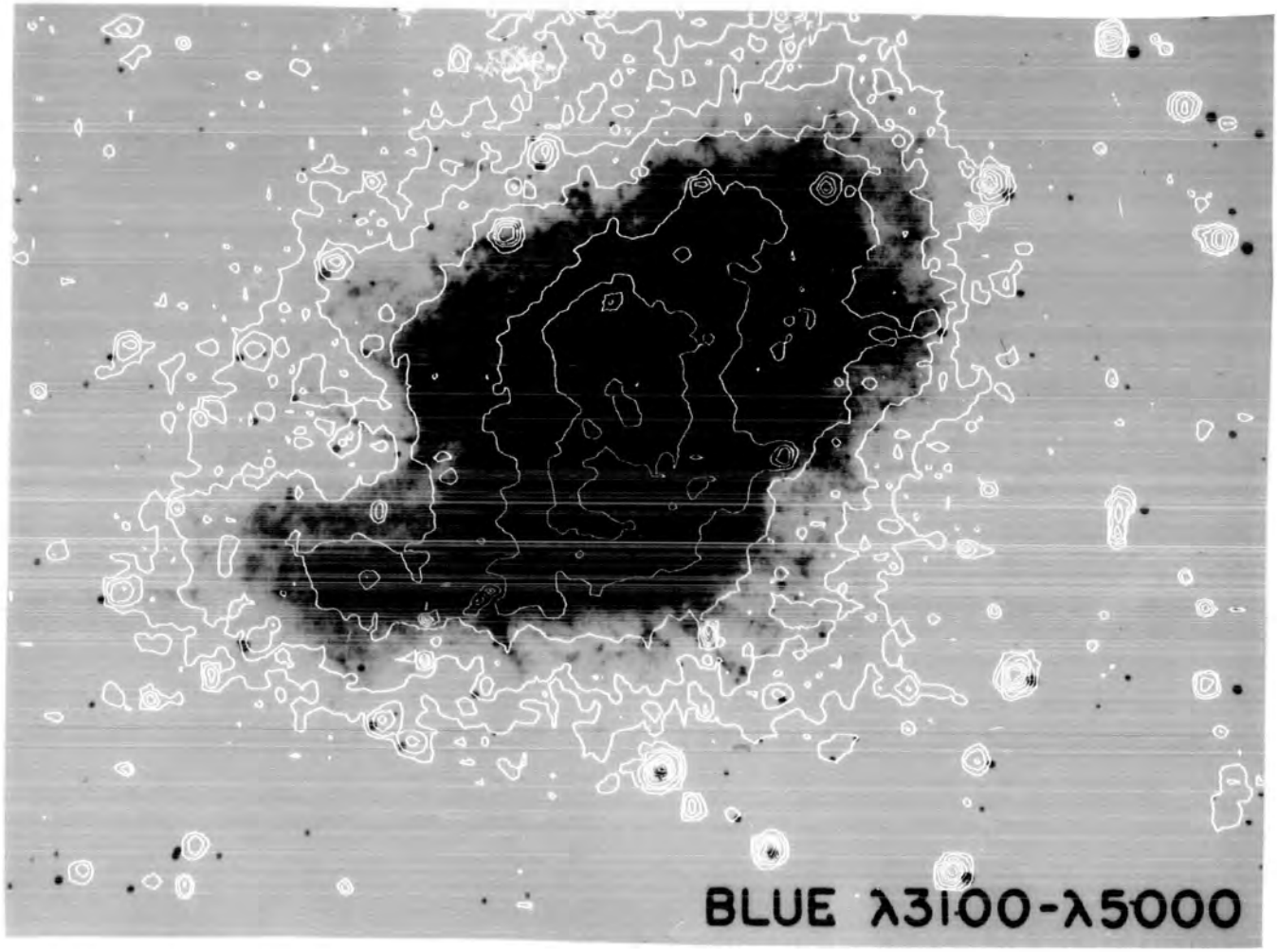

FIGURE 4.44 The present measurements of the optical linear polarisation of the Crab Nebula superimposed on a contour map of an electronograph taken in the blue (4000Å-5000Å)

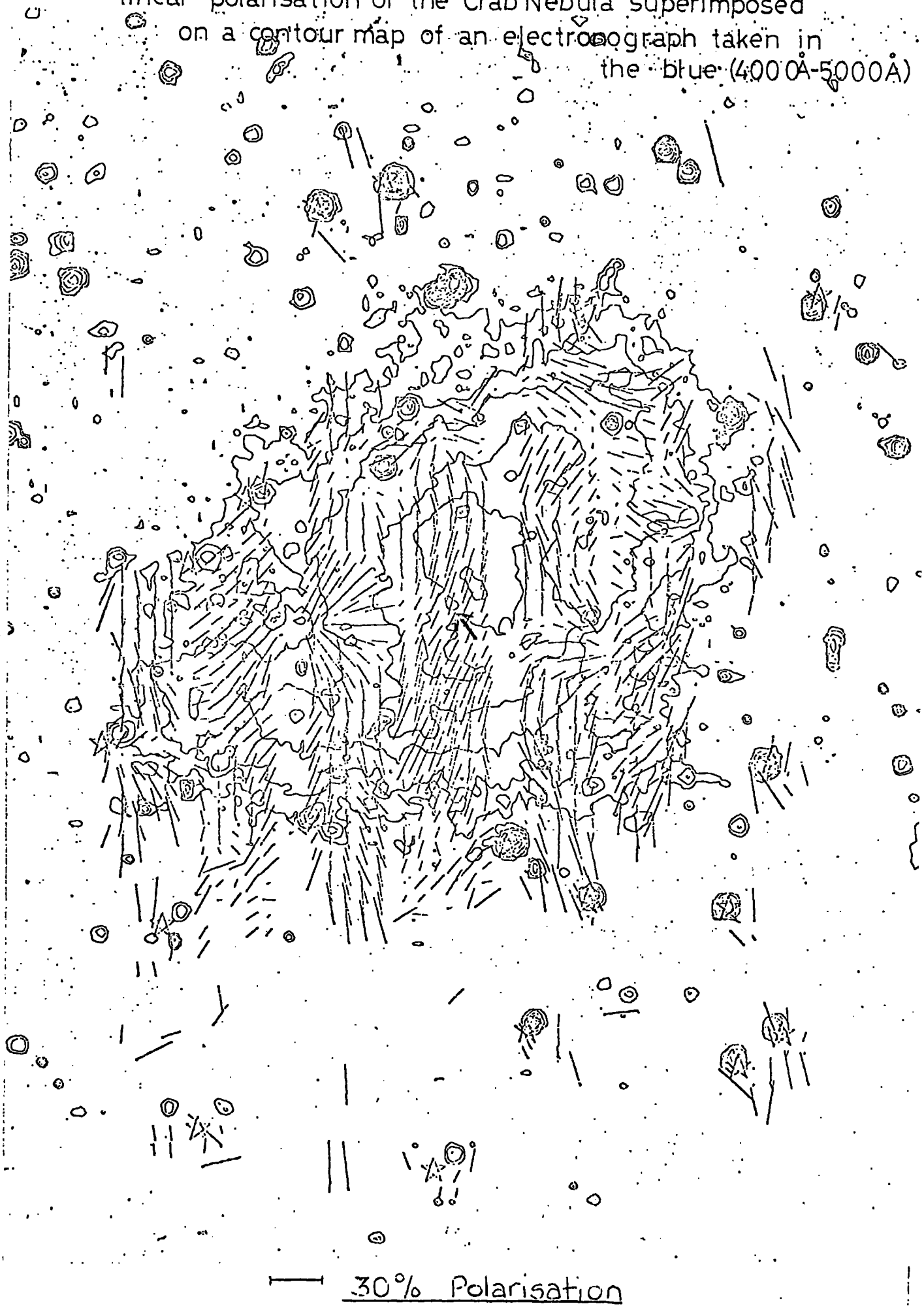

A plot of distribution of the value P1 - P2 against Intensity (figure 4.51) shows that the difference in the two estimates of the degree of polarisation falls off rapidly with increasing intensity.

More detailed estimates of the error on the degree of polarisation measured can be made by considering the difference in the two estimates of the degree of polarisation as a function not only of the intensity, but also of the degree of polarisation itself. Figure 4.52 shows the relationship between the difference of the two estimates of the degree of polarisation measurements, P1 - P2, with intensity, for various intervals of the degree of polarisation, P, less than 10%, 10%-20%, 20%-30%, 30%-40%, 40%-50%, 50%-60% and greater than 60%. The intensity scale used is logarithmic, in order to show more clearly the information measured, since figure 4.51 shows the distribution to be almost exponential.

It can be seen from figure 4.52, that for all intervals of the degree of polarisation the difference in the two estimates, P1 - P2, is greater than for lower intensity regions, the outer edges of the nebula, than for the more intense brighter regions of the nebula.

For low values of the degree of polarisation $0\% \leqslant P \leqslant 20\%$, P1 - P2 can be as great as 10% for the faint regions of the nebula, falling to less than 5% in the more intense regions. The shape of the error line is more or less linear, showing that for small values of polarisation the error is not so nearly dependant on the intensity as for higher values of the polarisation. As the degree of polarisation increases, to about 20%-40% the intensity plays a much more vital part in the error calculation. As the polarisation increases the value of P1 - P2 falls off more and more rapidly with intensity.

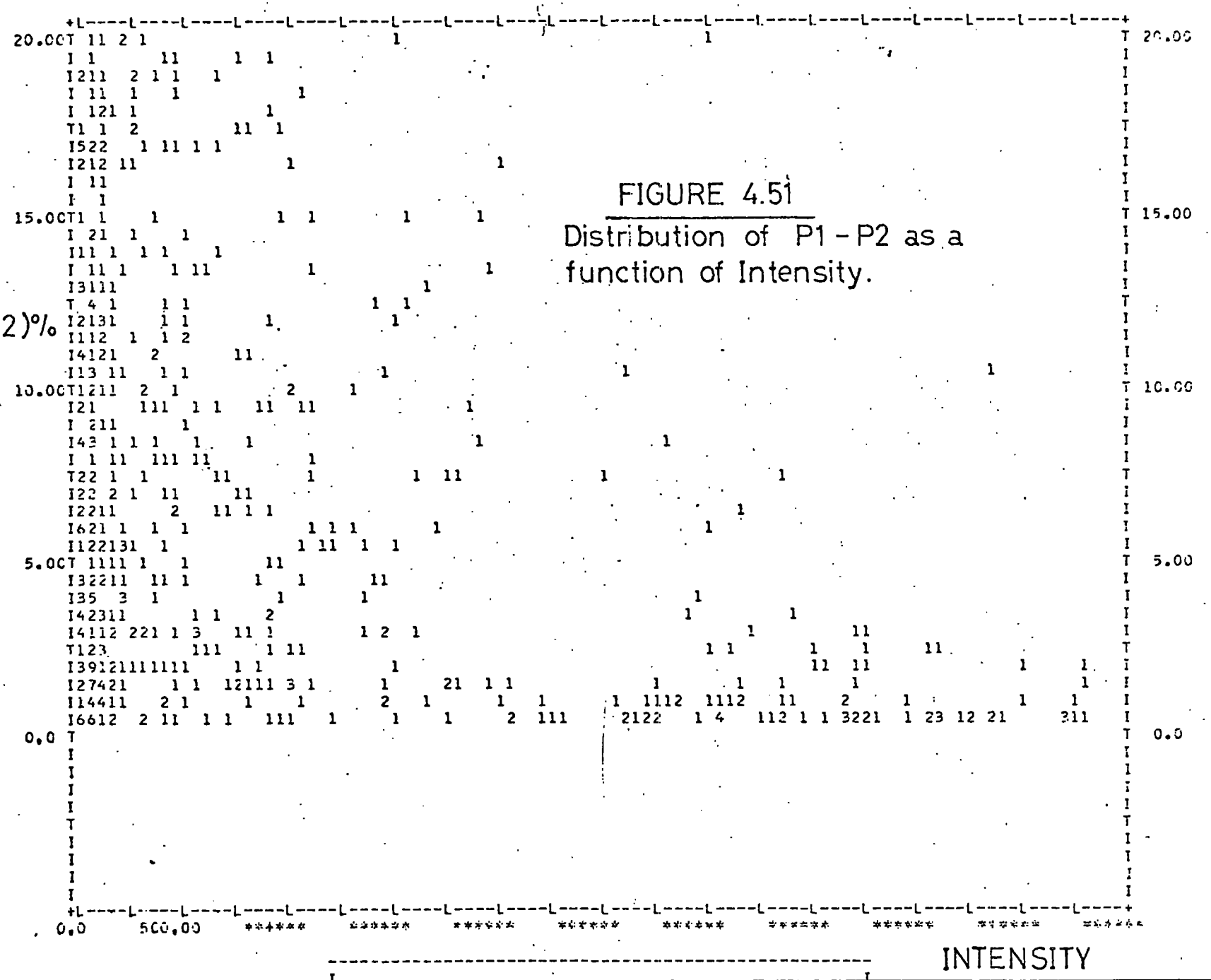

FIGURE 4.51

Distribution of P1 - P2 as a function of Intensity.

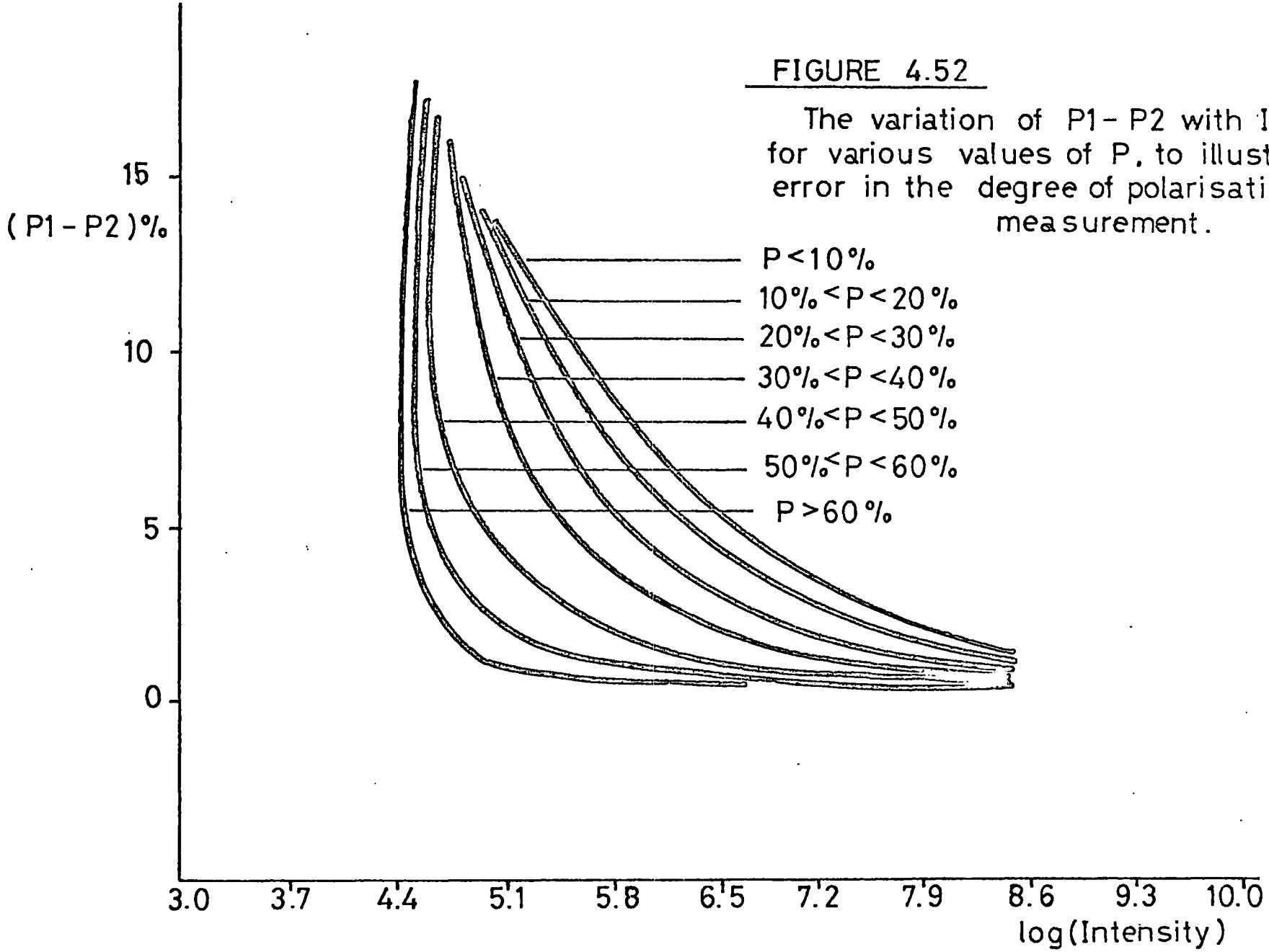

FIGURE 4.52

The variation of P1 - P2 with Intensity for various values of P, to illustrate the error in the degree of polarisation measurement.

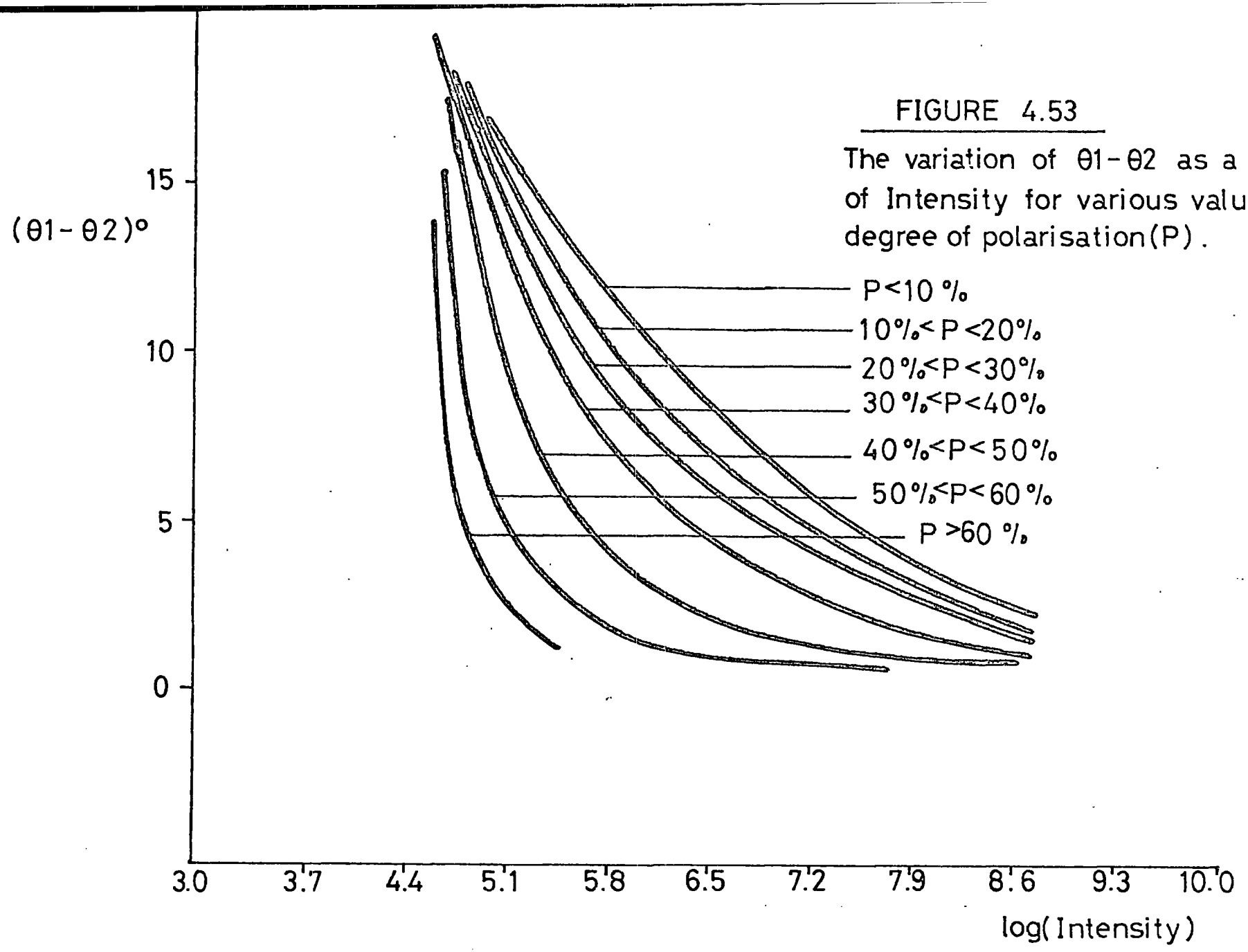

FIGURE 4.53

The variation of θ1 - θ2 as a function of Intensity for various values of degree of polarisation(P).

At the higher values of the degree of polarisation P $\geq$ 50%, even at low intensity the polarisation is well determined, that is P1 - P2 is less than 5%. Another factor to be introduced here is the non-linearity in the digitisation process of the electronographs. Although this effect is allowed for in the reduction technique, for large values of the degree of polarisation, this effect could produce systematic errors in the polarisation measured.

The conclusion to be drawn is, therefore, that the error on the degree of polarisation measured is intensity dependant, and that the error decreases with increasing value of the degree of polarisation.

The error on the angle, as shown in figure 4.53, where the difference in the two estimates of the angle, $\theta 1 - \theta 2$, is plotted as a function of intensity for the same intervals of P as for figure 4.52. Here the error on the angle measured is less dependant on the intensity, as would be expected, and more dependant on the degree of polarisation measured, which can be seen clearly in figure 4.53. Of course the less well determined values of the degree of polarisation are a function of the intensity and this is reflected in the fact that $\theta 1 - \theta 2$ is slightly greater, of the order of 10° for low intensity values falling to 5° at higher intensity levels.

4.6 Description of the Observed Optical Polarisation of the Crab Nebula

The results of the present observations (figure 4.4.1), superimposed on a blue photograph of the nebula show that the degree and angle of polarisation can be measured by this method for faint areas of the nebula which are not visible on the photograph. A superposition of the polarisation map on the contour map of a blue electronographic plate (figure 4.44) indicates that we do indeed measure the optical polarisation for the entire nebula.

The general pattern of the polarisation vectors resembles the results of the measurements of the optical polarisation of the nebula by Woltjer (1957) (figure 3.42). A more detailed comparison of the results of these two sets of observations is discussed in the following chapter.

In the brightest parts of the continuum image the polarisation vectors lie parallel to the general S shape of the nebula, lying perpendicular to the fibres in the continuum, indicating, if the usual theory of the synchrotron nature of the continuum radiation is correct, that the magnetic field in the nebula runs along these fibres. The value of the degree of polarisation in the central brightest part of the nebula, being about 20%-30% rising to over 70% in some outer regions of the continuum where the nebula is faintest.

The photograph in the blue shows in the north easterly region bright loops of continuum emission. The polarisation vectors in this region trace the contours of these loops and have a value of the degree of polarisation of the order of 30% to 40%.

Another notable feature of the polarisation map is the radial fan of vectors, which appears centred on the dark bay in the eastern region of the nebula.

The position of the pulsar in figure 4.41 is indicated by an arrow.

Implications of the Results

It is now widely accepted that the nebula continuum emission is synchrotron in nature. Therefore examination of the positional variations in the degree of optical polarisation gives some indication of the structure of the magnetic field in the nebula.

As described in Section 3.6 the expected value of the degree of polarisation for a uniform magnetic field for a spectral index of 2.5 is 70%.

Only in the central region of the nebula where the polarisation pattern is uniform can the magnetic field be said to be smooth and simple. In the bright central region the value of the degree of polarisation is about 20%, considerably lower than the expected value of 70%, and only in some areas in the outer regions is the degree of polarisation measured comparable to the expected value. This can be explained by the fact that in the central regions of the nebula we are looking across several crossed looped lines of force, whereas in the outer regions we see just a single looped line of force. However the problem of allowing for projection effects is not simple. Scargle (1969) has measured the spectral indices for various points in the north west and south east region of the nebula, and finds that the spectral index increases with increasing distance from the centre of the nebula, which is caused by the method by which energy is deposited throughout the nebula via damping of magnetohydrodynamic waves.

If a comparison is made between the results of the observations for integrated areas of 7" x 7" and 4" x 4", which is shown in figure 4.62, it can be seen that in the two cases the degree and angle of polarisation agree well. This indicates that the method of reduction of the data can be used for the smaller integrated area measurements and reveals that if more detailed measurements of the optical linear polarisation of the nebula are to be made the aperture size should be smaller than 4" x 4" to reveal any small scale structure in the polarisation pattern.

One of the reasons for the observations of the Crab Nebula, was to make a detailed comparison of the results of the present method of reduction of the data with the extensive previous measurements of Woltjer. Although the general pattern of the polarisation vectors from the present measurements resemble the results of Woltjer a detailed comparison is necessary and is described in the following chapter.

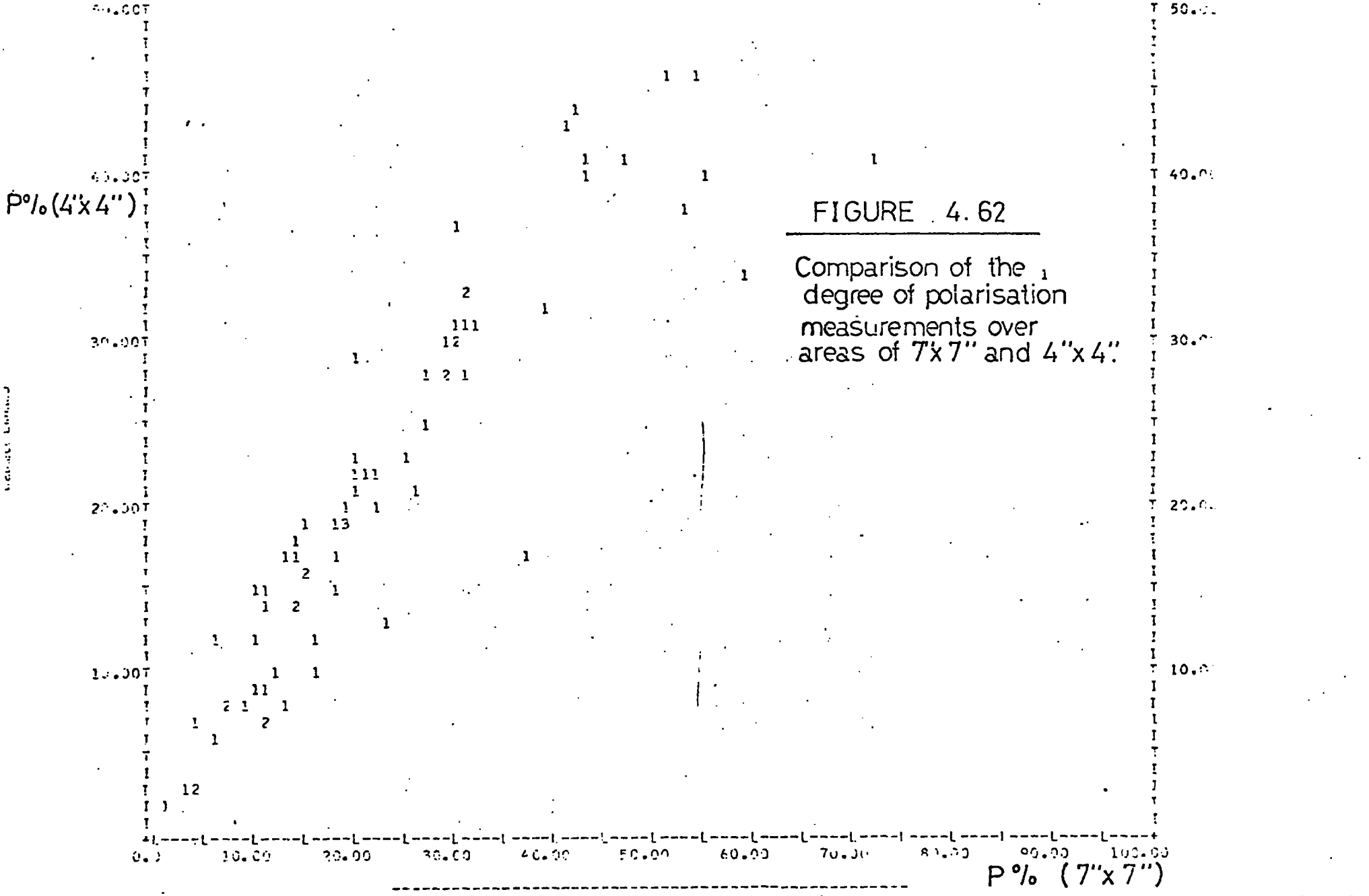

FIGURE 4.62

Comparison of the degree of polarisation measurements over areas of 7"x7" and 4"x4".

References

Scargle, J.D (1969) Ap. J 156 401

Woltjer, L. (1957) BAIN 13 301

Chapter Five Comparison of the Present Data of the Crab Nebula with Earlier Work

5.1 Introduction

The first map of the optical linear polarisation of the Crab Nebula was made by Woltjer (1957) using photographs taken by Baade (1955) on the 200 inch telescope at Mount Palomar.

Full details of the technique used to produce this map are given by Woltjer (1957). The main feature of the technique is that the photographic results had to be calibrated with photoelectric measurements made by Walraven (1957). The Woltjer map was made with a circular diaphragm of diameter 5 arc seconds and in the wavelength region 5200 Å - 6400 Å. In this part of the spectrum the contribution of filamentary radiation is small.

A point to point comparison between the Woltjer map and the Durham map is very informative as it will yield further confirmation of the validity of the electronographic technique to measure polarisation. It may also indicate any changes in the polarisation of light from the Crab Nebula in the period 1955 to 1975.

This chapter describes the procedure used to make the comparison and includes a discussion of the results of this comparison.

5.2 Procedure for the Comparison of the Durham Map with the Woltjer Map

To make a comparison between the two maps it is necessary to compare the measurements of the polarisation in each map corresponding to the same point in the nebula. The Durham map was transformed to the co-ordinate system that Woltjer used, using the field stars as fiducial marks, so that there was a one to one correspondance between measurements in the two sets of observations. The spatial correspondance between the two maps was better than 2 arc secs.

5.3 Results of the Comparison

The scatter plots shown in figures 5.31 and 5.32 show a general comparison between the two sets of results.

Figure 5.31 shows, for each corresponding pair of measurements, the scatter plot of the degree of polarisation for the Durham and Woltjer measurements. If there is good agreement between the measurements the points should lie close to a line at 45° to the axes. Although the general trend is a line at 45° the points are widely scattered about this line.

Figure 5.32 shows a similar plot for the angle of polarisation. There is excellent agreement between the two sets of observations in this plot.

The initial conclusion to be drawn from this comparison is that, although there is considerable agreement in the measure of the angle of polarisation, the measurements of the degree of polarisation disagree over the whole range of values of the degree of polarisation.

It is necessary, therefore to consider the possible causes for this discrepancy.

5.4 Possible Causes of Disagreement between the Durham Results and those of Woltjer

The discrepancy between the two sets of measurements could result from one of the following effects.

1. Either the measurements of the optical linear polarisation are wrong in places.
2. Calibration differences, the photographic plate technique requires calibration which may be in error. This would result in an effect where the two sets of results may agree in one range of nebular brightness but disagree in other ranges.

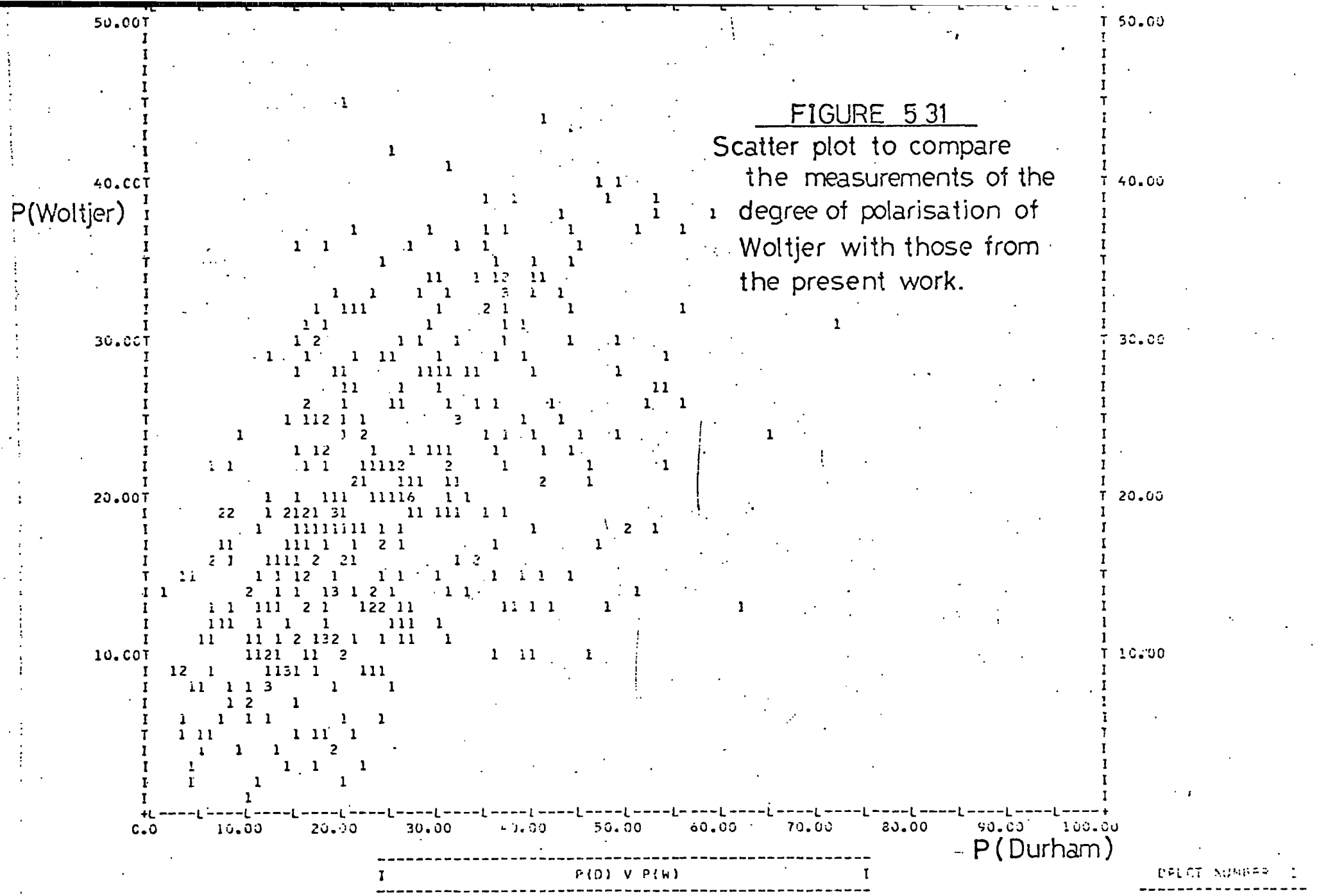

FIGURE 5 31

Scatter plot to compare the measurements of the degree of polarisation of Woltjer with those from the present work.

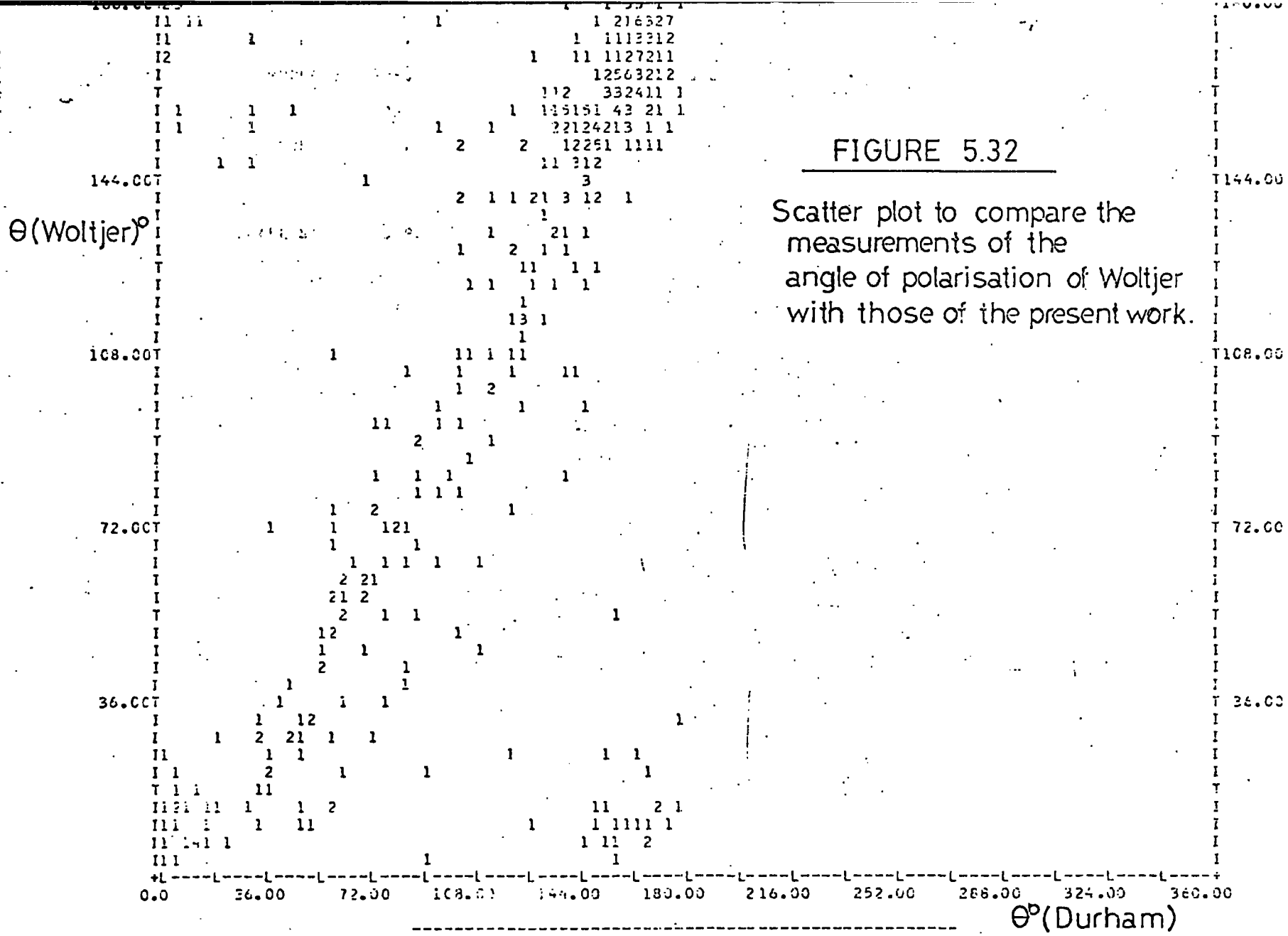

FIGURE 5.32

Scatter plot to compare the measurements of the angle of polarisation of Woltjer with those of the present work.

3. The difference in aperture size and shape, Woltjer used a near circular diaphragm of 5 arc seconds diameter, whereas a square aperture, dimensions 7" x 7", was used for the present measurements. The effect is important in areas of the nebula where there are considerable intensity gradients.
4. Errors in location of the comparison points.
5. Changes in size of the nebula in the twenty years between the two sets of measurements. The field stars used for the transformation of the Durham measurements to the co-ordinate system used by Woltjer will not have changed in relative position over this period, but since the nebula is expanding it is possible that there will not be point to point correspondance in the nebula itself.
6. A dependance on the waveband in which the observations were taken. The Durham map is in the wavelength region 4000 Å to 5000 Å, whereas the measurements of Woltjer were made in the region 5200 Å - 6400 Å. This would not affect the continuum synchrotron polarisation alone, since in the usual synchrotron theory the polarisation depends on the spectral index of the electrons rather than the wavelength. However the contribution of filamentary radiation may be different in one wavelength region than the other, which will affect the intensity distributions across the nebula for the two sets of observations, and therefore the degrees of polarisation measured.

5.5 Tests for the Causes of the Discrepancy

No reason can be proposed to accept the first suggestion (1) above. Various tests have been carried out to determine if suggestions (2), (3), (4) can cause the disparity between the present observations of the degree of polarisation measurements and those of Woltjer.

In none of these cases can any conclusive evidence be found to account for this discrepancy. The suggestion (5) that the nebula expansion in the 20 year period between the measurements can be sufficient to produce errors in location of the points compared can easily be ruled out by a simple estimate of the expected expansion in this time. Given the initial expansion velocities of the Crab Nebula to be 1700 km/sec and 1100 km/sec along the major and minor axes respectively, the convergence point to be 1140 AD and the acceleration, assumed constant to be 0.0014 cm/sec (Trimble 1971), the expansion in twenty years is of the order of 2", which is of too small a scale to result in major location errors.

Figures 5.51 and 5.52 show the Durham results superimposed of blue photographs of the nebula for points in which $|P(\text{Durham}) - P(\text{Woltjer})| < 10\%$, and $|P(\text{Durham}) - P(\text{Woltjer})| > 10\%$ respectively. It can be seen from these figures that there are certain areas in which a disparity in the measurements is seen, and that these areas contain a large amount of filamentary radiation, (see figure 5.53). It is felt therefore that varying amounts of filamentary radiation in the two wavebands is the main cause of the observed discrepancy. However one would expect the effect to be systematic, that is, one set of measurements consistently higher than the other, which does not appear to be the case. It could be that one of the maps is partially in error, but no evidence for this can be found for the present work.

5.6 Conclusion

It is evident from the previous discussion, that in many areas in the nebula the degree and angle of polarisation measured in the present work agrees well with the previous photographic work of Woltjer. However there are certain areas where agreement is not found.

FIGURE . 5.51

Polarisation measurements of M1 for P(Durham) - P(Woltjer) < 10% superimposed on a blue photograph.

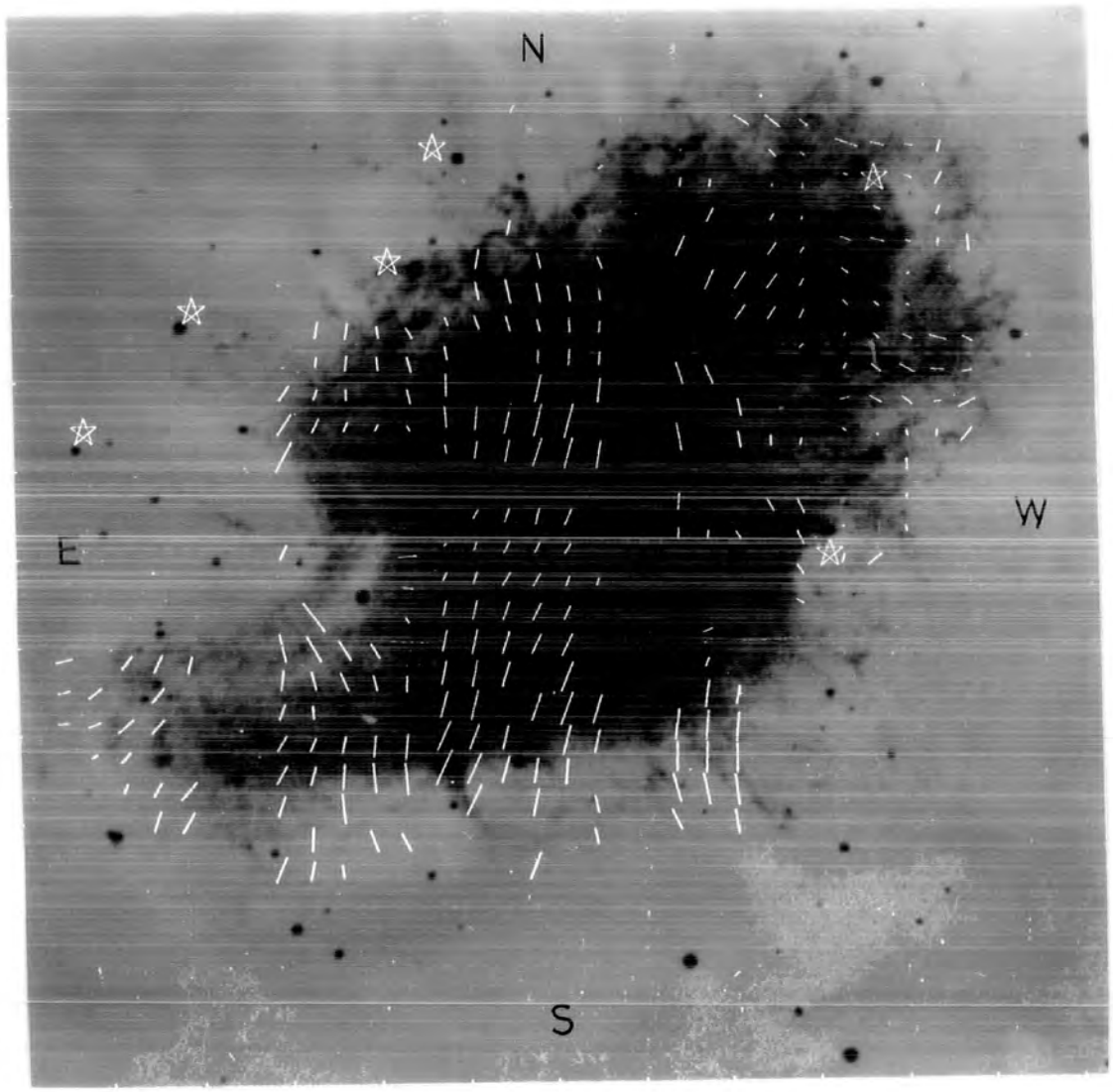

⊢ 30% polarisation

FIGURE 5.52

Polarisation measurements of the Crab Nebula for P(Durham) - P(Woltjer) > 10% superimposed on a blue photograph.

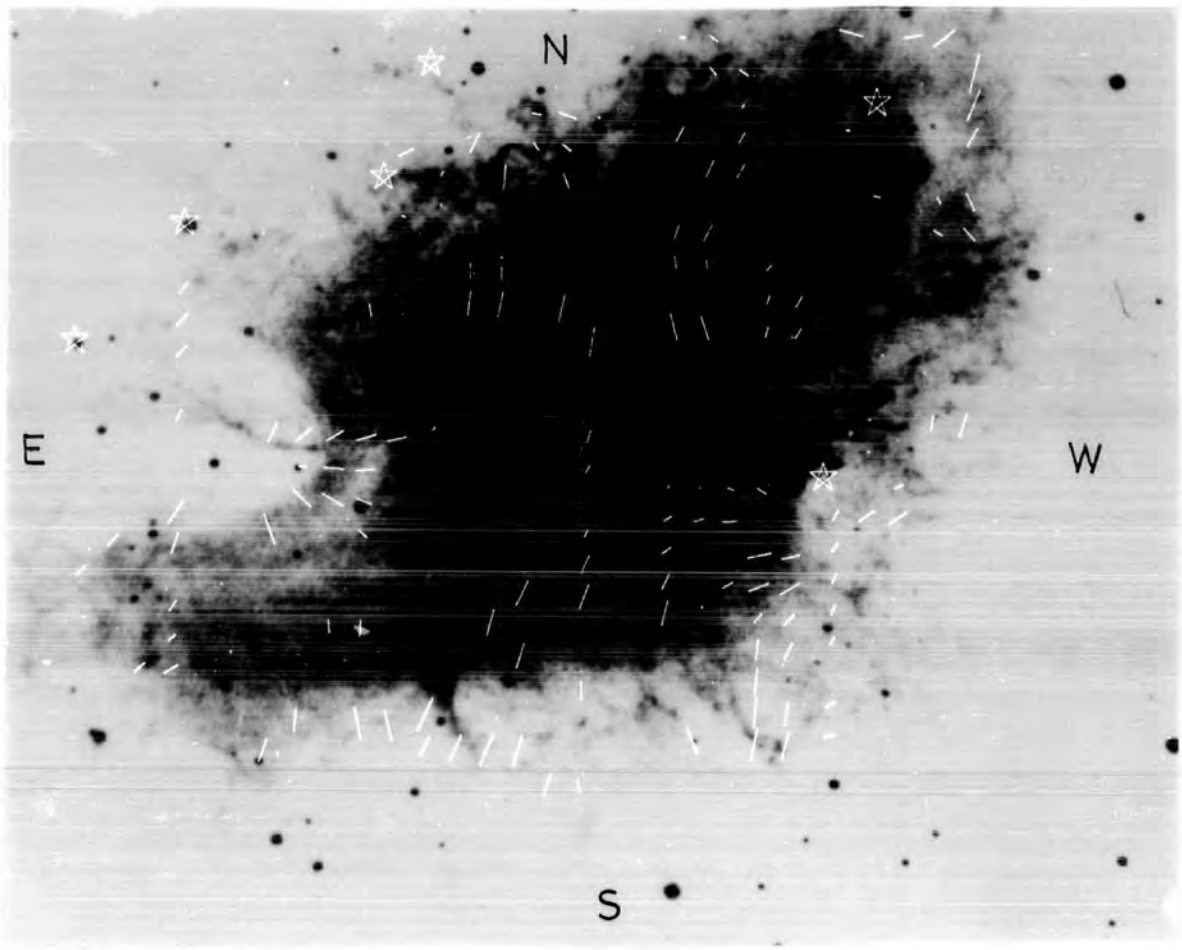

⊢ 30% polarisation

FIGURE 5.53

Polarisation measurements of the Crab Nebula for P(Durham) - P(Woltjer) > 10% superimposed on a red photograph.

⊢ 30 % polarisation

It is clear that this is not a function of intensity, errors in location of the compared points, or changes in the size of the nebula but is most certainly related to features in the nebula.

The features most likely responsible are the filaments, in that the waveband used in the present measurements contains a different contribution of filamentary radiation than the waveband in which the measurements of Woltjer were made. This will not account totally for the disparity in the measurements, however, but nevertheless is a tentative suggestion to explain the observed differences in the two sets of measurements.

References

Trimble, V. (1971) IAU Symposium No 46

Walraven, T (1957) BAIN 13 293

Woltjer, L. (1957) BAIN 13 301

Chapter Six Polarimetry of NGC 1569

6.1 General Remarks on NGC 1569

NGC 1569 is situated in Camelopardus, at RA (1950) 04^h 26'.0 and DEC (1950) + 64° 45'. The galactic longitude is l^{II} = 143.67° and galactic latitude b^{II} = 11.24°

Holmberg (1958) classified this galaxy as an IrrI and De Vaucouleurs (1964) in his catalogue gives classification IBm, and quotes the distance as 3.3 Mpc.

Blue plates published by Arp (1966) show the galaxy to be an amorphous mass having roughly elliptical outer isophotes, with stars resolved, especially noticeable in the south east region of the galaxy. The elliptical outer isophotes have mean axis ratio $\langle b/a \rangle$ of 0.49 (Ables 1971) which suggests that this is a late type disk system inclined at 63° to the line of sight, see figure 6.11.

An Hα survey, carried out to study galactic structure by Hodge (1974) contained both short and long exposure plates of NGC 1569 which revealed interesting features in the galaxy not previously seen on either deep red or deep blue plates. The plates show that the galaxy is contained in an intense Hα envelope about half the size again as the continuum image. External to this image, the long exposure plates reveal a system of faint narrow filaments roughly radial, but showing an intricate pattern of intertwining. Also seen is one bright filament, roughly spiral, in the south east region of the galaxy.

This system of filaments, which extend over twice the diameter of the galaxy, puts NGC 1569 in the class of filament galaxies, a typical example being M82 (Lynds + Sandage 1963), but there is as yet not enough evidence to distinguish whether these filaments consist of gas or dust.

FIGURE 6.11

Photograph of NGC 1569 in the blue from Arp (1966).

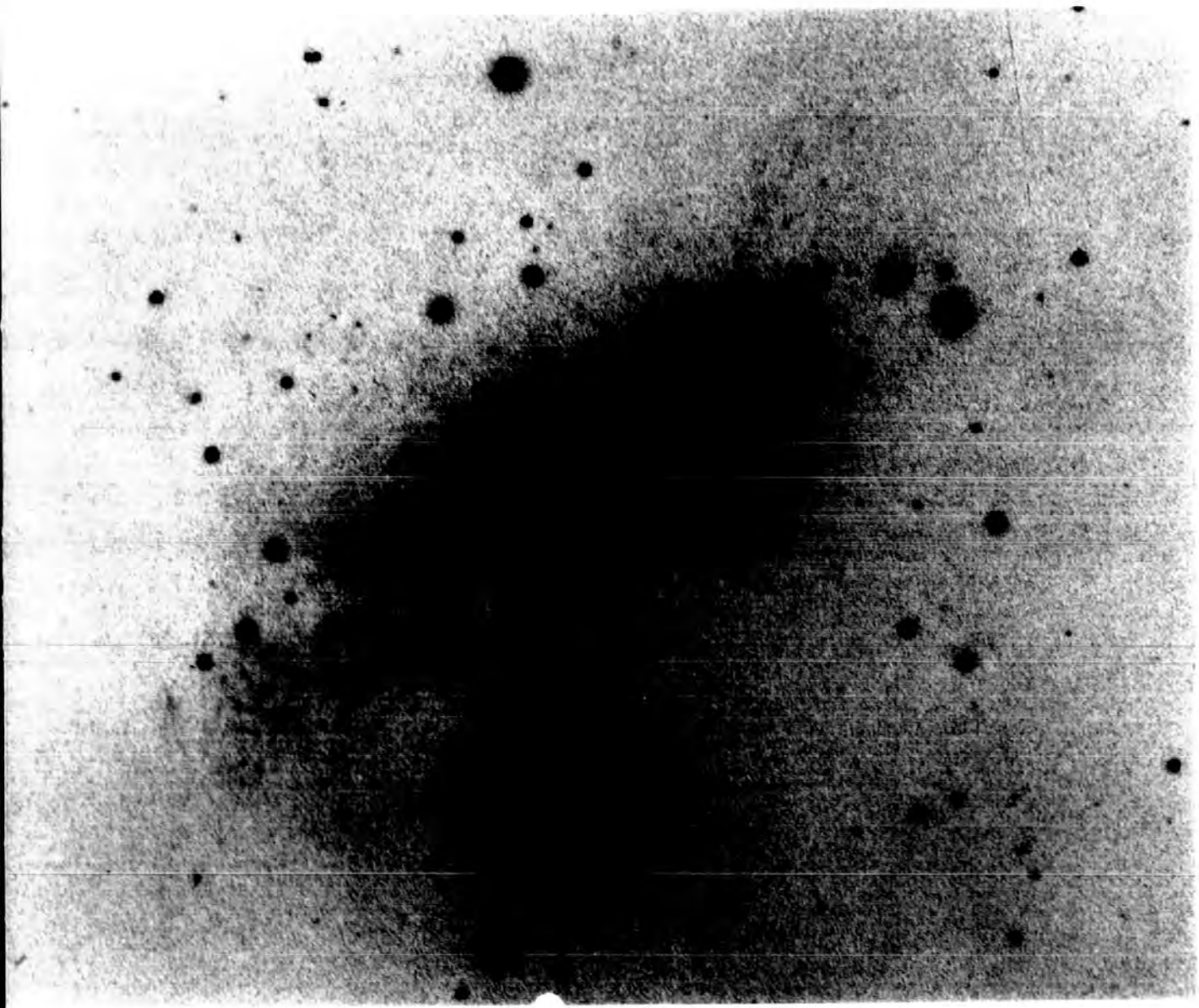

In a detailed photometric study of the galaxy NGC 1569, Ables (1971) identified two star like objects located near the centre of the galaxy, the brighter having RA (1950) $04^h\ 26^m\ 03^s.7$, DEC (1950) + 64° 44' 22" and the other with RA (1950) $04^h\ 26^m\ 05^s.3$ and DEC (1950) + 64° 44' 21".

These objects are of great interest, firstly because they are much bluer than nearby foreground stars, having B-V of 0.6 and 0.4 for the bright and fainter object respectively as opposed to B-V of $\geq$ 0.9 for the foreground stars in this region. Ables reports that if these objects belong to the galaxy the brighter has absolute magnitude $M_B =$ - 13.7. This second fact is significant, in that, the stars in the well resolved south east region of the galaxy have absolute magnitude -9.2, about 4.5 magnitudes smaller than the bright object. The bright object has magnitude comparable to the 30 Doradus complex in the LMC, but is much smaller, the diameter being $\sim$1" (20 pc) as opposed to 250 pc for the 30 Doradus nebula. However the bright object is about 1.5 - 2.5 magnitudes fainter than recognised Seyfert nuclei in their quiescent phases (De Vaucouleurs 1973) and no Seyfert nuclei have been identified in galaxies later than Sbc, which leads to the conclusion that the objects are not Seyfert nuclei, and although bright, resemble stars.

De Vaucouleurs (1974) traced the filaments described by Hodge, to their origin and reports that it is not unlikely that the filaments have been ejected by one or both of these objects.

The radio spectrum shows that NGC 1569 is a weak continuum source at 1400 MHz (McCutcheon 1973) with radio index + 2.3, not unusual for late type spirals and magellanic irregulars.

The spectral index is, however, more interesting. Measurements at 750 MHz by Heeschen and Wade (1964) and at 2695 MHz by Kazes, Le Squeren and Nguyen - Quang - Rieu (1970) give the flux density S (750) = 0.4 and S (2695) = 0.54 from which the average spectral index $\alpha = - \partial(\log s)/ \partial (\log f) = - 0.2$. All other normal galaxies have positive spectral indices for the same frequency range, for example M82, $\alpha = + 0.27$ ($f < 1400$ MHz). Negative spectral indices are usually associated with a small central source, so the spectral index measurement implies that either or both of the objects described by Ables, could be the source of the radio emission.

This hypothesis is strengthened by the results of the radio interferometric measurements of Lequeux (1971). He found that the radio emission could be divided into two components, extended disk component of intensity $S = 0.3 \mp 0.05$ Jy, consistent in dimensions with the optical image, and a point source of intensity 0.12 ∓ 0.05 Jy located at RA (1950) $04^h\ 26^m\ 5^s.6$ and DEC (1950) $+ 64^\circ\ 44'\ 4$. The error on these position measurements is 0.1", which makes the point source position consistent with either of the two bright objects. Therefore either of the objects described by Ables are candidates for the radio emission point source.

The velocity field measurements, carried out by de Vaucouleurs (1974) using a high resolution Fabry-Perot interferometer, reveal the velocity field to be highly chaotic, inconsistent with a typical rotation pattern of a disk galaxy inclined to the line of sight.

All this evidence led De Vaucouleurs (1974) to propose a tentative model based on the hypothesis of an explosive event in the centre of the galaxy giving rise to the Hα filaments.

In the galactic plane the ejected matter would be constrained by interaction with previously existing interstellar gas and may coincide with the anomalously blue central area of the galaxy covering an area 0.6 x 0.3 (600 pc in diameter). The age of the explosion estimated by de Vaucouleurs is 1.5×10^7 years.

6.2 Observations of NGC 1569

In February/March 1975, four plates of the galaxy NGC 1569 were taken using the Durham polarimeter and the Royal Greenwich Observatory electronographic camera , described earlier (Sections 2.1, 2.2) on the one metre telescope of the Wise Observatory, University of Tel Aviv, Israel. The f 13.5 focus was used and the blue filter BG 12, wavelength range 4000 - 5000 Å, was incorporated in the polarimeter. The very blue central region of the galaxy, of dimensions 0.6' x 0.3', was centred in one of the grid slits (width 45 arc secs), and therefore only four plates were needed to find the polarisation of the galaxy, observed in the exposure time of twenty minutes.

6.3 Results

The analysis revealed f1, f2 factor distributions shown in figure 6.31, and only those points with f factor lying between 0.95 and 1.05 were used in the determination of the polarisation.

The exposure factor distribution, initially revealed the necessity of taking a variable background for the clear plate subtraction and the final, acceptable e1, e2, e3 factor distributions are shown in figure 6.32.

The results of the analysis with the sky not removed, are shown in map form in figure 6.33, and for the galaxy alone in figure 6.34.

The vectors lie parallel to each other over a wide area of the galaxy, except for the outer regions, where in the southern area, the presence of a bright foreground star, distorts the pattern.

FIGURE 6.31

f1 distribution

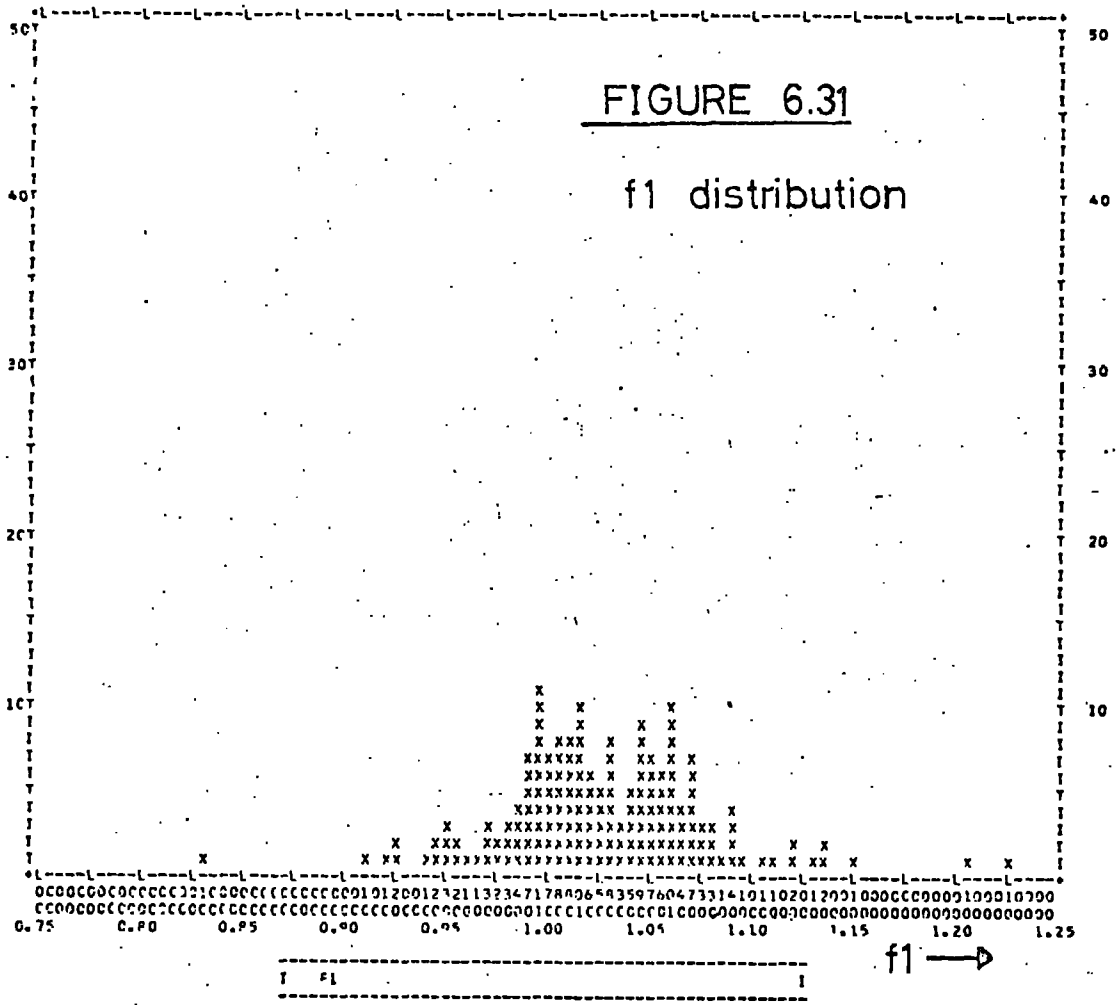

f2 distribution

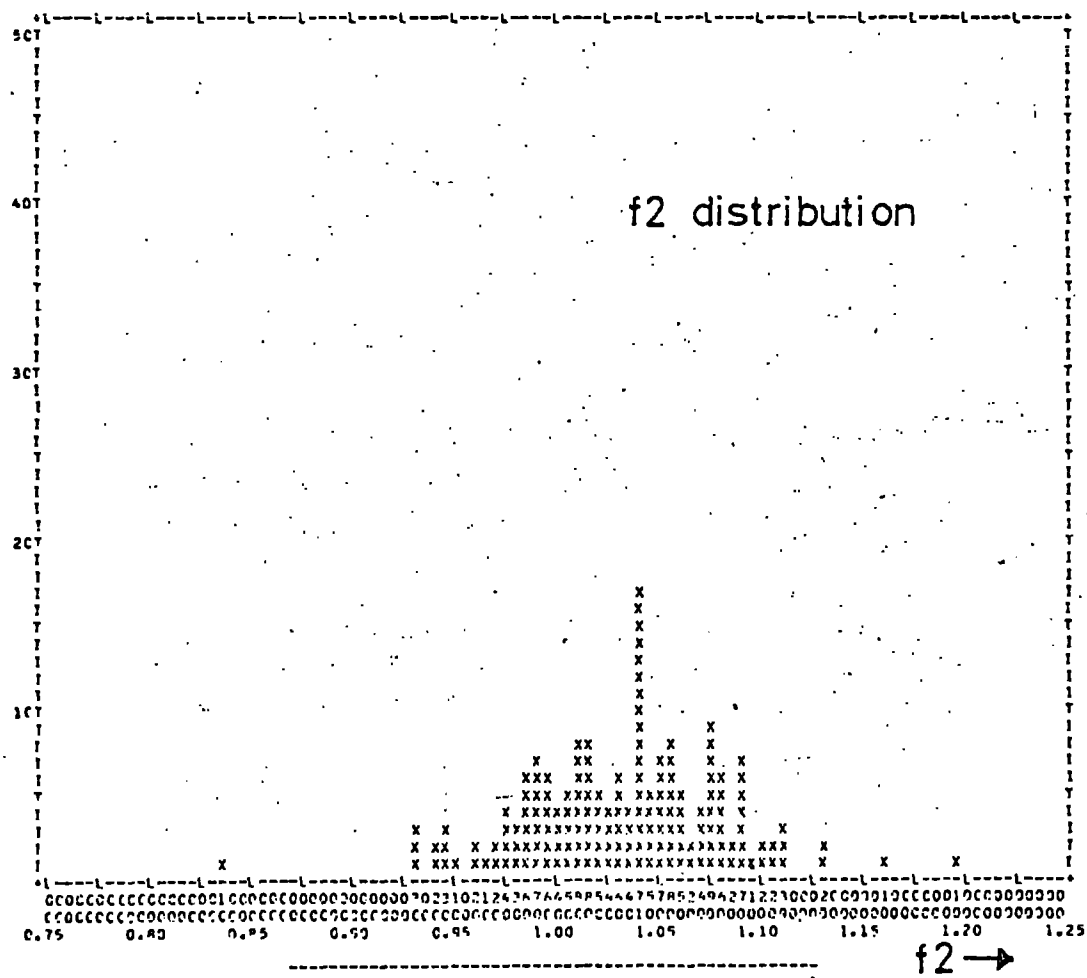

FIGURE 6.32

e1 distribution

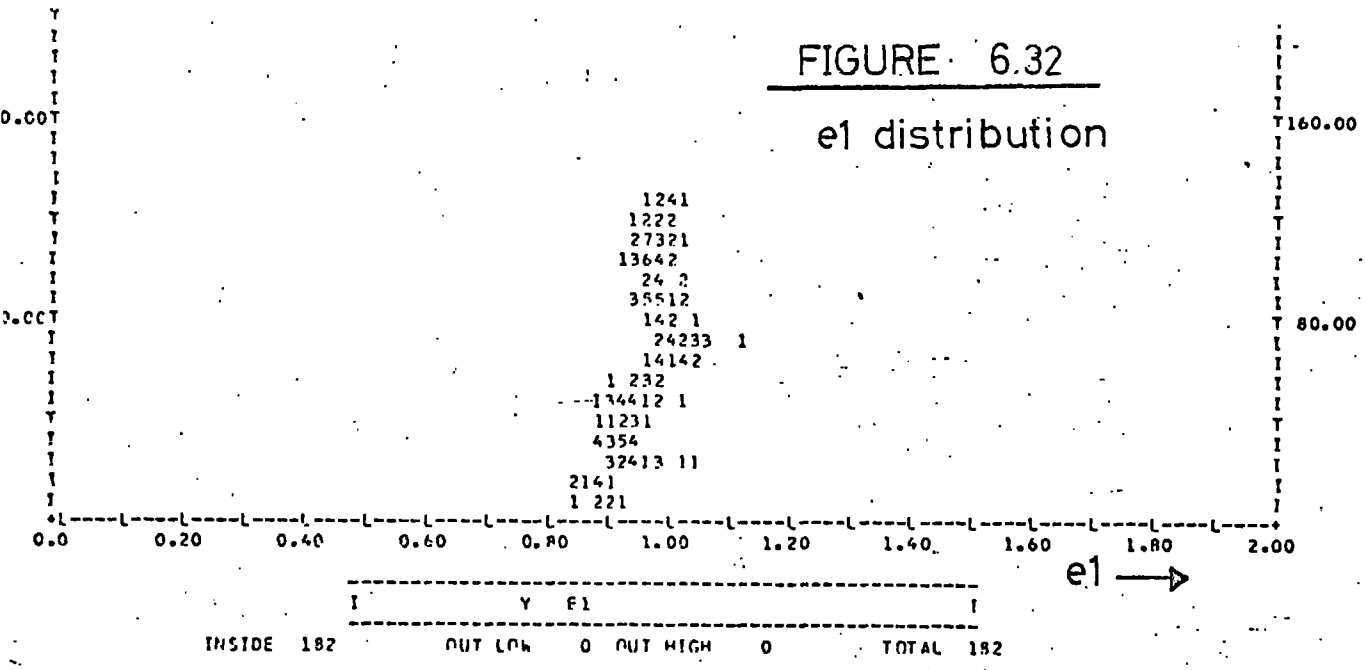

Y	E1

INSIDE 182 OUT LOW 0 OUT HIGH 0 TOTAL 182

e2 distribution

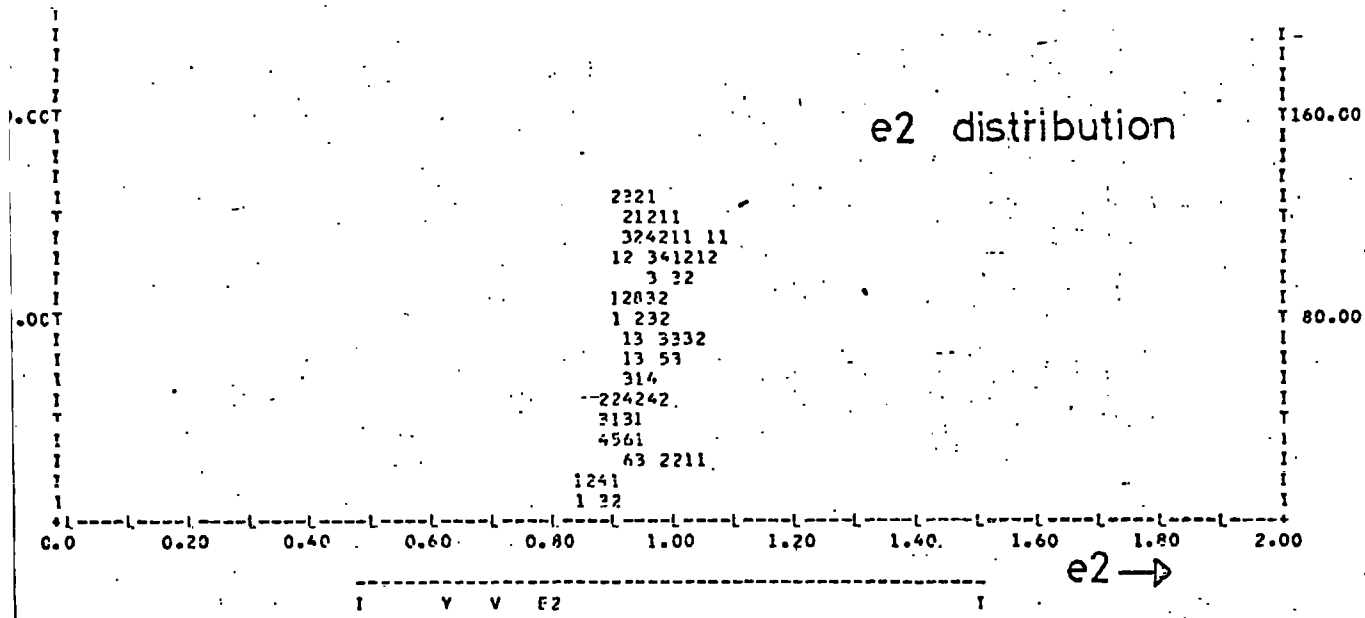

Y	V	E2

INSIDE 182 OUT LOW 0 OUT HIGH 0 TOTAL 182

e3 distribution

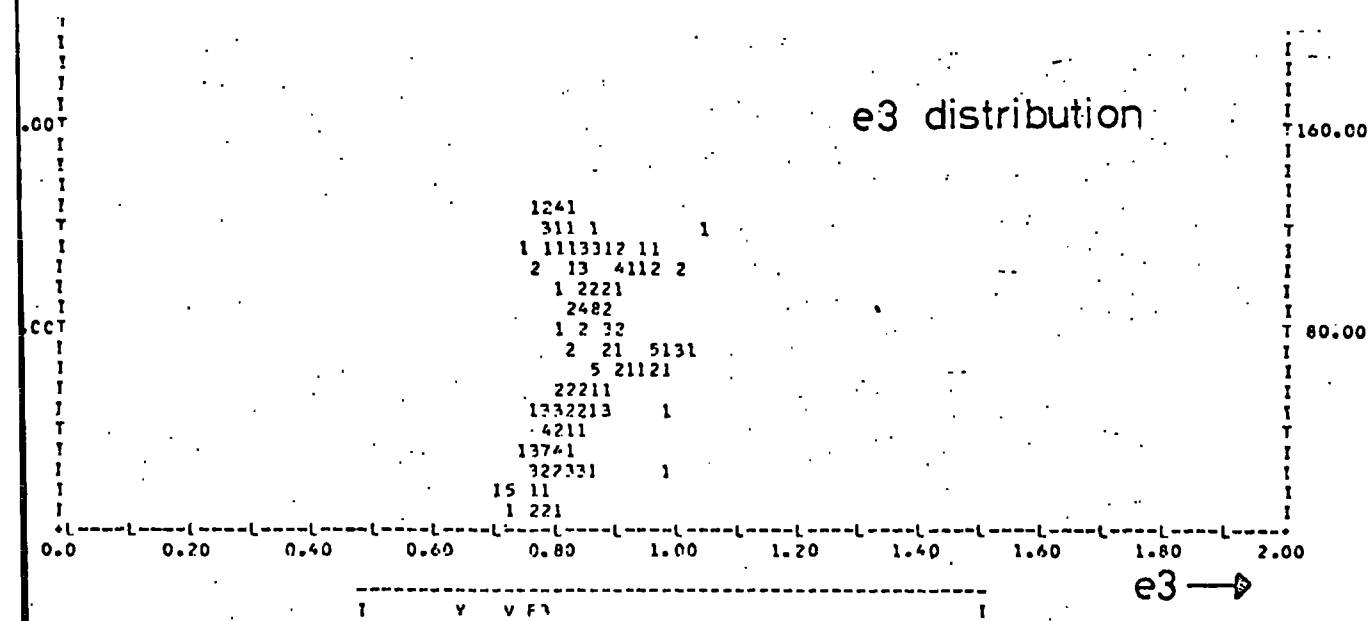

Y	V	E3

INSIDE 182 OUT LOW 0 OUT HIGH 0 TOTAL 182

FIGURE 6.33

Results of the analysis of data for NGC 1569 with no sky subtraction.

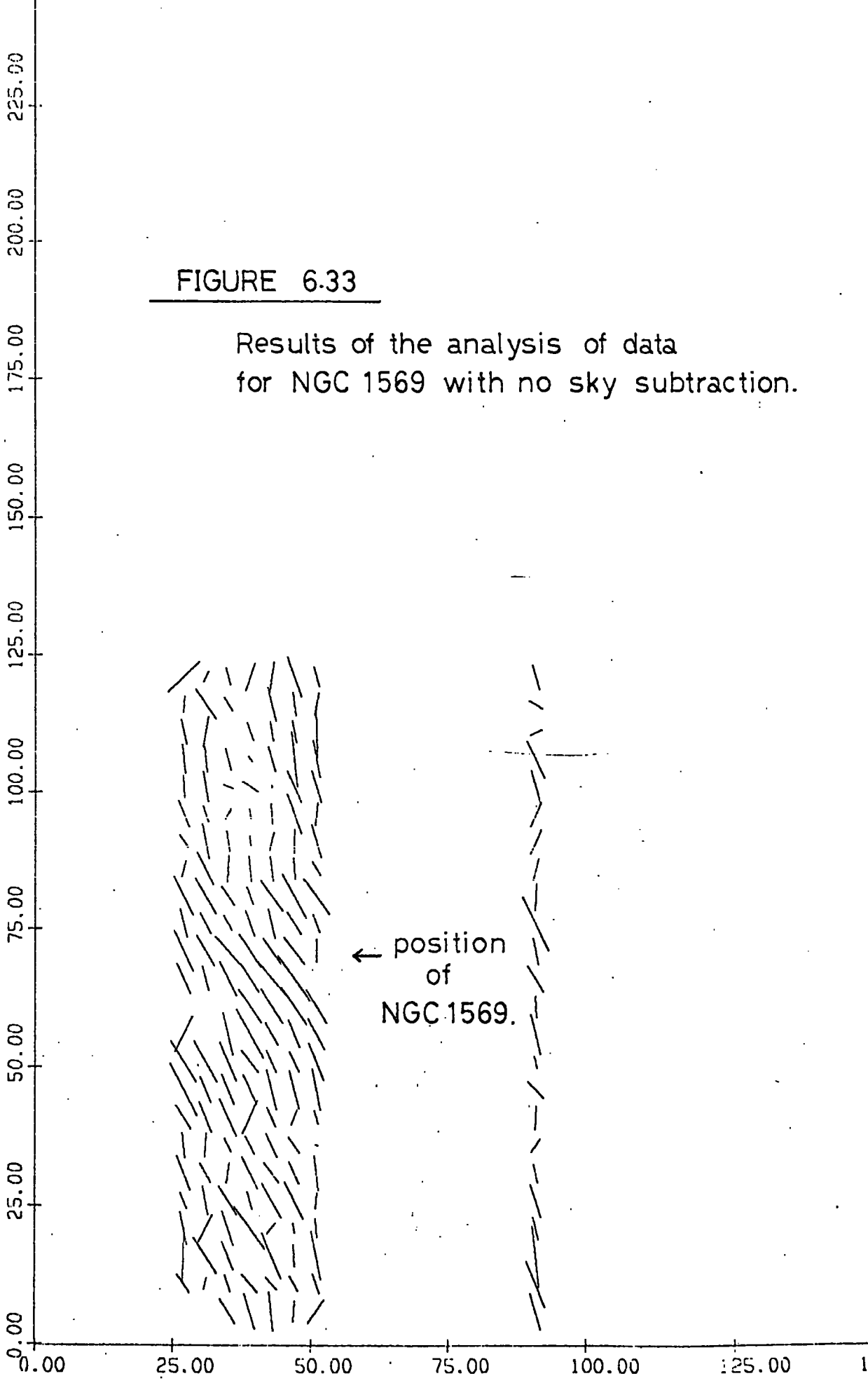

FIGURE 6.34 NGC 1569

(a) Polarisation map of galaxy superimposed on a photograph taken in the blue by Arp (1966)

(b) Contour map of the galaxy NGC 1569

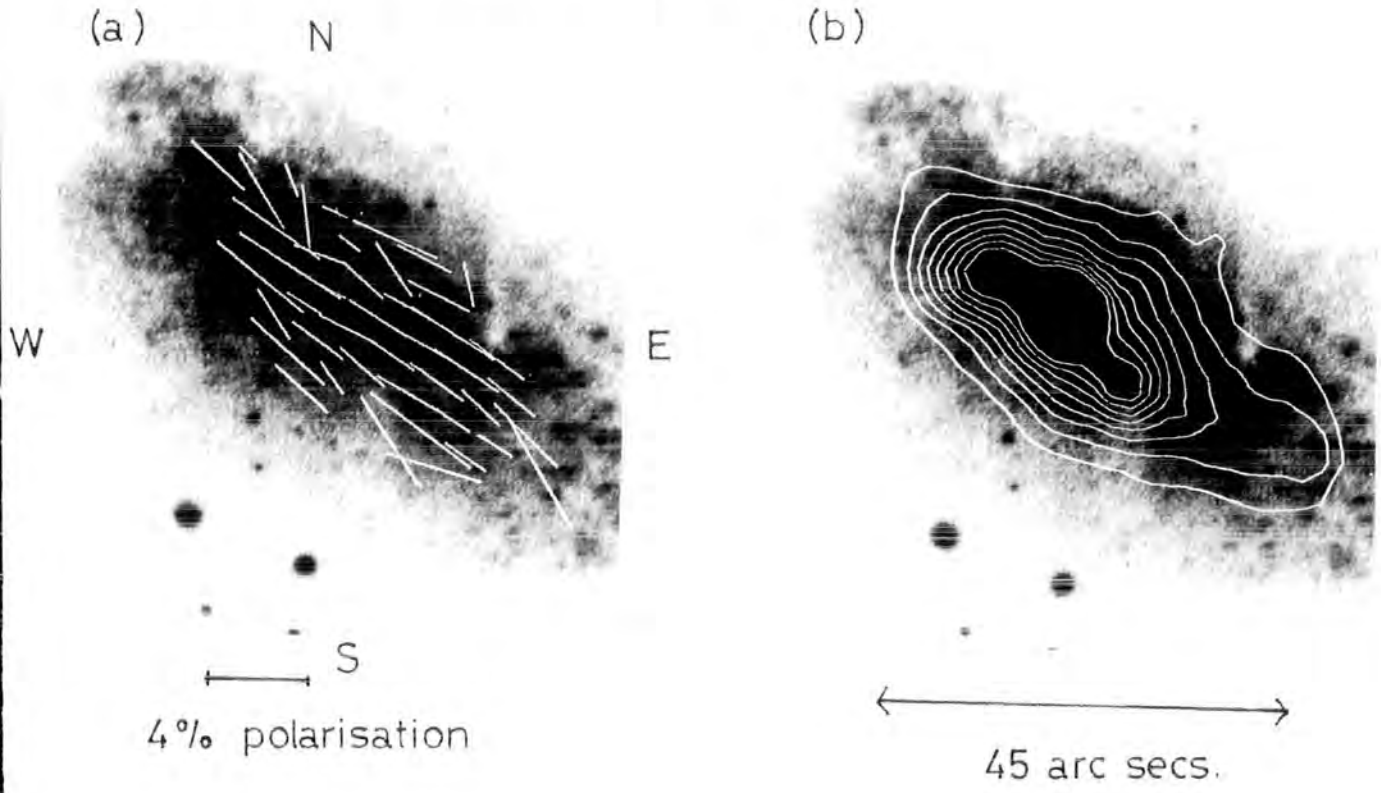

The standard deviation of the individual measurements for the degree of polarisation is ∓ 1% and both the mean polarisation, (calculated by summing over the polarisation measures assuming they are parallel) and the integrated polarisation (calculated by summing the Stokes parameters I, Q, U) were measured to be 4%.

The angle measured for the integrated polarisation is 146°∓5° measured positive from the North, anticlockwise through west to south.

6.4 Errors on the Observations

The method used for the estimation of the errors on the measurements, isthe same as that used for the error determination for the Crab nebula.

Figure 6.41 shows the distribution of the difference in the two estimates of the degree of polarisation P1 - P2 as a function of intensity for various intervals of the degree of polarisation measured.

For values of the degree of polarisation of about 4% the value of P1 - P2 is less than 2%, and since these values of P correspond to high intensity regions only the polarisation is well determined. Figure 6.41 also shows that the largest error on the degree of polarisation measured occurs in the outer regions of the galaxy, that is low intensity regions, where P1 - P2 can be as great as 5%, but the degree of polarisation P measured is 7%. One would expect that as P increases the error on P would decrease as in the case of the Crab Nebula, however the larger error in this region lends support to the proposal that the galaxy is uniformly polarised over its whole area.

Figure 6.42 shows the corresponding diagram for the error on the angle. For P about 4% the angles are well determined, to within 5°. However in the outer regions of the galaxy where the intensity is low, the value of $\theta 1 - \theta 2$ can be of the order of 10° or more.

FIGURE 6.41

The variation of P1 P2 as a function of Intensity for various values of degree of polarisation (P) measured.

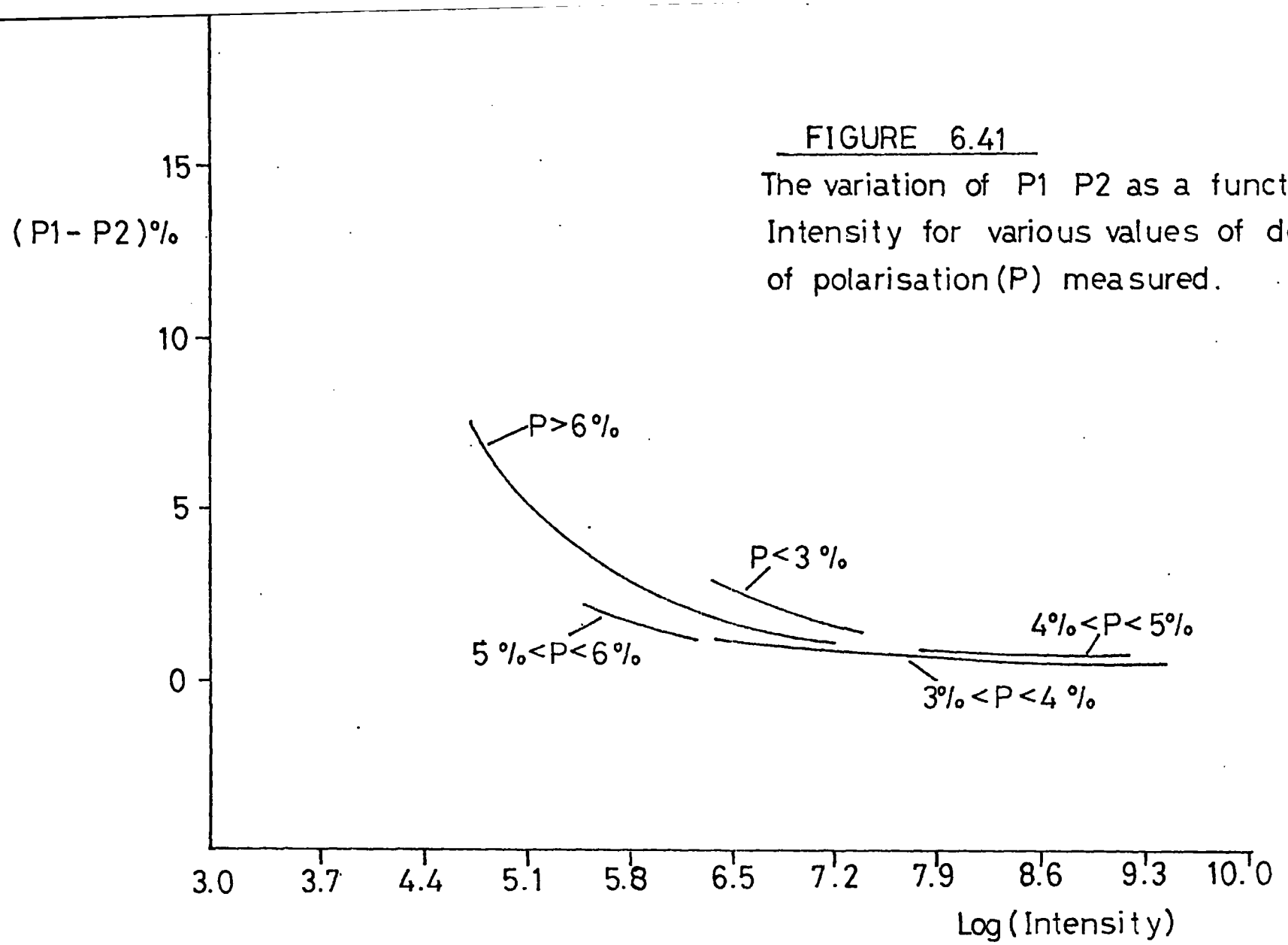

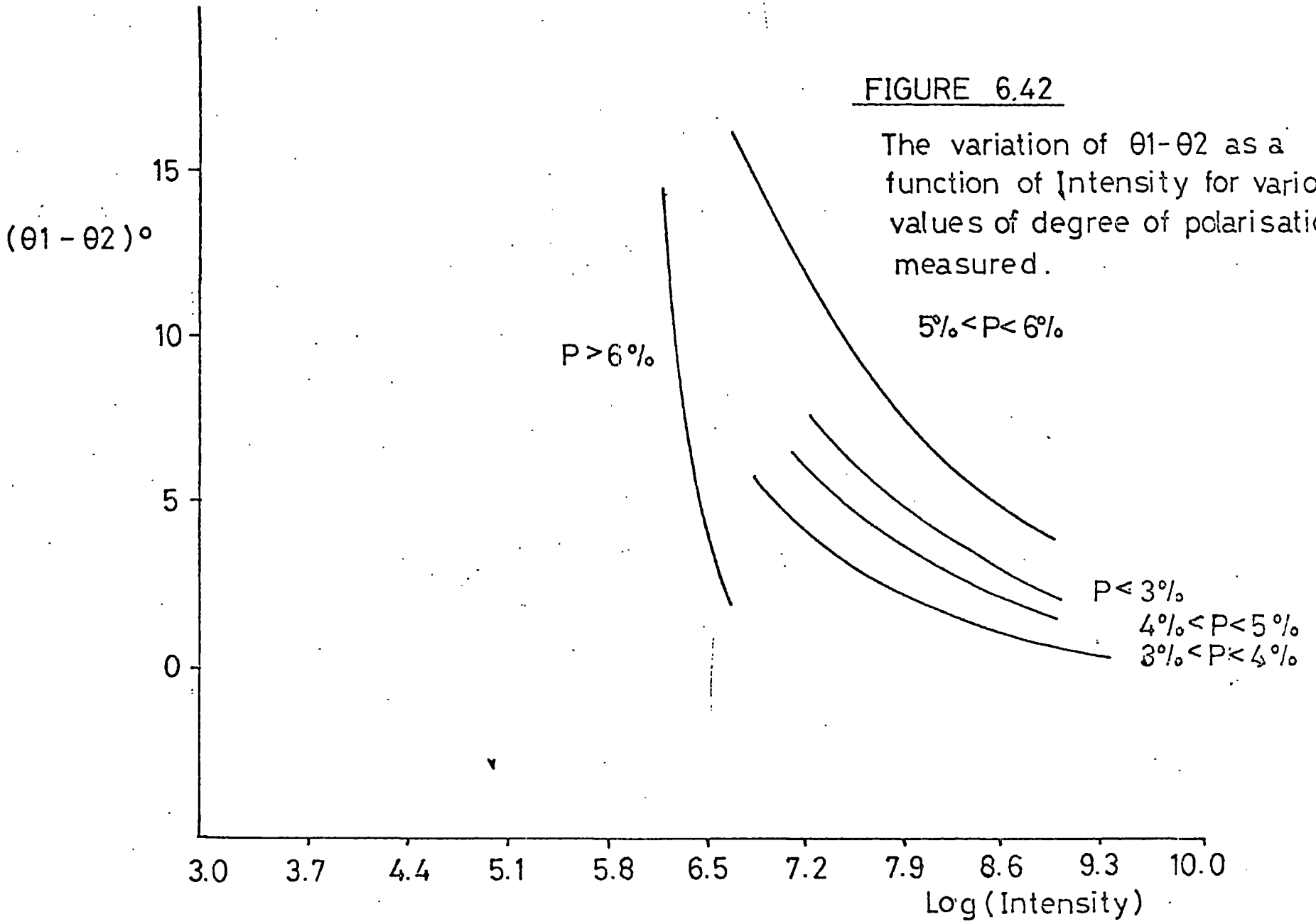

FIGURE 6.42

The variation of θ1 - θ2 as a function of Intensity for various values of degree of polarisation measured.

6.5 Interpretation of the Results

The polarisation pattern, since it is uniform over the whole of the galaxy, gives rise to problems in the interpretation. The production of this pattern, if the polarisation observed is intrinsic to the galaxy itself, demands a process which polarises the light uniformly over the whole area of the galaxy itself. If, however, the polarisation is produced in our own galaxy, which, since the galactic latitude of NGC 1569 is low $b^{II} = 11.24°$, is not unlikely, it is not difficult to see why the galaxy is uniformly polarised, as we see significant interstellar polarisation in this direction, due to the process described by Davis and Greenstein (1951). This process involves the selective absorption of light by interstellar dust grains aligned by a magnetic field.

To distinguish between these two alternative explanations the degree and angle of polarisation of one star, which seemed typical of the general pattern in this area, and was situated close, in both l^{II} and b^{II} ($l^{II} = 143.5°$ and $b^{II} = 9.6°$), to NGC 1569, was found from the catalogue of D Axon and R S Ellis (1976).

This star also had the advantage of being at distance 800 pc, which since NGC 1569 is extragalactic, is a good comparison, especially since Hiltner (1956) found no distance dependance for stars at distances greater than about 1 kpc.

The Stokes Parameters quoted for this star (HD 25443) are $Q/I = 0^m.11158$, $U/I = -0^m.02782$ which give degree of polarisation 5% at an angle of 83° measured from the galactic north pole.

Converting the results of the integrated polarisation of NGC 1569 to the same system we obtain $P = 4 \mp 1\%$ at angle $\theta = 81 \mp 3°$.

Hence the degree and angle of polarisation of NGC 1569 agree well with those of HD 25443 and we can conclude that the observed polarisation of NGC 1569 is produced by processes in our own galaxy.

6.6 Interstellar Polarisation

It is now widely accepted that most of the interstellar polarisation is produced by the mechanism proposed by Davis and Greenstein (1951) in which the selective absorbtion of light by interstellar dust particles aligned by a magnetic field produces linear polarisation. The E vectors represent the projection of the magnetic field in a plane perpendicular to the line of sight, and therefore they trace the structure of the magnetic field.

Interstellar polarisation was first discovered by Hall (1949) and Hiltner (1949).

Mathewson and Ford (1970) compiled all the observational data up to 1970, in a catalogue which contains 7000 stars as a function of galactic latitude and longitude. A more extensive catalogue compiled by Axon and Ellis (1976) gives information on the polarisation in the form of Stokes Parameters for 5700 stars as a function of galactic latitude and longitude, the source reference, and also the distance of the stars.

Both catalogues contain a series of plots which show the degree and angle of polarisation of the stars measured as a function of galactic latitude and longitude, for example figure 6.61.

The plots do not show regularity for distances up to 600 parsecs. Above this a well ordered pattern emerges, with the preference that the plane of polarisation lies in the galactic plane, the regularity of the alignment of the vectors depending on the galactic longitude.

FIGURE 6.61

The E-vectors of the optical polarisation measurements of 1800 stars at Siding Spring Observatory and of Northern Hemisphere observers are plotted in galactic coordinates.

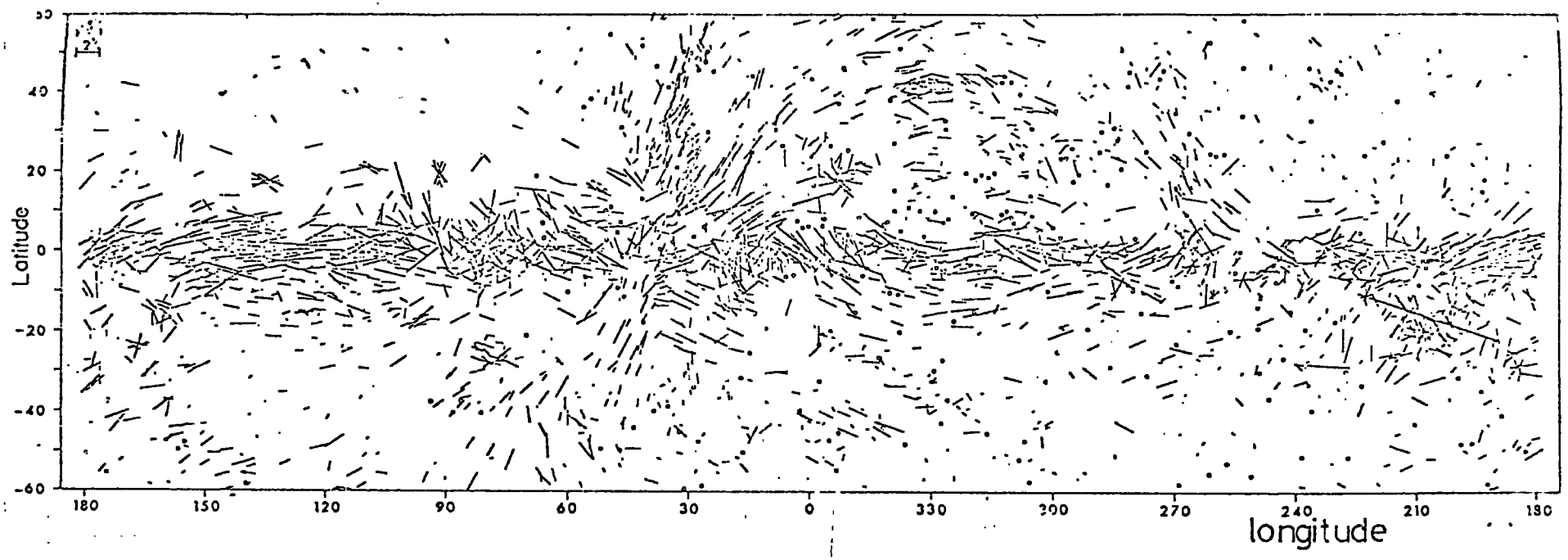

The length of each line is proportional to the percentage polarisation, and the angle is drawn relative to the galactic north pole in the direction of increasing longitude.

Reproduced from Mathewson and Ford (1970)

Hiltner (1956) found no distance dependance in the optical polarisation of stars for distances above 1 kpc, which indicates that most of the optical polarisation is produced relatively locally.

There are two major schools of thought as to the configuration of local magnetic fields, either a longitudinal field or a helical field.

Between $l^{II} = 100°$ and $l^{II} = 150°$, the well ordered field observed at large distances, suggests that the field is parallel to the plane and longitudinal. Radio continuum polarisation data at $l^{II} = 140°$, supports this hypothesis by suggesting that here we are looking normal to the local field.

Towards $l^{II} = 50°$, the data suggests we are looking along the local field. However at $l^{II} = 80°$, there are a confusion of vectors often associated with the field looking along our line of sight. However the cygnus X complex is situated at $l^{II} = 80°$, and therefore the observed polarisation pattern could be caused by processes in the complex, and can be regarded as an anomally in the field, and produced in the local spiral arm. Mathewson favoured the helical model on the grounds that, the polarisation vectors of many stars are perpendicular to the plane at low latitudes in many directions, whereas considering a longitudinal field, only in directions where we look normal to the field $l^{II} = 50°$ and $l^{II} = 230°$ would we expect this pattern. However the helical model does not explain the well ordered structure at $l^{II} = 140°$.

Of the two models, the more widely accepted is the longitudinal model, with axis down the local spiral arm.

Our results for the polarisation of NGC 1569 confirm the results of Hiltner (1956) in that the measurement of the degree of polarisation agrees extremely well with that of HD 25443, therefore since the galaxy is at distance 3 Mpc and the star, 800 pc, there seems no distance dependance on the polarisation for distances greater than 800 pc.

NGC 1569 is located at $l^{II} = 143.670$, the position where a well ordered interstellar polarisation pattern is seen. We confirm that the orientation of the polarisation vectors of NGC 1569 is the same as that of distant stars in our galaxy at this longitude, and therefore the results support the hypothesis that in this region we are looking normal to the local magnetic field.

6.7 Correction for Interstellar Polarisation

To extract information about the intrinsic polarisation of NGC 1569, it was decided to attempt to correct for the effects of interstellar polarisation.

The theory used was derived mainly by W S Pallister.

To correct for interstellar polarisation we consider:

1. The polarisation produced when an unpolarised beam of light passes through a series of aligned dust grains.
2. Using the results obtained from 1, we find the effect of a partially plane polarised beam passing through the same dust grains.

1. Let us take I as being the intensity of the unpolarised beam of light, k is the fraction of that light absorbed perpendicular to the short axis of the grains.

Parallel to the short axis of the grain the transmitted light component which remains unpolarised is I/2.

Perpendicular to this the transmitted component of the light is given by $(I/2)(1-k)$ and the absorbed component is given by $(I/2)k$.

The observed polarisation after passing through aligned dust grains is given by

$$P = \frac{k\ I/2}{I/2 + (I/2)(1-k)}$$

Therefore $k = \frac{2P}{1+P}$ 1.

2. Now we consider a partially polarised beam of light passing through the same dust grains.

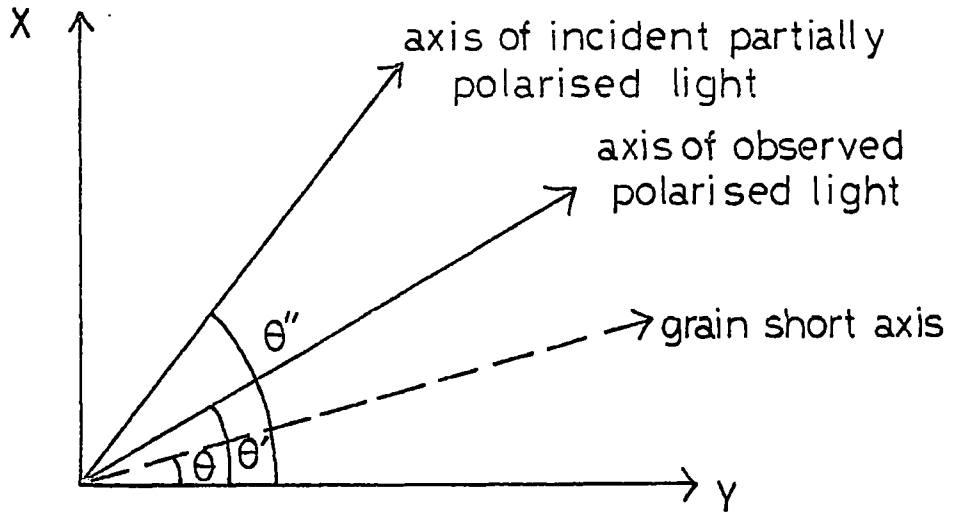

FIGURE 6.71

Figure 6.71 indicates the frame of reference we used, plane X, Y, where angles observed are measured from the Y direction.

θ is the angle between the grain short axis and the Y direction, that is the angle of polarisation observed after an unpolarised beam of light passes through a series of aligned dust grains.

θ'' is the angle of polarisation of the partially plane polarised light, that is, the incident beam.

θ' is the observed angle of polarisation.

Now we will treat the unpolarised components of the light after passing through the dust grains and the initially polarised components separately.

(a) Unpolarised Components

Taking components parallel to and perpendicular to the grain short axis.

Parallel to the grain short axis the transmitted unpolarised component is given by

$(I_i - p_i I_i)/2$

where Ii is the total intensity of the incident light (i.e light from the galaxy) and pi is the intrinsic polarisation of light from the galaxy.

Perpendicular to this, the transmitted unpolarised component is given by

$$\left[(Ii - pi\ Ii)/2\right] \quad (1-k)$$

where k is the fraction of light absorbed perpendicular to the short axis of the grain. Therefore the perpendicular component absorbed is $k\left[Ii\ \left(\frac{1 - pi}{2}\right)\right]$

(b) Polarised Components

The component of the polarised light from the galaxy after passing through the aligned dust grains that is transmitted is given by

$pi\ Ii\ Cos^2\ (\theta"-\theta)$

Perpendicular to the short axis of the grain the component of the transmitted light is

$pi\ Ii\ Sin^2\ (\theta"-\theta)\ (1-k)$

The absorbed perpendicular component is therefore

$pi\ Ii\ Sin^2\ (\theta"-\theta)\ k$

FIGURE 6.72

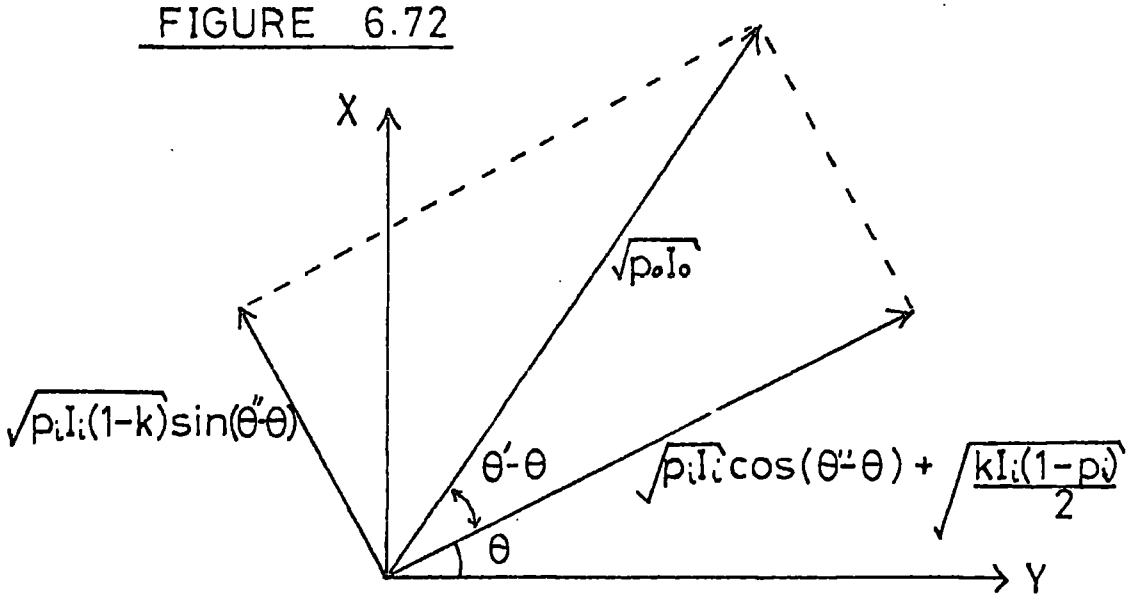

Figure 6.72 shows the components of the amplitude of the light which produce the observed intensity Io, where po is the observed fractional polarisation, from partially polarised light passing through the aligned dust grains.

The Intensity of the Unpolarised Component

$$(Io - po\ Io) = (Ii - pi\ Ii)\ (1-k) \qquad \text{---------- 1.}$$

Intensity of the Polarised Component

$$poIo = pi\ Ii\ Sin^2\ (\theta''-\theta)\ (1-k) + \left[\sqrt{pi\ Ii}\ Cos\ (\theta''-\theta) + \sqrt{k\ Ii\ \frac{(1 - pi)}{2}}\right]^2 \qquad \text{---------- 2.}$$

Angle of Observed Polarisation

$$Sin\ (\theta'-\theta) = \frac{\sqrt{pi\ Ii\ (1-k)}\ Sin\ (\theta''-\theta)}{\sqrt{po\ Io}} \qquad \text{---------- 3.}$$

Solving these we obtain

$$pi = \frac{2\ kpo\ Sin^2(\theta'-\theta) + 2po - pok - k}{2\ kpo\ Sin^2(\theta'-\theta) + 2 - pok - k} \qquad 4.$$

$$\text{and } Sin\ (\theta''-\theta) = Sin\ (\theta'-\theta) \sqrt{\frac{po\ (1-pi)}{pi\ (1-po)}} \qquad \text{---------- 5.}$$

6.8 Results of the Correction for Interstellar Polarisation

Equations (4) and (5), above were used to remove, from the observed polarisation, the effect of the interstellar polarisation. The value of interstellar polarisation P, and θ were determined from the quoted results for HD 25443.

The results are shown in map form in figure 6.81. The map shows that there is little or no polarisation over a wide area of the galaxy, the small polarisation values being of the order of 1% or less which is the error on making the measurements.

FIGURE 6 81

The optical polarisation of NGC 1569
after correction for interstellar polarisation

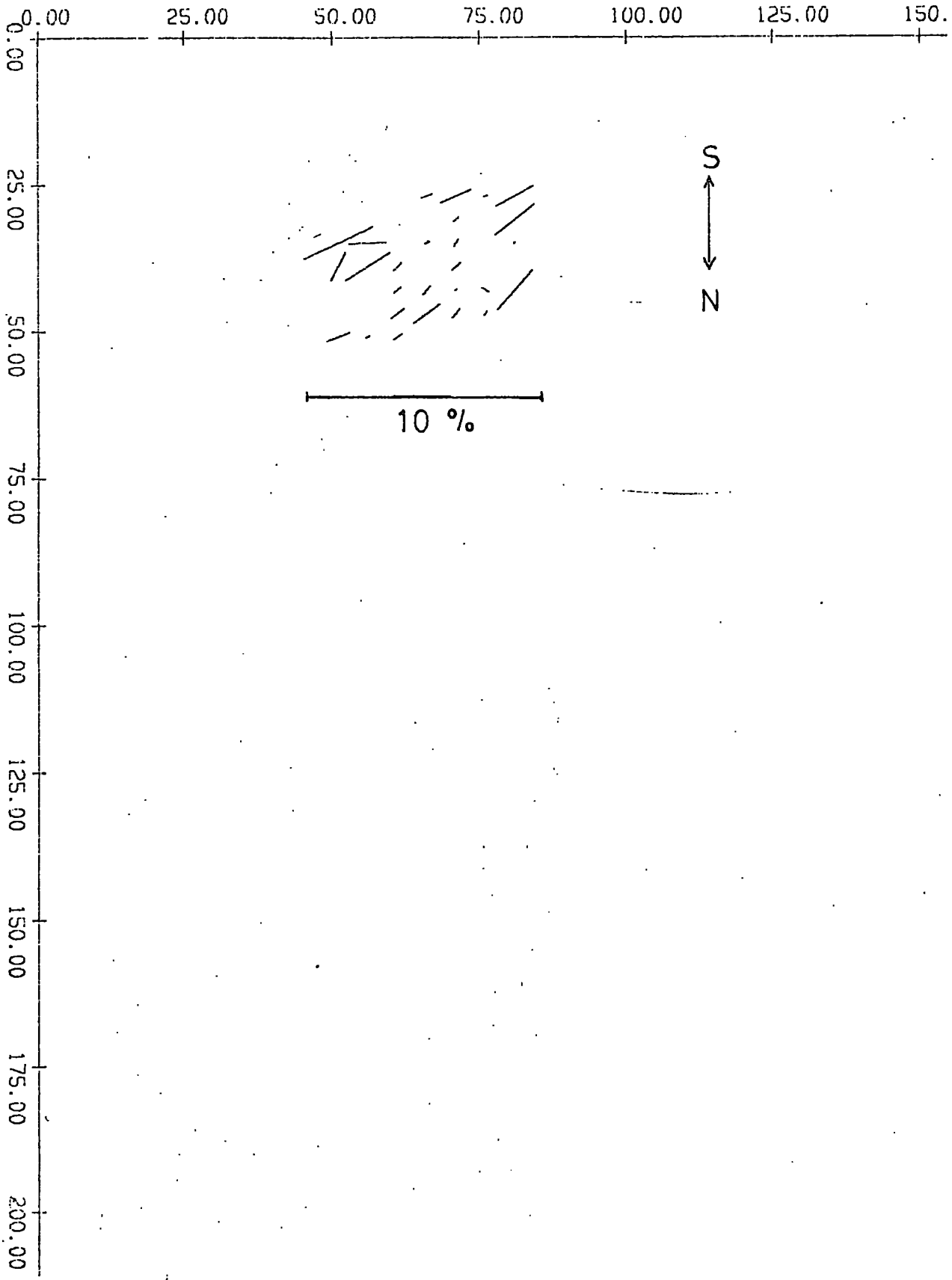

The outer edges of the galaxy show larger values for the degree of polarisation, of the order of 3-4%, but are randomly orientated, and in these regions the intensity is low thus introducing more error, of the order of the degree of polarisation measure itself (see section 6.4).

It can therefore be concluded that, over the area of the galaxy observed, there is no intrinsic polarisation, and that all the polarisation observed in the first place is induced as the light from NGC 1569 passes through our own galaxy.

6.9 Conclusion

NGC 1569 is unpolarised at source in the wavelength range 4000 Å - 5000 Å. The observed polarisation measured by our system agrees in degree and angle with that of distant stars in our own galaxy, therefore the polarisation measured is interstellar polarisation.

NGC 1569 is included in the class of filament galaxies typified by M82, on the results of the Hα plates taken by Hodge, but the polarisation pattern at source for NGC 1569 in no way resembles that of M82 in this wavelength range (Pallister 1976).

References

Ables, H.D. (1971) Pub. US Naval Obs 20 Part IV 60

Arp, H.C. (1966) Atlas of Peculiar Galaxies (Pasadena: California Institute of Technology)

Axon, D.J. and Ellis, R.S. (1976) MNRAS (in press)

Davis L. and Greenstein J.L. (1951) Ap. J 114 206

De Vaucouleurs, G, de Vaucouleurs, A. (1964) Reference Catalogue of Bright Galaxies (Austin: Univ Texas)

De Vaucouleurs, G, de Vaucouleurs, A and Corwin, H.G (1973) Bull, A.A.S 5 Part 1 40

De Vaucouleurs, A, de Vaucouleurs, G, and Pence, W. (1974) Ap J (Letts) 194 L119

Hall, J.S. (1949) Science 109 166

Heeschen, D.S and Wade, C.M (1964) A.J 69 227

Hiltner, W.A. (1949) Science 109 165

Hiltner, W.A. (1956) Ap J Suppl 2 389-462

Hodge, P.W. (1974) Ap J Letts 191 L21

Holmberg, E. (1958) Medd. Whd. Obs Ser 2 No 136

Kazes, I, Le Squeren, A.M. and Nguyen-Quang-Rieu (1970) Ap Letts 6 1973

Lequeux, J. (1971) Astr + Ap 15 30

Mathewson, D.S. and Ford, V.L. 1970 Mem. RAS 74 139-182

McCotcheon, W.H. (1973) A J 78 18

Pallister, W.S. (1976) Ph.d Thesis (Durham)

General Conclusions

The use of the Durham polarimeter together with the Royal Greenwich Observatory electronographic camera provides a fast and accurate method of measuring the optical linear polarisation of extended astronomical objects. The technique used for the reduction of the data once formulated can be used to analyse the results of observations of many objects with only slight modifications needed to meet the requirements of the different individual sets of measurements, as has been illustrated in this thesis, for the optical polarisation studies of the Crab Nebula.

The comparison of the present results for the Crab Nebula with earlier work by Woltjer shows that in most areas of the nebula the two sets of measurements agree well, although there appear some regions where agreement is not good. It is possible, since in these regions the filamentary structure is evident, that differing contributions of filamentary radiation in the two wavebands used in the two sets of measurements, could in some part account for the discrepancy.

The observed polarisation of light from the galaxy NGC 1569 would appear to be induced as the light passes through our own galaxy and not intrinsic to NGC 1569. After the interstellar polarisation has been removed, there is no evidence to suggest that the light from NGC 1569 is polarised at source.

In conclusion therefore, this technique provides a powerful tool for measuring the optical linear polarisation of extended astronomical sources.

Acknowledgements

The author wishes to thank Professor A.W. Wolfendale for making available the facilities of the Physics Department of the University of Durham, and the Science Research Council for its financial support.

She expresses gratitude to all members of the Astronomy group for their guidance and help in obtaining the data, and Dr. R.G. Bingham of the Royal Greenwich Observatory for his valuable advice and help.

Finally the author wishes to thank her sister-in-law Mrs. G Lockett for the great care she took in typing this thesis.